Fabrication and Characterization of PCDTBT:$PC_{61}BM$ Based Bulk Heterojunction Organic Solar Cell

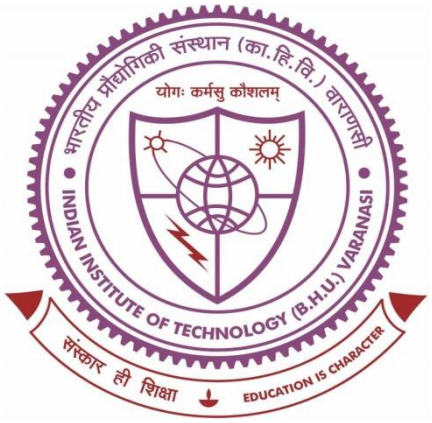

Thesis submitted in partial fulfillment for the Award of Degree

Doctor of Philosophy

By

Amit Kumar

DEPARTMENT OF ELECTRONICS ENGINEERING

INDIAN INSTITUTE OF TECHNOLOGY

(BANARAS HINDU UNIVERSITY)

VARANASI – 221005

INDIA

ROLL NO: 15091005

2021

CERTIFICATE

It is certified that the work contained in the thesis titled **"Fabrication and Characterization of PCDTBT:PC_{61}BM Based Bulk Heterojunction Organic Solar Cell"** by **"Amit Kumar"** has been carried out under our supervision and this work has not been submitted elsewhere for a degree.

It is further certified that the student has fulfilled all the requirements of Comprehensive, Candidacy and SOTA for the award of Ph.D. Degree.

(Prof. Satyabrata Jit)
Supervisor
Department of Electronics Engineering
IIT (BHU), Varanasi

(Dr. Bratindranath Mukherjee)
Co-Supervisor
Department of Metallurgical Engineering
IIT (BHU), Varanasi

DECLARATION BY THE CANDIDATE

I, Amit Kumar, certify that the work embodied in this thesis is my own bonafide work and carried out by me under the supervision of Prof. Satyabrata Jit and Dr. Bratindranath Mukherjee from "21/07/2015" to “12/04/2021”, at the Department of Electronics Engineering, Indian Institute of Technology (BHU), Varanasi. The matter embodied in this thesis has not been submitted for the award of any other degree/diploma. I declare that I have faithfully acknowledged and given credits to the research workers wherever their works have been cited in my work in this thesis. I further declare that I have not willfully copied any other's work, paragraphs, text, data, results, *etc*., reported in journals, books, magazines, reports, dissertations, theses, *etc*., or available at websites and have not included them in this thesis and have not cited as my own work.

Date: **Signature of the Student**

Place: **Amit Kumar**

CERTIFICATE BY THE SUPERVISOR

It is certified that the above statement made by the student is correct to the best of my knowledge.

(Prof. Satyabrata Jit)
Supervisor
Department of Electronics Engineering
IIT (BHU), Varanasi

(Dr. Bratindranath Mukherjee)
Co-Supervisor
Department of Metallurgical Engineering
IIT (BHU), Varanasi

Signature of Head of Department
"SEAL OF THE DEPARTMENT"

COPYRIGHT TRANSFER CERTIFICATE

Title of the Thesis: **Fabrication and Characterization of PCDTBT:$PC_{61}BM$ Based Bulk Heterojunction Organic Solar Cell.**

Name of the Student: **Amit Kumar**

Copyright Transfer

The undersigned hereby assigns to the Indian Institute of Technology (Banaras Hindu University), Varanasi all rights under copyright that may exist in and for the above thesis submitted for the award of the Doctor of Philosophy.

Date: **Signature of the Student**

Place: **Amit Kumar**

Note: However, the author may reproduce or authorize others to reproduce material extracted verbatim from the thesis or derivative of the thesis for the author's personal use provided that the source and the Institute's copyright notice are indicated.

ACKNOWLEDGEMENTS

Foremost, I would like to express my sincerest regards and love for my father Late-Sri Changur Prasad Gour, and my mother Late- Smt. Kunnan Devi for their constant support and love throughout my life. I will always be in debt no matter what I do, and I will always be your reflection.

Besides my parents, I would like to express my immense gratitude to my supervisor Prof. Satyabrata Jit and co-supervisor Dr. Bratindranath Mukherjee for their excellent guidance and motivation. The completion of this research work is indeed an outcome of their constant untiring support, valuable ideas, and suggestions during my research work. The insightful discussions with them always provided me great enthusiasm.

I wish to extend my sincere gratitude towards my research performance evaluation committee (RPEC) members, Prof. V. N. Mishra and Dr. Bhola Nath Pal for their encouragement and insightful comments. I would also like to thank all the faculty members for their kind cooperation and encouragement during this journey.

I am grateful to my M. Tech. supervisor Dr. Mousumi Saha for enlightening me for further research.

I would like to express my special thanks to Dr. Hemant Kumar, Dr. Gopal Rawat, Dr. Balraj Singh, Dr. Kunal Singh, Dr. Ekta Goel, Dr. Sanjay Kumar, Dr. Yogesh Kumar, Dr. Sweta Chander, and Dr. Chandan Kumar for their valuable assistance from personal to the technical level.

I am very much thankful to many research scholars of the CRME laboratory for providing a stimulating and friendly environment. My thanks go to Dr. Lalit Chandra, Dr. Praveen Kumar Sahu, Mr. Smrity Ratan, Mr. Deepak Kumar Jarwal, Mr. Ashwini Kumar Mishra, Mr. Prince Kumar Singh, Mr. Kamalaksha Baral, Mr. Abhinav Pratap Singh, Mr. Rishibrind Kumar Upadhyay, Mr. Deep Chandra Upadhyay, Mr. Manas Ranjan Tripathy, Mr. Ashish Kumar Singh, Mr. Jogindra Singh Rana, Mr. Abhishek Kumar Singh, Mr. Ankit Verma, Mr. Prashant Kumar, Mr. Vijay Kumar, Mr. Ashutosh Kumar Dixit and Mr. Sanjeev Mani Yadav.

I am indebted to research scholars, Mr. Prabhakar Tripathi, Mr. Arjun Kumar, Mr. Akash Kumar, Mr. Mumtaz Ali Ansari, Mr. Rahul Pal, Dr. Aman Sikari, Dr. Vinit Kumar Singh, Dr. Rajnish Singh, and Mr. Shyam Gopal Yadav for providing a fun-filled environment.

My thanks and sincere appreciations also go to all staff members of CRME laboratory, especially to Mr. M. K. Saxena, Dr. V. K. Singh, Mr. L. Bahadur, Mr. S. Narayan, Mr. S. C. Yadav, and Mr. S. Srivastava for their kind co-operation.

I am indebted to some of my close friends, Ms. Anushka, Mr. Vijay Kumar, Mr. Manish Deo, Mr. Ravi Singh, Mr. Rahul Kumar, and Mr. Srinivas for their constant encouragement and support.

My most profound appreciation towards my sisters and brothers for their continuous support and encouragement. They are the source of strength for me and remain an invaluable asset to me.

I also would like to give the special thanks to MeitY, Government of India for providing research fellowship to me under the Visvesvaraya Ph.D. scheme <MEITY-PHD-216>.

Finally, I heartily express sincere thanks to my big family. For their unconditional love, extreme patience and constant support over the years. They provide me strength and confidence to attain this task.

Above all, I thank Lord Vishwanath and Maa Durga for providing me strength and courage in completing the work.

Date: **(Amit Kumar)**

Dedicated
To
My Family

CONTENTS

LIST OF FIGURES

LIST OF TABLES

LIST OF ABBREVIATIONS

Abbreviation	Details
OPV	Organic photovoltaic
OSC	Organic solar cell
BHJ	Bulk heterojunction
EPBT	Energy payback time
EQE	External quantum efficiency
MEH-PPV	Poly[2-methoxy-5-(2'-ethylhexyloxy)-1,4-phenylene vinylene]
PCDTBT	poly[N-9′-hep- tadecanyl-2,7-carbazole-alt-5,5-(4′,7′-di-2-thienyl-2′,1′,3′-ben- zothiadiazole)]
PCBM	[6,6]-phenyl-C_{61}-butyric acid methyl ester
ETL	Electron transport layer
HTL	Hole transport layer
P3HT	Poly(3-hexylthiophene)
PQT-12	Poly(3, 3‴-dialkylquaterthiophene) or
	Poly(3,3‴-didodecylquaterthiophene)
FTM	Floating-film transfer method
IL	Interface layer
HOMO	Highest occupied molecular orbital
LUMO	Lowest unoccupied molecular orbital
AM	Air mass
PBTTT	Poly[2,5-bis(3-tetradecylthiophen-2-yl)thieno[3,2-b]thiophene]
PEDOT	Poly(3,4-ethylenedioxythiophene)
PSS	Polystyrene sulfonate
eV	Electron volt
V_2O_5	Vanadium oxide
PPV	Poly(p-phenylene vinylene)

TiO_2	Titanium dioxide
PCE	Power conversion efficiency
MDMO-PPV	([2-methoxy-5-(3',7'-dimethyloctyloxy)]-1,4-phenylenevinylene)
HRSEM	High resolution scanning electron microscopy
UV-Vis	Ultraviolet-visible
PL	Photoluminescence
ZnO	Zinc oxide
PET	Polyethylene terephthalate
CdSe	Cadmium selenide
QDs	Quantum Dots
SnO_2	Tin oxide
Au	Gold
Ag	Silver
Al	Aluminum
MoO_3	Molybdenum trioxide
ITO	Indium-doped tin oxide
FTO	Fluorine-doped tin oxide
Si	Silicon
In_2O_3	Indium oxide
MEA	Monoethanolamine
PVDF	Polyvinylidene fluoride
DI	Deionized
IPA	Isopropanol alcohol

LIST OF SYMBOLS

Symbol	Details
λ	Wavelength
η	Power conversion efficiency
n	Ideality factor
R	Responsivity
α	Absorbance coefficient
IV	Current-voltage
JV	Current density-voltage
Eg	Energy band gap
IP_D	Ionization potential of the donor
EA_A	Electron affinity of the acceptor
E_B	Binding energy of the excitons
μ	Mobility
E_{HOMO}	Energy level of HOMO
E_{LUMO}	Energy level of LUMO
e	Charge of electron
I_{dark}	Dark current
I_d	Diode current
I_{so}	Reverse saturation current
I_{ph}	Photo generated current
Jo	Reverse saturation current density
V_T	Thermal equivalent voltage
Rs	Series resistance
Rsh	Shunt resistance

Isc	Short circuit current
Jsc	Short circuit current density
Voc	Open circuit voltage
FF	Fill factor
Vm	Maximum voltage
Im	Maximum current
Pmax	Maximum output power
Pin	Input incident power

PREFACE

Bulk heterojunction (BHJ) based organic solar cells (OSCs) are gaining greater attention for clean energy production due to various features, namely low-cost, easy fabrication process, the feasibility of solution process, mechanical flexibility, non-toxicity, and biodegradability. Recently, the low bandgap polymer, poly[N-9′-hep-tadecanyl-2,7-carbazole-alt-5,5-(4′,7′-di-2-thienyl-2′,1′,3′-benzothiadiazole)] (PCDTBT) has been considered to be more suitable p-type donor polymer for the OSC. The PCDTBT is blended with the commonly used acceptor polymer $PC_{61}BM$ for the fabrication of OSC and provides better stability as well as improved photovoltaic parameters. Considering the above aspects, the present thesis is focused to fabricate and characterize the PCDTBT:$PC_{61}BM$ active layer based BHJ OSC by modifying the interface layer, transport layers, and the photoactive layer. The works of the thesis are intended to enhance the photovoltaic parameters through thin film engineering. The thesis consists of five chapters which are briefly outlined in the following sentences.

Chapter-1 introduces the inorganic and organic semiconductors and charge conduction mechanism through them. A brief discussion on solar cells is included. Further, various types of organic solar cells, including the BHJ OSC, are discussed along with working principles and important photovoltaic parameters. A detailed literature survey followed by the scope of the present thesis has been finally outlined in this chapter.

Chapter-2 reports the PQT-12 polymer-based interface layer (IL) effect for the improvement in the photovoltaic parameters of the BHJ OSC. The floating film transfer method (FTM) is adopted for the deposition of PQT-12 thin film. Two distinct BHJ

OSCs have been fabricated in the device structure of ITO/ZnO QDs/PCDTBT:$PC_{61}BM$/PEDOT:PSS/Ag and ITO/ZnO QDs/PCDTBT:$PC_{61}BM$/PQT-12/PEDOT:PSS/Ag for the comparative study. The effect of PQT-12 IL has been investigated by several characterizations, namely current-voltage characteristics, absorbance, photoluminescence (PL), impedance spectroscopy, and external quantum efficiency. The OSC with the PQT-12 based IL has shown improved photovoltaic parameters.

Chapter-3 investigates the effect of thickness variations of the electron transport layer (ETL) as well as hole transport layer (HTL) on the performance of PCDTBT:$PC_{61}BM$ based BHJ OSCs. The BHJ OSCs are fabricated in ITO/ZnO QDs/PCDTBT:$PC_{61}BM$/PQT-12/Ag structure, where ZnO QDs and PQT-12 are used as ETL and HTL, respectively. ZnO QDs ETL has been deposited by a solution-processed spin coating method, whereas PQT-12 HTL has been deposited using the FTM technique. The best OSC device performance has been obtained with the 35 nm ZnO QDs and 20 nm PQT-12 thicknesses.

Chapter-4 deals with the fabrication and characterization of two distinct BHJ OSCs in the device structures, ITO/ZnO QDs/PCDTBT:$PC_{61}BM$/MoO_3/Ag and ITO/ZnO QDs/PCDTBT:$PC_{61}BM$:CdSe QDs/MoO_3/Ag. The synergistic effect of CdSe QDs and $PC_{61}BM$ is investigated in the ternary OSC device, where ZnO QDs and MoO_3 are used as ETL and HTL, respectively. The device structure, ITO/ZnO QDs/PCDTBT:$PC_{61}BM$:CdSe QDs/MoO_3/Ag has shown the improved photovoltaic parameters compared to other OSCs described in Chapter-2 and Chapter-3. The maximum efficiency of 5.02% is achieved due to the synergistic effect of CdSe QDs and $PC_{61}BM$.

Chapter-5 includes the major findings of the thesis along with a brief outline for the future scope of research related to the present thesis.

----XXX----

CHAPTER 1

Introduction and Scope of the Thesis

Contents

CHAPTER 1

Introduction and Scope of the Thesis

1.1 Introduction

Industrial development, automation, and the fast-growing population have increased the global requirement for energy. The energy demands in economically emerging countries are estimated to be increased by 90% in 2035 [1]. Moreover, energy production (electricity) is still less than the current demand, and about 20% of the global population are facing electricity problem [1]. Presently, most of the electricity is produced by traditional fossil fuels, namely coal, oil, and gas. However, the decreasing natural stock of fossil fuels will affect future energy requirements. The generation of electrical energy from fossil fuels also creates severe environmental issues such as global warming through the greenhouse effect and air pollution by releasing carbon monoxide, sulphur dioxide, carbon dioxide, nitrogen dioxide, and other gases [2]. Therefore, the sustainable and green energy source is adopted nowadays to overcome the environmental issues and the shortage of fossil fuels. Renewable energy sources such as sun, wind, geothermal, hydroelectric, and biomass are examples of sustainable and green energy resources, as shown in Figure 1.1 [3]. The sun is one of the most important renewable energy sources among the various renewable energy resources due to the abundant sunlight availability. A photovoltaic device converts solar radiation (photon energy) into electrical energy similar to the natural photosynthetic process (convert solar radiation energy into another form of energy such as the chemical potential) in plants [4].

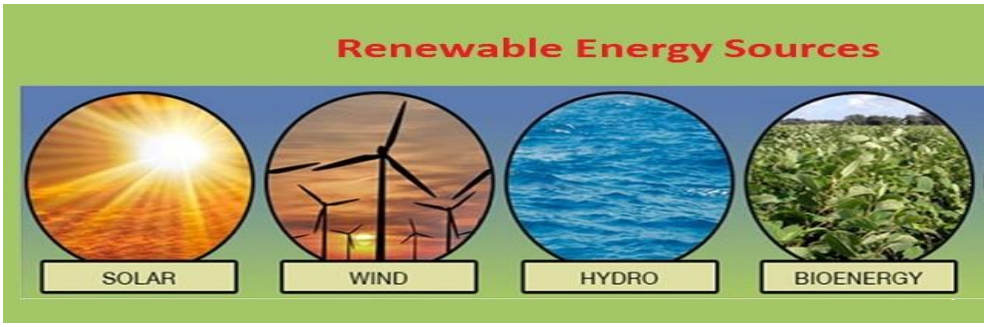

Figure 1.1: Renewable energy resources [3].

1.2 Photovoltaic Devices

The 'photovoltaic effect' is a phenomenon in which photon energy is converted into electrical energy (voltage and current). The photovoltaic effect was first observed by French physicist A. E. Becquerel in 1839 [5]. He found a generated voltage and current in his experiment when he placed silver chloride in an acidic solution and illuminated it with light. Initially, this effect was also known as the "Becquerel effect"[5]. In 1876, photoconductivity was found by William Adams and Richard Day in a thin layer of selenium when sandwiched between two heated platinum contacts [6]. In 1883 C.E. Fritts has given a new form of selenium cells which was extremely sensitive to light than any other cells discovered before. In 1914, Goldman and Brodsky observed that the photovoltaic effect is due to the existence of a barrier that drives the charge carrier in the opposite direction in the photodiode-like structures. The flow of charge carriers constitutes the photocurrent, and the conduction mechanism at semiconductor/semiconductor or semiconductor/metal interfaces was developed by Walter Schottky in 1941 [7].

On the other hand, the manufacturing of good quality silicon wafers in the 1950s gave rise to the development of solid-state electronics and efficient photovoltaic devices

[8]. Further, the realization of the positively (p) and negatively (n) doped silicon led to the manufacturing of silicon p-n junction structures, which have shown a much better-rectifying property than Schottky barriers and better photovoltaic behaviour. In 1954, Daryl Chapin, Calvin Fuller, and Gerald Pearson, scientists of Bell Laboratories, accidentally found while doing experiments with semiconductors that silicon doped with certain impurities was very sensitive to light [9]. They invented the first practical device for converting sunlight into useful electrical power, resulting in the production of the first practical solar cell with an efficiency of around 6% [9]. Later, the researchers have shown a lot of effort to improve the silicon solar cell's performance. Commercially, silicon is the most widely used material for the fabrication of solar cells, but the high fabrication cost of silicon-based devices (due to high-temperature processing) [10], high energy payback time (EPBT) (due to large energy requirement for converting silica into silicon) [11] and difficulties in managing the electronic waste resulted from silicon devices have led to a new area of research in organic solar cells (OSCs).

1.3 Organic Photovoltaic (OPV) Devices

Silicon photovoltaic technology currently dominates the commercial production of photovoltaic cells, but whenever cost and mechanical properties come into consideration over the performance and lifetime, organic photovoltaic technology comes into the picture. The beginning of the 20^{th} century or the end of the 19^{th} century was the era of organic devices. Organic devices opened the scope of OSC and developed the interest among the researchers to work in OSC at the commercial level. The organic materials have shown synthesis-dependent several favourable properties, such as bandgap tuning, electronic and optical properties enhancement, etc. The first

photo conducting phenomenon in the organic compound was observed in anthracene and analyzed by Pochettino in 1906 [12]. The first organic photovoltaic (OPV) device was fabricated by Tang in 1986 [13] with a power conversion efficiency of 1%. Recently, organic photovoltaic technology has shown a more considerable impact in the field of photovoltaic over inorganic photovoltaic technology. The charge carrier conduction mechanism in the organic materials is not identical to the inorganic materials. Therefore, the organic materials properties are briefed in the next subsection before discussing different types of organic solar cells and their working mechanisms.

1.3.1 Materials for Organic Photovoltaic Cells

The electronics structures of organic and inorganic semiconductors are entirely different from each other. In inorganic semiconductors, atoms are bonded with the covalent bond to form a crystalline structure where electrons are spatially delocalized over the crystalline lattice. These electrons are distributed over energy states that comprise the semiconductor valence band and conduction band. These bands are continuous energy bands separated by an energy gap, known as energy bandgap (Eg). In inorganic photovoltaic, electrons of the valence band are jumped into the conduction band upon light absorption, and these excited electrons in the conduction band are driven to the electrodes utilizing an electrical field.

On the other hand, organic semiconductors are conjugated molecular or polymeric compounds whose energy band gap is defined by the difference between the highest occupied molecular orbital (HOMO) to the lowest occupied molecular orbital (LUMO). Polyaniline was the first organic semiconductor, synthesized by the anodic oxidation of aniline in 1862 [14]. Carbon and hydrogen atoms are the basic building blocks for any

organic semiconductor, and also some other heteroatoms such as nitrogen, sulphur, oxygen, etc., are used depending upon electronics application. Conjugated polymers are those where alternating C-C bonds (σ-bonds) and C=C bonds (π-bonds) exist in the polymer chain, which makes them conducting in nature and used for the optoelectronic application [15]. The valence band (VB) theory describes the covalent bond between the atoms but has limitation that it can not describe the alternating double and single bonds associated with the conjugated polymers. Therfore, molecular orbital (MO) theory was developed to describe the covalent bonds in the conjugated polymers. According to the MO theory electrons are distributed in a set of molecular orbital and can be extended over entire molecule. MO theory includes the two different combination of molecular orbital, one is bonding orbital and another is anti bonding orbital. Bonding orbitals are formed by σ-orbital and π-orbital whereas, anti bonding orbitals are formed by σ*-orbital and π*-orbital as shown in Figure 1.2. The σ-orbital is completely filled and at the lowest energy level, whereas the σ*-orbital is empty and at the highest energy level. The strong net attractive interaction among the nuclei is due to the bonding and anti-bonding in σ-orbital that holds the molecule together. However, due to the less attractive interaction of π-bonds, splitting takes place to form π- and π*-orbitals. π-orbitals are filled whereas, π*-orbitals are empty. Similar to the valence band in the inorganic semiconductor, there is the highest occupied molecular orbital (HOMO) consisting of π-orbitals. On the other hand, like conduction band in an inorganic semiconductor, there is a lowest unoccupied molecular orbital (LUMO) consisting of π*-orbitals. The comparison of the simplified energy band diagram of a conjugated polymer and inorganic semiconductor is shown in Figure 1.2.

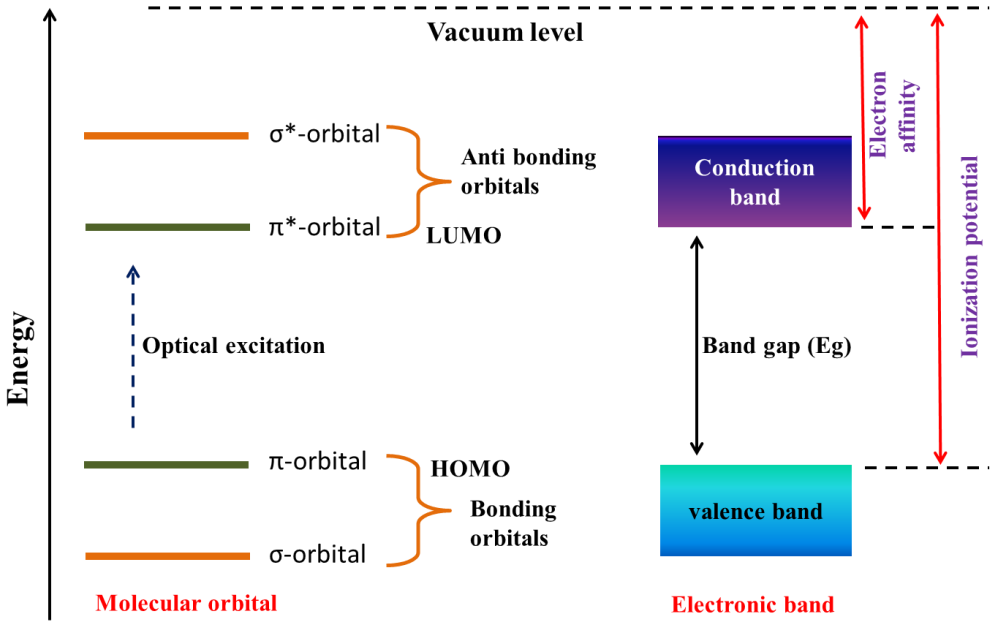

Figure 1.2: The comparative energy band diagram for conjugated polymer and conventional inorganic semiconductor.

The charge generation mechanisms in inorganic and organic photovoltaic devices are entirely different from each other due to the intrinsic electronic diversity between inorganic and organic materials that cause significant differences in the interfacial processes in inorganic and organic photovoltaic devices. The generation of free charge carriers in inorganic PV takes place directly upon light absorption under normal conditions. Whereas in the case of organic PV, the light absorption results in the production of a mobile excited state which dissociates into free charges only at the heterointerface where the tightly bonded (due to the Coulombic interaction) excitons are get dissociated by the driving force [16]. These generation phenomena affect the active material structure at the micro and nanoscopic scale, which is important for organic PV to be performed efficiently.

Another aspect of the inherently different electronic structure of inorganic and organic semiconductors is its charge transport phenomenon. In an inorganic semiconductor, typically band transport mechanism is observed where the surrounding lattice efficiently screens the delocalized charges due to the inorganic materials' high dielectric constant. Transportation of these delocalized charges takes place through the material in the continuous conduction band of the semiconductor without any energy losses, whereas, in amorphous organic semiconductors, the conductive electronic states are more localized. The dielectric constant is lower in organic semiconductors due to which charges are poorly screened by the neighboring molecules [17]. These poorly screened charges polarize and distort the surrounding lattice and form the polarons, which diffuse between adjacent molecules through a less efficient hoping mechanism, comparing to band transport, results in lower charge mobility in organic semiconductors as compare to that of inorganic semiconductors [15].

The entirely different cohesion forces in the amorphous organic solids and crystalline inorganic solids also explain these two materials' physical and mechanical properties. The inorganic semiconducting materials are rigid, highly brittle, and have very high processing temperatures, making them costly. On the other hand, organic semiconducting materials are semi-crystalline in nature, lightweight, flexible, and have very low processing temperature compared to inorganic semiconductors, which makes them cheaper materials for industrial processes [10]. The light absorption phenomenon in both semiconductors is different due to differences in their electronic structure. The absorption coefficient (α) ($\sim 10^5\ cm^{-1}$) of organic semiconductors in the visible range is higher when compared with the inorganic semiconductor ($\sim 10^3$ - $10^4\ cm^{-1}$). In general,

the bandgap of the conducting organic semiconductors lies between 1 eV- 2 eV, which is well suited for the visible spectrum to be absorbed [18].

Finally, the numbers of synthetically available inorganic semiconductors are much lower than that of their organic counterparts. Also, the electrical and optical properties of the organic semiconductors are effectively changed/tuned during the synthesis process by accurately designing the molecular structure and thus increasing the control on the performance optimization. All these advantages of organic PV over inorganic PV are well enough to develop the researchers' interest to work in the field of organic PV rather than the inorganic counterpart.

1.3.2 Type of Organic Photovoltaic Devices

Three types of structures, namely single-layer, bilayer heterojunction, and bulk heterojunction, are commonly used to fabricate organic photovoltaic cells. The brief introduction of these three types of photovoltaic devices is discussed in the following subsections.

1.3.2.1 Single-Layer OPV Device

A single photoactive film sandwiched between transparent and non-transparent electrodes with different work functions is used to fabricate a single-layer OPV device, as shown in Figure 1.3 (a). The first single-layer OPV was reported with very low quantum efficiency [19]. The low quantum efficiency was due to low charge mobility (μ) of organic semiconductor ($10^{-3}cm^2/V{\cdot}s$) in comparison with the inorganic semiconductor, i.e., single crystalline silicon ($10^{3}cm^2/V{\cdot}s$). The single-layer OPV device's power conversion efficiency was also very low (around 0.01%) due to the

lower charge mobility of organic photoactive semiconductor sandwiched between the charge extracting electrode [20].

In the single-layer OPV device, a Schottky barrier is formed between a low work function electrode and a semiconducting photoactive film (p-type semiconductor). The Schottky barrier creates a thin layer of depletion region that develops a built-in electric field. The developed built-in electric field facilitates the dissociation of generated excitons upon light absorption in such a way that generated excitons diffuse into the depletion region, and electrons are collected by the low work function electrode while holes are collected by high work function electrode, as shown in Figure 1.3 (b). The major concern with this type of structure is the low diffusion length of generated excitons. Therefore, most of the excitons are get recombined before dissociation and do not contribute to the photocurrent. Hence, the power conversion efficiency exhibited by the single-layer OPV devices is very low (0.01%) [20].

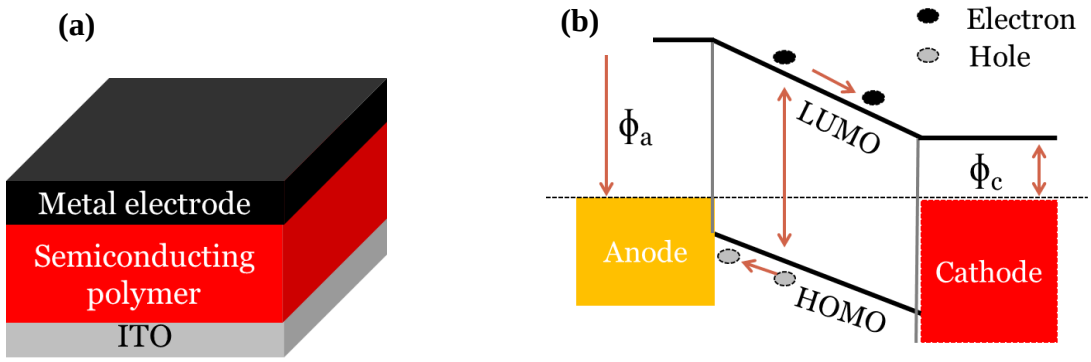

Figure 1.3: (a) Device structure and (b) Energy band diagram of single-layer OPV cell.

1.3.2.2 Bilayer Heterojunction OPV Device

To overcome the low-efficiency problem associated with the single-layer OPV device, a new device structure, i.e., donor/acceptor bilayer heterojunction, was

introduced by C. Tang in 1986 [13] with remarkable efficiency of 1%. The high-efficiency in bilayer OPV was made possible due to the pn junction formation using p-type and n-type organic semiconductor, generally called electron donor and electron acceptor material, respectively, as shown in Figure 1.4 (a). This bilayer of p-type and n-type semiconductor is worked as a photoactive layer. In particular, most of the time, the photogeneration of excitons takes place at the bilayer interface. The dissociation of the excitons occurs due to the presence of the built-in electric field at the junction (interface). The dissociation takes place in such a way that electrons are moved towards the acceptor by crossing the junction to the cathode and holes remain in the donor side and move towards the anode, as shown in Figure 1.4 (b). The probability of recombination of the electron-hole pairs is less as compared to that of single-layer OPV devices because this structure allows the excitons to cross the interface and separate in two different phases. However, the efficiency of the OPV devices is still low compared to the inorganic PV devices, mainly due to the low diffusion length of around few tens of nanometer and low interface area.

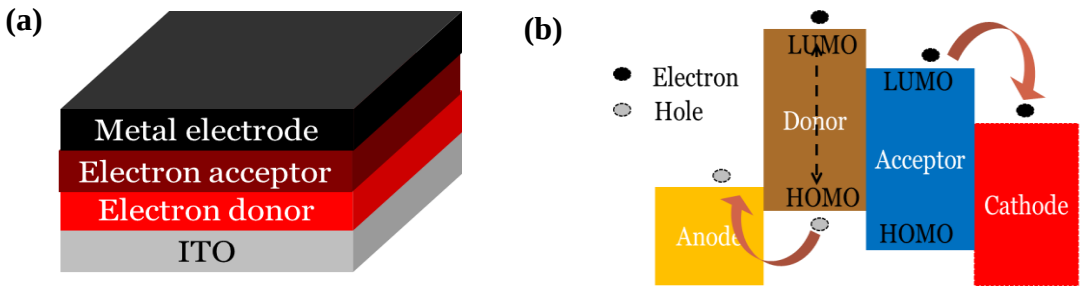

Figure 1.4: (a) Device structure and (b) Energy band diagram of bilayer heterojunction OPV device.

1.3.2.3 Bulk Heterojunction (BHJ) OPV Device

To further improve the efficiency of the OPV device new concept of bulk heterojunction was introduced where donor and acceptor semiconductors are blended to enhance the interface area so that generation of the electron-hole pair could be increased. The excitons generated near the interface can easily cross the junction to participate in the photogenerated current, rather than excitons generated far from the interface area. The BHJ OPV device and energy band diagram structures have been shown in Figure 1.5 (a) and (b), respectively. Significant improvement in efficiency has been obtained in BHJ OPV devices compared with the single-layer or bilayer OPV devices. Various p-type polymeric materials such as poly(p-phenylene-vinylene) (PPV), MEH-PPV, P3HT, PQT-12, PTB7-Th, PBDTTPD, MDMO-PPV and, PCDTBT etc., have been extensively used as a donor [21]–[26]. Whereas n-type fullerene derivatives such as C_{60}, C_{70}, $PC_{61}BM$, $PC_{71}BM$, etc., as well as some non-fullerene materials, have been used as an acceptor [27]. The higher efficiency in the BHJ OPV devices compared to bilayer OPV devices could be attributed mainly to the reduced exciton losses due to the large interfacial area and the reduced dimensions of donor and acceptor phase/ domains in which excitons are generated and diffuse to reach the donor/acceptor interface [28]. If the size or length of the donor/acceptor domain is comparable to that of the excitons diffusion length, then possibility of crossing the donor/acceptor interface by the excitons will be increased. this may lead to increase in photo-generated current and thereby increasing the efficiency of the BHJ OPV devices.

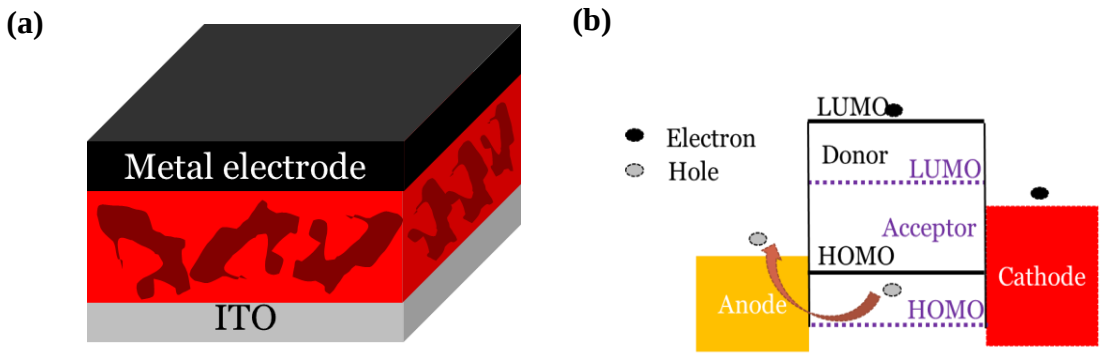

Figure 1.5: (a) Device structure and (b) Energy band diagram of bulk heterojunction (BHJ) OPV device.

The different device structures for the OPV are used for the improvement in the power conversion efficiency. Apart from the photoactive layer variation, buffer layers are also used to reduce recombination and improve OPV efficiency. The buffer layers are chosen in such a way that one type of charge carrier (i.e., electrons) can move one side, and another type of charge carrier (i.e., holes) can move another side so that no recombination can take place. These buffer layers are called the electron transport layer (ETL), and hole transport layer (HTL) as shown in Figure 1.6. ETL allows passing the electron through it and blocks the hole, whereas HTL allows the hole to pass through it and blocks the electrons. Sometimes interface layer (IL) is also used for better energy band alignment between the transport layer (ETL or HTL) and the photoactive layer. The suitable morphology of the different layers also plays a vital role in achieving high-efficiency BHJ OPV devices. Despite several difficulties in the performance improvements of BHJ OPVs, Zhu et al. [29] have recently reported a highly efficient BHJ OPV with the maximum efficiency ~ 16.88 %.

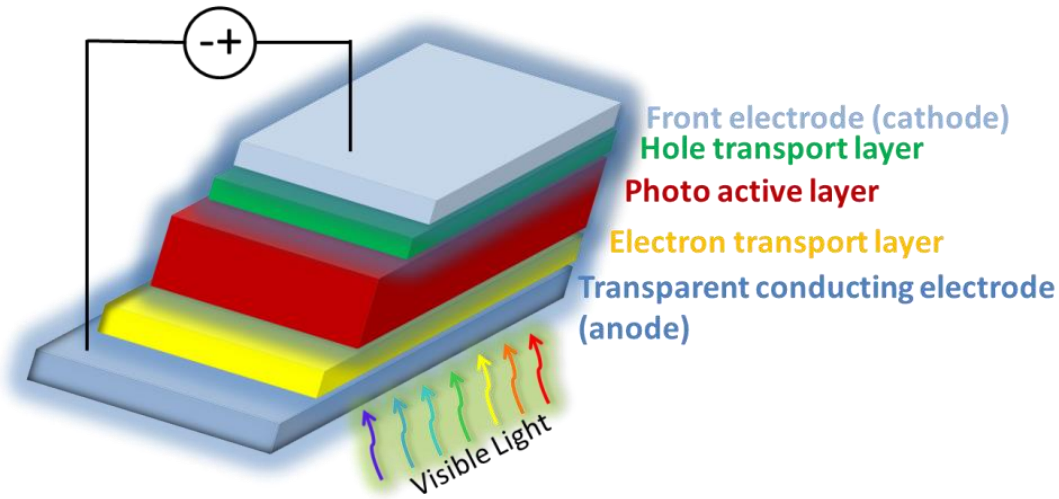

Figure 1.6: Bulk heterojunction (BHJ) OPV device with buffer layer.

1.3.3 Working Principles of BHJ OPV Device

To develop a better understanding of the performance of OPV devices, a comprehensive discussion on the working mechanism of the OPV devices is important. Therefore, for the deeper analysis, the working principle of OPV devices is discussed in this section. Figure 1.7 shows the basic working principle of OPV devices. Primarily, it consists of four basic steps that are (1) light absorption, (2) exciton diffusion, (3) Exciton dissociation, and (4) charge collection, as shown in Figure 1.7. In BHJ OPV devices, donor material absorbs most of the solar spectrum due to low bandgap (absorption coefficient of acceptor material is much lower and band gap is high). The following subsections describe the working principle of OPV devices in more detail.

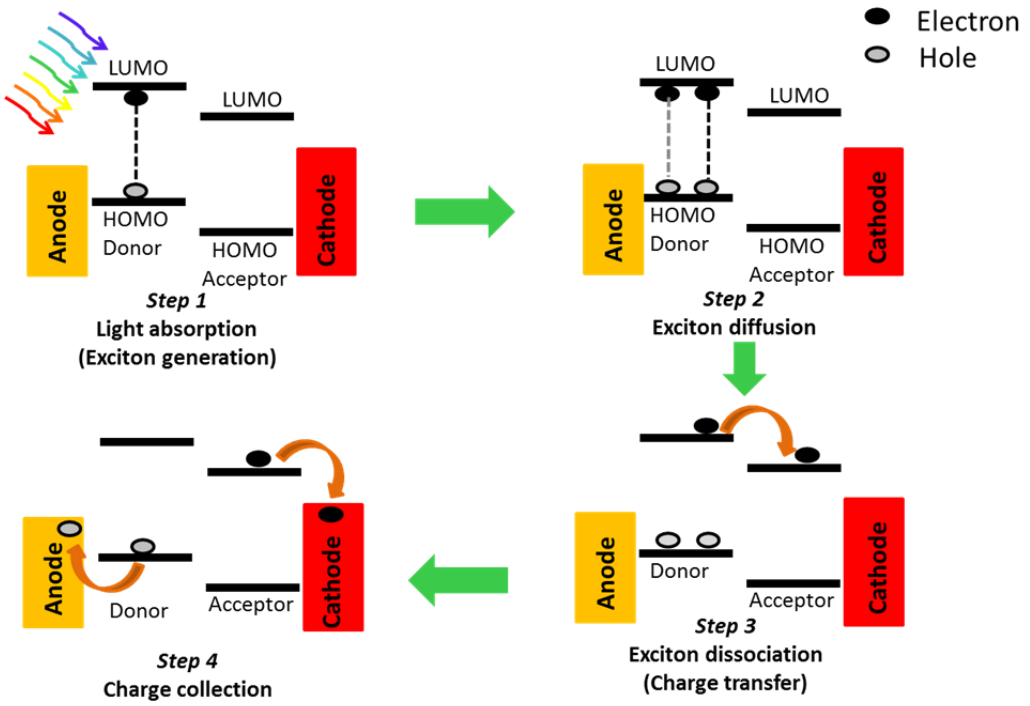

Figure 1.7: Working of BHJ OPV device: Step 1 to 4 [30].

1.3.3.1 Light Absorption

Light absorption is mainly due to the donor/acceptor blend (photoactive material), and within the donor/acceptor phase, absorption occurs mostly in the donor material. Penetration of the incident photons into the photoactive layer is taken place after illumination of the light on the device. The amount of light to be absorbed by the absorbing material depends primarily on the absorption coefficient of the donor and acceptor material. This absorption coefficient mainly depends on their molar extinction coefficient (i.e., the intrinsic capacity of light absorption by a single molecule), density, and absorption cross-section area. Moreover, light absorption also depends upon the bandgap (Eg) of semiconductors, defined by the difference between HOMO and LUMO. Only photons with energy > Eg could be absorbed. Therefore, the accurate tuning of the electronic structure of semiconductor molecular is required to maximize

light absorption. Another factor influencing light absorption is film thickness. As the absorption coefficient of organic semiconductor is much higher than that of the inorganic counterpart (Si), the thickness of organic semiconductor less than 100 nm is enough for 60% to 90% absorption of the incident light when reflective back contact is used [31].

Furthermore, the light pathway length inside the photoactive film also influences light absorption. The reflection, refraction, and scattering affect mostly this pathway length at the device layers interfaces and the device/air interface. Light absorption is also influenced by the format of the solar spectrum, which depend upon atmospheric condition. The emission of photons is distributed over the wavelength range of 2500 nm, and it is equivalent to the emission of a black body at 5960 K for the extra-terrestrial solar spectrum (AM0), as shown in Figure 1.8. However, this solar spectrum is filtered by the atmosphere when reached at the earth's surface, as shown in Figure 1.8. But the spectrum pattern remains the same, and it is called terrestrial solar spectrum (AM1.5), a standard for the calculation of PV parameters.

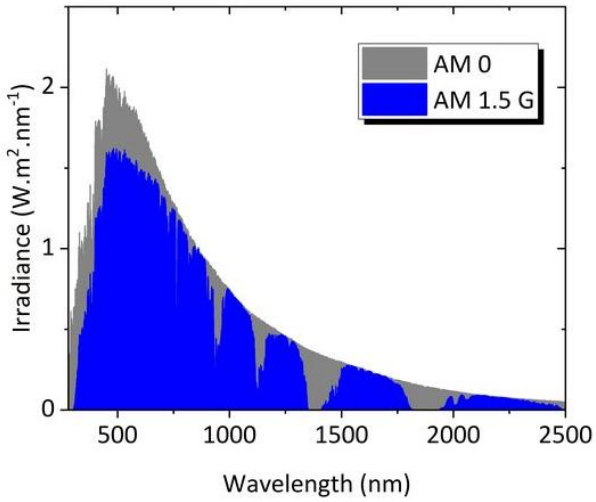

Figure 1.8: Extraterrestrial solar spectrum (AM0, gray) and terrestrial solar spectrum (AM1.5, blue) [32].

1.3.3.2 Exciton Diffusion

Once the solar light is absorbed in the donor material, the electrons are transferred from the ground state to one of the excited states of the semiconductor and results in a generation of excitons. The separation of these generated excitons can take place only when diffusion is allowed to the donor/acceptor interface. Diffusion is continued deeper till the recombination does not take place. The domain size of the donor material in the BHJ OPV device must be kept comparable to the exciton diffusion length so that the exciton recombination mechanism could not dominant and effective diffusion can take place. Typically, the exciton diffusion length of the donor phase in the BHJ OPV device ranging from 5 nm to more than 100 nm depending upon the donor material used [33].

1.3.3.3 Exciton Dissociation

After surviving the recombination process, the remaining excitons are diffused into the donor or acceptor phase and finally reached the donor/acceptor interface. Commonly, excitons dissociation has been described as a two-step process. In the first instance, at the donor/acceptor interface, the exciton state evolves into a charge transfer (CT) state between the donor (+ve) and acceptor (-ve). Then either recombine to the ground state or dissociates into free carriers via several charge-separated (CS) states (states where the electron and hole are weakly bounded with the Coulombic attraction force or freed from one another) [34]**.** The energy of the final CS state corresponds to the energy associated with the completely unbound electron-hole pair and related to the ionization potential of the donor (IP_D) and electron affinity of the acceptor (EA_A) (i.e $E_{final} = IP_D + EA_A$). The favorable condition for the excitons to be dissociated is when the difference between ionization potential of the donor (IP_D) and electron affinity of the

acceptor (EA_A) is greater than that of binding energy (E_B) of the excitons. The condition is as follow:

$$IP_D - EA_A > E_B \quad (1.1)$$

The rate of the charge transfer at the donor/acceptor interface is very efficient and fast, typically in the range of < 100 fs. Once the excitons are dissociated, the holes stay in the donor molecule itself, whereas electrons are moved towards the acceptor molecules. In this way, the charge carriers are spatially separated and reside in two different molecules that results in low recombination rates.

1.3.3.4 Charge Collection

The possible conditions for charge collection at their respective positive and negative electrodes are when the work function of the cathode is lower than the LUMO level of the acceptor material, and the work function of the anode is higher than the HOMO level of the donor material. Depending upon the difference between the work function of the electrodes and LUMO of the acceptor and HOMO of the donor, two types of contacts are formed, i.e., ohmic contact and non-ohmic contact. Non-ohmic contact causes electrical losses for the device, whereas ohmic contact facilitates better charge collection at their respective electrode, and higher efficiency could be expected. The most common electrodes used in the organic solar cell are silver (Ag), gold (Au), and aluminium (Al) as a non-transparent electrode and indium-doped tin oxide (ITO) and fluorine-doped tin oxide (FTO) as a transparent electrode [35]. ITO is a highly conducting semiconductor made up of SnO_2 (10%) and In_2O_3 (90%), and highly transparent for the visible light due to its high bandgap of approximately 3.7 eV and its high conductive is because of oxygen vacancies [36].

Charge extraction does not depend only on band alignment but also on various physical and chemical characteristics of the interface of electrode and semiconducting materials such as wave function hybridization, dipole formation, chemical reactions, and physical intermixing, etc. [37]. All these factors affect the mechanisms and efficiency of the charge extraction process at the interface of electrodes and semiconducting materials. For example, a thin oxide layer formed at the interface causes a potential barrier for charge extraction. On the other hand, while depositing the metal by using the evaporation method, the thermal energy of the metal causes hot metal atoms and clusters to diffuse into the semiconducting layer that creates non-geminate charge recombination sites and also results in damaging of the semiconducting layer due to high metal condensation energies. A buffer layer (ETL, HTL, IL) is used between the active and electrode layers to overcome these problems [38]. Commonly used HTLs are PEDOT:PSS (polymer) and some metal oxides such as vanadium oxide (V_2O_5), molybdenum oxide (MoO_3). On the other hand, primarily used ETLs are metal oxide of TiO_2 and ZnO.

1.3.4 Equivalent Circuit of BHJ OPV Devices

The structure and operation of BHJ OPV devices are similar to heterojunction diode; hence it is represented by the equivalent circuit using a simple diode connecting with a load resistance R_L when no light falls on it, as shown in Figure 1.9 (a). Upon the light illumination on the BHJ OPV device, a potential difference is developed when the terminals are open, and this developed voltage is called open-circuit voltage (Voc). On the other hand, a short circuit current (Isc) is drawn when terminals are connected. For any intermediate resistance R_L, a solar cell develops a voltage in the range of 0 to Voc and delivers a current I, such a way that $V = I*R_L$. The load resistance R_L connected to

the BHJ OPV device develops a potential difference between terminals even under dark condition. This potential difference is responsible for the diode current in the direction opposite to the photocurrent. The diode current is termed as dark current I_{dark}. Since most of the BHJ OPV device under dark condition behaves like a simple diode, the dark current is equal to diode current. It varies according to the diode behaviour shown by equation 1.2, known as Shockley's equation.

$$I_d = I_{so}\left[e^{\frac{V}{nV_T}} - 1\right] \tag{1.2}$$

Where, I_{so} is reverse saturation current, n is ideality factor of the diode, V_T thermal equivalent voltage and V is the voltage across the diode.

When light is illuminated on the solar cell, a photogenerated current I_{ph} occurs, and the total current will be denoted by equation 1.3.

$$I = I_{ph} - I_d \tag{1.3}$$

$$I = I_{ph} - I_{so}\left[e^{\frac{V}{nV_T}} - 1\right] \tag{1.4}$$

Some resistive elements, known as series resistance (Rs) and shunt resistance (Rsh), are also associated with practical OPV devices due to which the equivalent circuit of the solar cell gets modified, which includes Rs and Rsh [39], as shown in Figure 1.9 (b). Accordingly, equation 1.4 is modified to equation 1.5. For better performance of any solar cell, the value of series resistance must be as low as possible and Rsh must be as high as possible.

$$I = I_{ph} - I_{so}\left[e^{\left\{\frac{V-IRs}{nV_T}\right\}} - 1\right] - \frac{V-IRs}{Rsh} \tag{1.5}$$

Where, I_{ph} is photocurrent.

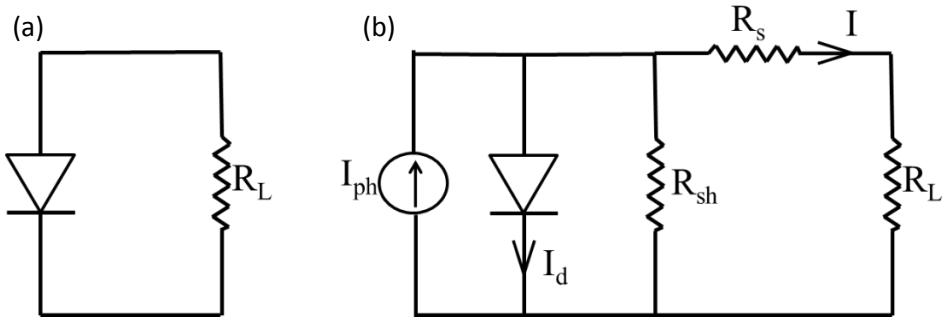

Figure 1.9: Equivalent circuit of OPV device under (a) Dark and (b) Solar light.

1.3.5 Parameters of BHJ OPV Devices

The BHJ OPV devices work as a simple diode under dark, and the current flowing through it follows the diode curve shown by the blue curve in Figure 1.10. When light falls on the BHJ OPV device, the current-voltage (I-V) curve follows the superposition of dark (I-V) and generated current upon illumination of light and gets sifted to the fourth coordinate, as shown in Figure 1.10 (red curve). All the important parameters of BHJ OPV devices, namely power conversion efficiency (η), short circuit current (Isc), open-circuit voltage (Voc), and fill factor (FF) are calculated directly from the solar cell current-voltage (I-V) characteristics, as shown in Figure 1.10. The parameters are briefly described in the following subsections.

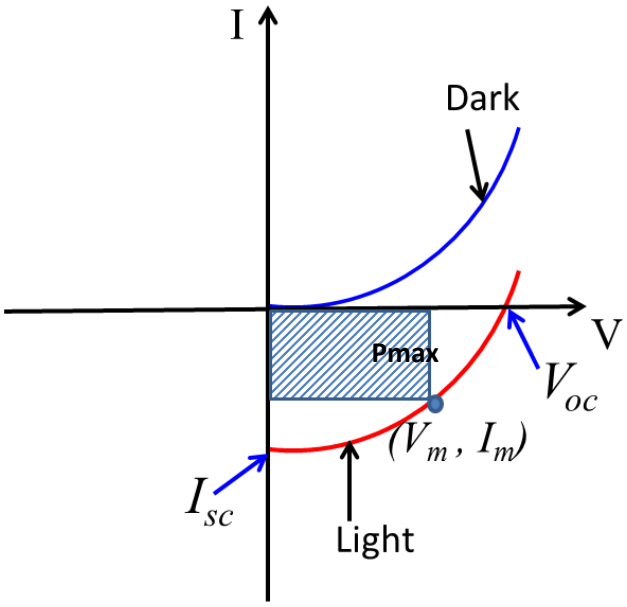

Figure 1.10: Current-voltage (I-V) characteristics of BHJ OPV.

1.3.5.1 Short Circuit Current (Isc)

A short circuit current is a current flowing through the cell when the voltage across the cell is zero (V=0), as shown in Figure 1.10**.** It is the maximum current that any BHJ OPV device can draw and deliver to the load against light illumination. The generation of short circuit current takes place due to the excitons generation and collection by the respective electrode. It can also be described as the total number of charge carriers generated and finally collected by their respective electrodes when there is no applied voltage. For any ideal BHJ OPV devices, the value of short circuit current (Isc) and photocurrent (Iph) must be equal. In general, the value of short circuit current depends on device area, and therefore most of the time, it is used as short circuit current density (Jsc in mA/cm^2) for the efficiency calculation purpose. Following are the factors upon which short circuit current depends on:

1. Directly proportional to the intensity of light falling on the device.
2. Electrical and optical properties of the photo absorber material.

3. Device area upon which light strikes and the overall spectrum of the incident light.
4. It also depends on the interface between the active layer and buffer layer through which the generated carriers have to be crossed.
5. Minority carrier lifetime. So that generated carriers can be collected by the electrode to convert in the current before recombination.

1.3.5.2 Open Circuit Voltage (Voc)

Open circuit voltage is one of the most important parameters to define the BHJ OPV devices' efficiency. It is the maximum voltage developed by the BHJ OPV device upon illumination of light when there is no external load connected, i.e., when the current flowing between the terminals is zero, as shown in Figure 1.10. Generally, the maximum limit of Voc depends on the energy offset between the HOMO of the donor material and LUMO of the acceptor material, as shown in Figure 1.11. Various factors that influenced the open-circuit voltage are shown in Figure 1.12. The most commonly used formula for calculating the open-circuit voltage (Voc) of the BHJ OPV device is described by equation 1.6 [40]. Where "e" is the electronic charge.

$$Voc = \frac{1}{e}[E_{LUMO}Acceptor - E_{HOMO}Donor] - 0.3 \quad (1.6)$$

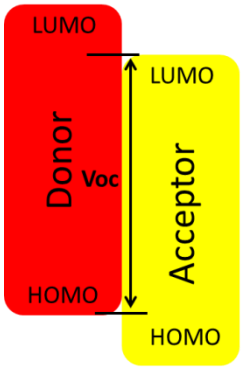

Figure 1.11: Maximum limit for open-circuit voltage in OPV.

Figure 1.12: Factors influencing the open-circuit voltage in OPV [40].

1.3.5.3 Fill Factor (FF)

The fill factor of any BHJ OPV device primarily gives an idea about the shape of the current-voltage (I-V) characteristic under light illumination condition. In other words, the fill factor defines the ideality of the BHJ OPV device. The maximum value of the fill factor could not be greater than one. It is defined as the ratio of the product of maximum voltage (Vm) and maximum current (Im) to the product of Voc and Isc. It is calculated by the formula described in equation 1.7. Graphically, it defined the

squareness of the current-voltage (I-V) characteristic of the BHJ OPV device and represented by the area under the shaded region, which also shows the region where the device delivers the maximum power to the load, as shown in Figure 1.10. The most important parameters that affect the fill factor are series resistance (Rs) and shunt resistance (Rsh) [41].

$$FF = \frac{V_m * I_m}{V_{oc} * I_{sc}} = \frac{P_{max}}{V_{oc} * I_{sc}} \quad (1.7)$$

1.3.5.4 Power Conversion Efficiency (PCE)(η)

Power conversion efficiency is the most discussed performance parameter of the BHJ OPV devices. This parameter shows the amount of light converted into electricity and is denoted by the ratio of output power to the input power, as shown by equation 1.8.

$$(PCE) = \frac{P_{out}}{P_{in}} = \frac{FF * V_{oc} * I_{sc}}{P_{in}} \quad (1.8)$$

Where Pin is input incident power falling on cell. The intensity of the sunlight changes depending upon the geographical location, so one standard is commonly maintained for the intensity of sunlight while calculating the power conversion efficiency of the solar cell. The standard test conditions are 25 C^o temperature, AM 1.5 spectral shape as standard air mass index, and 1000 W/m^2 intensity of light [42] for the calculation of power conversion efficiency. The most important factor that affects the power conversion efficiency is the fill factor. Suppose two cells have the same Voc and Isc but different fill factors, as shown in Figure 1.13. Despite having the same Voc and Isc the power conversion efficiency of cell 2 is higher than that of cell 1 due to a higher fill factor for cell 2 compared to cell 1.

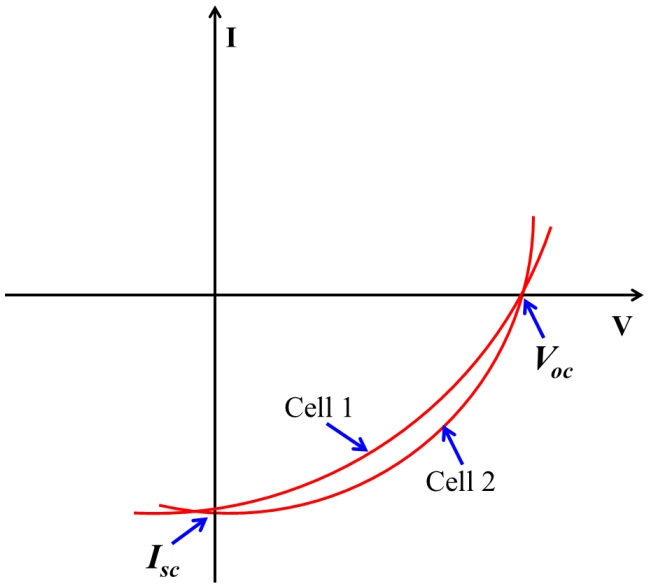

Figure 1.13: Comparison of power conversion efficiency of cell 1 and cell 2.

1.4 Literature Review

The present thesis primarily focuses on the effect of various layers on the performance parameters of the bulk heterojunction (BHJ) organic solar cell (OSC). To accomplish the motive of this thesis, we had already discussed the literature on inorganic-based photovoltaic devices to investigate the gap between inorganic and organic photovoltaics. Now, we have reviewed the literature based on organic photovoltaic to discuss the various aspects of the OPV device's performance depending on various layers associated with the BHJ OPV.

1.4.1 Review of BHJ OSCs

The organic solar cell using a single layer of small-molecule organic semiconductor deposited by the vacuum evaporation method was first reported by Calvin in 1958 [43]. Reucroft and Simpson investigated the photovoltaic effect in the monolayer of chlorophyll [44]. Merritt and Hovel fabricated an organic solar cell using a single-layer of hydroxy squarylium as an organic semiconducting dye in 1976 and achieved a power

conversion efficiency of only 0.2% [45]. Ghosh and Feng reported an organic solar cell based on Merocyanine-type photosensitizing dyes and achieved an efficiency of 0.7% in 1978 [46]. Later, a breakthrough occurred when Tang [13] gave the donor/acceptor bilayer-based organic polymer solar cell concept in 1986. He used the bilayer of copper phthalocyanine and perylene tetracarboxylic derivative for photoabsorption and reported the power conversion efficiency of 1%.

The small molecule blended junction was first reported by Hiramoto *et al.* in 1991 [47], [48]. They investigated the composite materials in the three-layer structure and achieved a maximum efficiency of 0.7%. MEH-PPV as a donor polymer and C_{60} as an acceptor polymer were used Sariciftci *et al.* and fabricated the bi-layer heterojunction photodiode as well as solar cell [49]. Whitlock *et al.* have investigated various materials and device structures for the organic solar cell [50]. In 1995, Yu, *et al.* [51] have given the concept of bulk heterojunction by using MEH-PPV donor and C_{60} acceptor and got the efficiency two times higher than that of the simple bilayer structure. Yang and Heeger have investigated the morphology of semiconducting polymer composites mixed with C_{60} used in the organic solar cell [52]. Chen *et al.* [53] have fabricated OPV using the multilayer of donor polymer MDMO-PPV and $PC_{61}BM$ as an acceptor polymer. They have also compared the performance of BHJ OPV to the single layer of MDMO-PPV. The relation between efficiency and morphology of donor-acceptor phase in BHJ OSC was investigated by Padinger *et al.* [54]. Fromherz *et al.* [55] have done a comparative study on the organic photovoltaic devices containing various blends of polymer and fullerene derivatives.

Chirvase *et al.* [21] have fabricated the OSC based on the P3HT donor and $PC_{61}BM$ acceptor and investigated the electrical and optical properties. Riedel and Dyakonov

have explored the charge transport in the P3HT:$PC_{61}BM$ based BHJ OSC [56]. Yuen *et al.* [57] have reported the comparative study of BHJ OSC based on PQT-12:$PC_{61}BM$ and P3HT: $PC_{61}BM$, and they found better stability in the case of OPV device fabricated with PQT-12: $PC_{61}BM$, but the power conversion efficiency was only ~0.45% rather than ~2.5% in case of device P3HT: $PC_{61}BM$. This report shows that PQT-12 could also be used as HTL or interface layer with another donor polymer to improve the stability as well as the efficiency of the BHJ OSC. From starting era to the current scenario of the OSC, several organic polymers have been explored to be utilized in the OSC [19], [21]–[23], [49], [58]–[60][24]. Beaupre and Leclerc have studied the performance of P3HT as well as PCDTBT based BHJ OSC separately and found that PCDTBT based BHJ OSC performed well [61]. Zhang *et al.* have performed the stability analysis of PCDTBT:$PC_{71}BM$ based BHJ OSC [26].

Apart from the organic semiconducting materials used as a photoactive layer, other layers such as transport layers (ETL and HTL) [62] [63] and interface [64] layer also play an important role in improving the performance parameters of the BHJ OSC. Metal oxides are extensively used material for the transport layer in BHJ OSC due to their better transparency in the visible region and good ohmic contact with the donor and acceptor polymers [65]–[69]. On the other hand, PEDOT:PSS is the most widely used organic polymer used as HTL in BHJ OSC [63], [70]. One of the earliest works on the solution-processed ZnO ETL layer in P3HT: $PC_{61}BM$ based OSC was carried out by White *et al.* in 2006 [71]. They achieved the certified power conversion efficiency of 2.58% by inserting solution-processed ZnO between ITO and active layer P3HT: $PC_{61}BM$. Hori *et al.* [72] have fabricated the C60/poly(3-hexylthiophene)(PAT6) based OSC where they used ZnO and MoO_3 as ETL and HTL layer, respectively.

Comparatively, they improved efficiency from 0.49% to 1.46% when ZnO and MoO_3 transport layers were inserted as ETL and HTL layers, respectively. Kundu *et al.* [73] have fabricated and characterized two different devices with structure, i.e., ITO/ZnO/P3HT: $PC_{61}BM$ /MoO_3/Ag and ITO/MoO_3 /P3HT: $PC_{61}BM$ /ZnO/Ag where solution-processed ZnO has been used as an ETL and thermally evaporated MoO_3 as an HTL layer. They found the efficiency enhancement from 2.86% to 3.48% when ITO/ZnO/P3HT: $PC_{61}BM$ /MoO_3/Ag device structure is used rather than ITO/MoO_3 /P3HT: $PC_{61}BM$ /ZnO/Ag device structure.

1.4.2 Review of PCDTBT: PCBM based BHJ OSCs

Semiconducting polymer have shown the great interest in the field of BHJ OSC in the recent year [22], [23], [58], [59], [74], [75]. Among various semiconducting polymer, poly[N-9′-hep- tadecanyl-2,7-carbazole-alt-5,5-(4′,7′-di-2-thienyl-2′,1′,3′-benzothiadiazole)] (PCDTBT) has shown great impact in BHJ OSC due to its superior properties over other semiconducting polymer [58], [61], [76]–[79]. Blouin *et al.* [58] have reported the highly conjugated and stable poly(N-alkyl-2,7-carbazole) derivative, namely poly[N-9′-hep- tadecanyl-2,7-carbazole-alt-5,5-(4′,7′-di-2-thienyl-2′,1′,3′-benzothiadiazole)] (PCDTBT) for the BHJ OSC. They have achieved a maximum efficiency of 3.6% in the PCDTBT: $PC_{61}BM$ based organic solar cell. They have also studied stability improvement using PCDTBT instead of mostly used donor polymer P3HT. Chu *et al.* [80] have reported the PCDTBT:$PC_{61}BM$ based BHJ OSC and examined the effect of PCDTBT:$PC_{61}BM$ thickness to improve the light absorption and hence increase the performance of the device.

Investigation on the effect of solvent on the morphology, charge transportation, and performance of PCDTBT:$PC_{70}BM$ based BHJ OSC have been carried out by Alem *et al.* [76]. Etzold *et al.* [79] have studied the charge dissociation and recombination phenomenon in PCDTBT:$PC_{61}BM$ based BHJ OSC. Effect of the nanostructured morphology of the PCDTBT:$PC_{70}BM$ film in the BHJ OSC has been reported by Sun Moon et al. [78]. Ratcliff *et al.* [81] have discussed the influence of energy level alignment between the buffer layer and the PCDTBT:$PC_{70}BM$ active layer in the BHJ OSC. Parlak *et al.* [58] have synthesized the Ag nanoparticle and utilized the same in PCDTBT:$PC_{61}BM$ based BHJ OSC for the comparative study of the performance of the two distinct devices fabricated with and without Ag nanoparticle.

Researchers have introduced several approaches to improve the performance of PCDTBT:$PC_{61}BM$ based BHJ OSC in the recent year [61], [77], [84]–[88]. Further, one of the most critical investigation of the stability of the PCDTBT:$PC_{71}BM$ based BHJ OSC has been carried out by Zhang *et al.* [26] recently in 2016. They have fabricated and characterized the PCDTBT:$PC_{71}BM$ based BHJ OSC and reported the outdoor stability analysis of one year. Tuning of PCDTBT:$PC_{71}BM$ and nanoparticles blend have been performed by D'Olieslaeger *et al.* [89] for the eco-friendly solution processing of polymer solar cell. Pratyusha *et al.* [90] have fabricated PCDTBT:$PC_{70}BM$ based BHJ OSC incorporating the ternary polymer made of PCDTBT, $PC_{70}BM$, and PCPDTBT to enhance the absorption range and reported the improved performance of the device.

Furthermore, the analysis of traps' effect due to the disorder assembly of the donor-acceptor phase on the charge transport between donor and acceptor polymer in PCDTBT:$PC_{70}BM$ based BHJ OSC has been reported by Khan *et al.* [91]. Aghassi and

Fay have reported the effect of the isopropyl alcohol (IPA) treatment on the performance of the PCDTBT:$PC_{70}BM$ and (p-DTS($FBTTh_2$)$_2$: $PC_{70}BM$ based BHJ OSC [92]. Recently in 2020, Piralaee *et al.* [83] have analysed the effect of random dispersion of Ag nanoparticles in the P3HT:$PC_{61}BM$ and PCDTBT:$PC_{61}BM$ photoactive blends. They found the enhancement in the photocurrent and thus the improved performance of the BHJ OSC.

1.4.3 Major Observation from the Literature Review

In this section, we will summarise the major observations derived from the literature survey, as given in the following:

- The donor/acceptor polymer-based bulk heterojunction type organic solar cells [47], [48] have shown great interest in the field of OPV due to its several advantages such as low cost and easy fabrication processing technique, flexibility, and the possibility of enhancement in the power conversion efficiency by utilizing the various approaches [83], [91], [92].
- Among various donor polymers, the polymer poly[N-9′-hep- tadecanyl-2,7-carbazole-alt-5,5-(4′,7′-di-2-thienyl-2′,1′,3′-ben- zothiadiazole)] (PCDTBT) [58], [61], [76]–[79] has been reported as a better candidate to replace the most widely used donor polymer poly(3-hexylthiophene) (P3HT) due to its higher stability and performance when blended with the fullerene derivative $PC_{61}BM$ (electron acceptor) in BHJ OSC [80].
- Among the various metal oxides, used as a transport layer in the BHJ OSC, ZnO and MoO_3 is the most promising candidate for the ETL and HTL, respectively due to its high transparency in the visible region [65]. Whereas

PEDOT:PSS [63] is extensively used as organic HTL in BHJ OSC due to its high transparency and easy solution processability.

- PQT-12 is used as a donor polymer and shows higher stability than extensively used donor polymer P3HT [57]. Although PQT-12 offers lower power conversion efficiency than P3HT, it may also be used as HTL as well as interface layer in the BHJ OSC due to its higher stability and higher mobility than P3HT [24].
- It has been observed from the literature that inverted structure (transparent electrode/ETL/active layer/HTL/metallic electrode) of the BHJ OSC is more stable than the conventional structure (transparent electrode/HTL/active layer/ETL/metallic electrode) of the BHJ OSC [73].

1.5 Challenges in the BHJ OSC

It has been discussed that the BHJ OSCs, where organic polymers are used as photo absorbing material, are gaining more popularity due to their various advantages, namely low cost, easy fabrication process, the possibility of flexible, roll to roll fabrication (large area fabrication) process, and non-toxicity (due to organic material). However, BHJ OSCs are facing several challenges in achieving high efficiency as well as stability. Further, due to the use of several layers, they also face the challenge of achieving a better interface between the different layers, leading to lower charge transportation and lower performance. Many approaches have been employed to improve the performance of BHJ OSC, such as using an interface layer between the transport layers and active layer (PCDTBT:$PC_{61}BM$), optimizing the thicknesses of various layers, and incorporation third material in the active layer to improve the charge transportation.

1.6 Motivation and Problem Definition

In the previous section, we have already discussed the challenges related to the BHJ OSC, which includes the stability issue, lower efficiency, and low charge transportation due to the degradation issue of active layer material as well as the inappropriate interface between the various layers. Because of the relatively high performance of the PCDTBT donor polymer over the extensively used donor polymer P3HT in BHJ OSC, the PCDTBT polymer is believed to have a vast opportunity to improve the performance of the BHJ OSC when used with the different buffer layers. In the continuation of the above discussion, a highly stable PCDTBT donor polymer and $PC_{61}BM$ acceptor polymer are used for fabricating the BHJ OSC and characterize the performance parameters when used with the various buffer configuration layers. In addition, PQT-12 is used as HTL as well as interface layer deposited by floating film transfer method (FTM) to achieve better phase matching. Further, CdSe QDs are also used with the active layer (PCDTBT:$PC_{61}BM$) to enhance the BHJ OSC performance.

1.7 Scope of the Thesis

The present thesis deals with the fabrication and characterization of PCDTBT:$PC_{61}BM$ based BHJ OSC. The thesis consists of FIVE chapters, including the present chapter. The contents of the remaining FOUR chapters are briefly described in the following sentences:

Chapter-2 deals with the fabrication and characterization of PCDTBT:$PC_{61}BM$ based BHJ OSC, where FTM deposited PQT-12 polymer is used as interface layer in between active layer (PCDTBT:$PC_{61}BM$) and hole transport layer (PEDOT:PSS). The entire device is fabricated on the ITO-coated glass substrate. Here, PQT-12 provides

better band alignment and phase matching for the efficient charge extraction at their respective electrodes. The effect of PQT-12 interface layer on the device has been primarily carried out by electrical and optical characterization. The incorporation of the PQT-12 interface layer in PCDTBT:$PC_{61}BM$ based BHJ OSC improves performance and stability.

Chapter-3 includes the fabrication and characterization of PCDTBT:$PC_{61}BM$ based BHJ OSC device in ITO/ZnO QDs/ PCDTBT:$PC_{61}BM$/PQT-12/Ag structure, where ZnO QDs, PCDTBT:$PC_{61}BM$, and PQT-12 are used as ETL, active, and HTL layer, respectively. Several devices have been fabricated with different thicknesses of ZnO QDs and PQT-12 to optimize thicknesses of the individual layers for achieving the high-performance OPV device. Electrical and optical characterizations have been carried out to compare different fabricated devices. Among the various set of fabricated devices, it has been found that the BHJ OSC device with the thickness of 35 nm, 100 nm, and 20 nm for ZnO QDs, active and PQT-12 layer, respectively, provide the best performance.

Chapter-4 investigates the fabrication and characterization of PCDTBT:$PC_{61}BM$ based binary and ternary BHJ OSC. CdSe QDs are mixed with the PCDTBT:$PC_{61}BM$, and the complete device is fabricated on the ITO coated glass substrate in ITO/ZnO QDs/ PCDTBT:$PC_{61}BM$:CdSe QDs/MoO_3/Ag structure. All the layers are deposited by spin coating technique except MoO_3 and Ag, which are deposited by the thermal evaporation method. The comparative studies have been carried out for two different BHJ OSC devices fabricated without CdSe QDs and with CdSe QDs. CdSe QDs incorporated ternary BHJ OSC device has shown the superior solar cell performance compared to without CdSe QDs based binary BHJ OSC.

Finally, **Chapter-5** summarizes the major objectives and concludes the important findings of the present thesis. This chapter also outlines some future scope of works related to this thesis.

CHAPTER 2

Effect of PQT-12 Interface Layer on the Performance of PCDTBT:$PC_{61}BM$ Bulk Heterojunction Organic Solar Cells

Contents

*Part of this work has been published as:

Amit Kumar et al., "Effect of PQT-12 interface layer on the performance of PCDTBT:PCBM bulk heterojunction solar cells," *Material Research Express*, vol. 6, no. 11, 115514, 2019.

CHAPTER 2

Effect of PQT-12 Interface Layer on the Performance of PCDTBT:$PC_{61}BM$ Bulk Heterojunction Organic Solar Cells

2.1 Introduction

Importance of the solar cell in context of green energy harvesting has already been discussed in detail in Chapter-1. Organic solar cells (OSCs) have drawn considerable attention from researchers in the last few years due to their lightweight, environment-friendly nature, fabrication possibility on flexible substrates, high throughput, and potentiality of cost-effective, fast roll-to-roll (R2R) production [93], [94]. Among the various organic solar cell (OSC) structures, bulk heterojunction (BHJ) OSC is a promising solar cell technology having the general structure of (ITO or FTO coated glass substrate)/ETL/Active layer/HTL/Metallic electrode shows the better capability for superior performance. It has opened up several design aspects such as controlling the photoactive layer's morphology, interface layer insertion, and feasibility of multilayer deposition through the solution process, etc. [26], [93], [95]–[100].

In the recent few years, among various donor-acceptor polymers, poly[N-9′-hep-tadecanyl-2,7-carbazole-alt-5,5-(4′,7′-di-2-thienyl-2′,1′,3′-benzothiadiazole)] (PCDTBT): Phenyl-C_{61}-butyric acid methyl ester ($PC_{61}BM$) [58], [61], [76]–[79] has shown considerable interest as the active material in the BHJ OSCs. The large bandgap metal oxides (e.g. ZnO, TiO_2 etc.) are widely used for the electron trnasport layer (ETL) [65]. Among them, ZnO is the most commonly used metal oxide for the electron transport layer (ETL) [71], [72] in OSCs.

Because, ZnO has a large bandgap energy which is suitable for complete absorption of the UV light. Further, it has a good level allignment property with the $PC_{61}BM$ which allows only the transporation of electrons while blocking the transportation of holes. Moreover, ZnO can be easily synthesized by low-cost solution process which enables to fabricate low-cost BHJ OPVs. The non-toxic environ-friendly nature of the ZnO also makes it a favorable for electronic and optoelectronic applications. In general, various nanostructures of the ZnO are used for the ETL [65], [71], [72]. However, colloidal ZnO quantum dots (QDs) based ETL layer has not been explored in the BHJ OPVs. It is interesting to note that the energy bandgap of the ZnO QDs can be tuned by tuning the sizes of the QDs [101]. Therefore, we have explored the colloidal ZnO QDs for the ETL in the BHJ OPV considered in this chapter.

PEDOT: PSS is extensively used for the hole transport layer (HTL) [102] [103], [104]. However, direct deposition of PEDOT:PSS on the active layer may degrade the quality of the underneath active material and hence the performance of the BHJ OSCs [100], [104]. The poly (3, 3’’’- dialkylquaterthiophene) (PQT-12) may be used as an interfacial layer in between the HTL and active layer due to its good phase matching and energy band alignment with the active layer to achieve improved charge transport in the device [105]–[108]. The floating-film transfer method (FTM), originally proposed by Morita et al. [109] and later optimized by others [110]–[113], is a relatively new cost-effective thin film deposition technique for obtaining thin PQT-12 films [114] in organic devices.

The present chapter investigates the effect of FTM based PQT-12 film on the performance of ZnO quantum dots (QDs)/PCDTBT:$PC_{\mathbf{61}}BM$/PQT-12/ PEDOT:PSS based

OSCs where the layer of ZnO QDs acts as the ETL, PCDTBT:$PC_{61}BM$/ acts as the active layer, PQT-12 film acts as an interfacial layer (IL) and PEDOT: PSS layer acts the HTL in the device. The ZnO QDs are synthesized by the low cost-cost solution method. The performance parameters of the BHJ OSCs with and without the PQT-12 IL have been compared. The outline of the rest of this chapter is as follows:

Section 2.2 exhibits the experimental details of the fabrication of PCDTBT:$PC_{61}BM$ BHJ OSC. The results and discussion related to the electrical and optical characterizations of the fabricated device have been included in Section 2.3. Finally, Section 2.4 concludes the objectives and outcomes of the research carried out in this chapter.

2.2 Experimental Details

2.2.1 Materials and Synthesis

The polymer PCDTBT was purchased from Sigma-Aldrich (India), $PC_{61}BM$ and PEDOT:PSS were purchased from Ossila (United Kingdom), and PQT-12 was purchased from American Dye Source (Canada). All the other chemicals were purchased from Merck Chemicals (India). The colloidal ZnO QDs were synthesized from zinc acetate dehydrate as a precursor illustrated in Figure 2.1. It was dissolved in 2-methoxyethanol (as coordinate ligand) under flow of nitrogen gas in a three-neck flask and then equivalent molar of monoethanolamine (MEA) was added as a reagent for stabilization purpose using the technique described in [101]. The prepared colloidal ZnO QDs solution was then stirred for 24 h in an inert atmosphere. Finally, the resulting solution was filtered using a polyvinylidene fluoride (PVDF) membrane (0.22 μm) to obtain ZnO QDs of uniform size by discarding the unreacted particles [101].

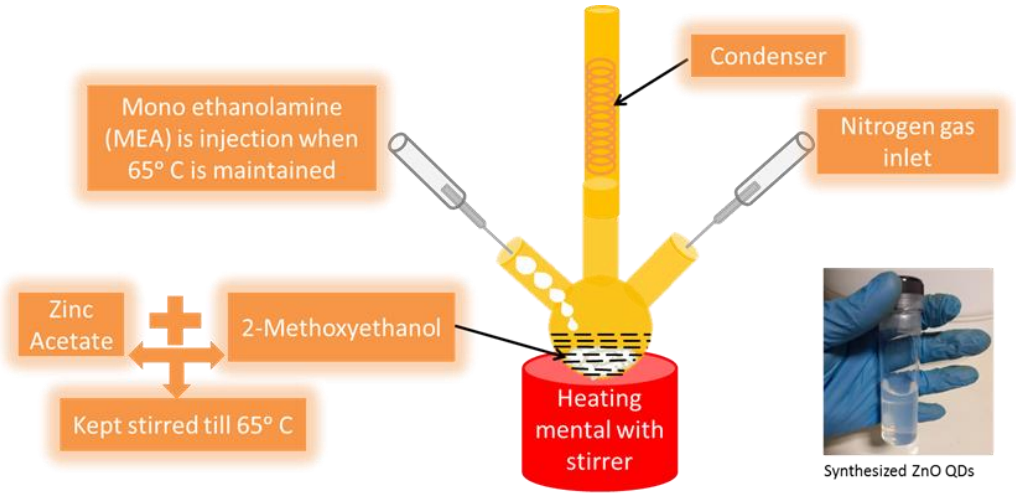

Figure 2.1: Synthesis process of ZnO QDs.

2.2.2 Device Fabrication

The BHJ OSC devices were fabricated on ITO coated soda-lime glass substrate in an ambient air atmosphere unless and otherwise specific conditions are mentioned. The fabrication of the OSCs was started with the cleaning of ITO-coated glass substrates (15×15 mm^2) for all types of devices. The ITO-coated glass substrates were cleaned ultrasonically in a soap solution, deionized (DI) water, acetone, and isopropanol for 10 minutes, sequentially. The substrates were dried at 100°C in the oven under nitrogen gas flow for 15 minutes. The synthesized ZnO QDs solution of 100 mM was deposited on ITO film by the spin coating technique at 2000 rpm for 40 s. The film was dried at 110°C for 10 minutes, and then the spin coating was repeated for one more time. Finally, the film was annealed at 200°C in an ambient air atmosphere for 30 minutes to achieve a ~30 nm thickness of ZnO QDs to work efficiently as the ETL of BHJ OSC. For the deposition of the active layer, a blend solution of PCDTBT (5 mg/ml in dichlorobenzene) and $PC_{61}BM$

(15 mg/ml in chloroform) was prepared by stirring overnight. The blend solution was deposited on the ZnO QDs layer by spin coating technique at 1500 rpm for 40 s and then dried at 120°C in the oven under a nitrogen environment for 30 min.

Two types of devices were fabricated: "Device 1" used the ITO/ZnO QDs/PCDTBT:$PC_{61}BM$/PEDOT:PSS/Ag structure and "Device 2" used a PQT-12 IL to form the structure of ITO/ZnO QDs/PCDTBT:$PC_{61}BM$/PQT-12/PEDOT:PSS/Ag under study. The PEDOT:PSS HTL was deposited by the conventional spin coating at 2000 rpm for 40 s and dried it at 120°C for 30 min to obtain a thickness of ~40 nm. The PQT-12 was deposited using the FTM technique, as illustrated in Figure 2.2 [110] [112]. It should be noted that the PQT-12 was dissolved in chloroform (a non-polar solvent), and this hydrophobic solution was dispersed on the hydrophilic (ethylene glycol and glycerol in 1:1 ratio) liquid (liquid substrate). Also, the surface of the active layer (a blend of PCDTBT and $PC_{61}BM$) was of hydrophobic nature. Thus, the surface of the active layer (hydrophobic) promotes adhesion for PQT-12 during film stamping using the FTM technique and thus offers a better interface [112], [114]. The PQT-12 film of ~20 nm was obtained over the active layer and was then dried at 120°C for 10 min in a nitrogen environment. Finally, a 100 nm thin Ag metal electrode of 2 mm diameter was deposited by a thermal evaporation method (Model no. FL400 SMART COAT 3.0 A from Hind High Vacuum) using shadow masking technique at a vacuum level of ~3×10^{-6} mbar and a constant rate of 0.2 Å/s. The complete device structures of the BHJ OSCs are shown in Figure. 2.3.

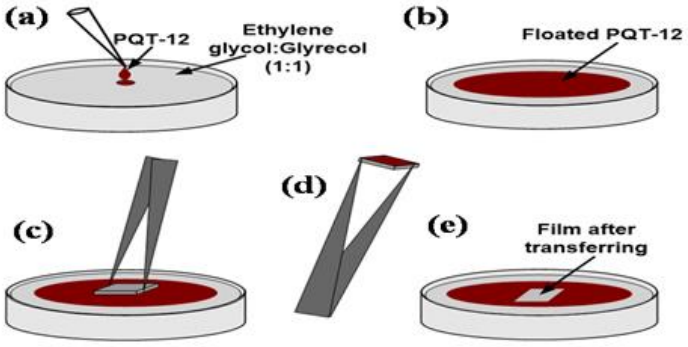

Figure 2.2: The schematic diagram of floating film transfer method (a) Dropping of PQT-12 on the hydrophilic solution (ethylene glycol and glycerol in 1:1 ratio), (b) Thin film of PQT-12 over the liquid surface, (c) Transferring of the film on the substrate, (d) PQT-12 coated substrate and (e) Empty space in PQT-12 film in the liquid surface.

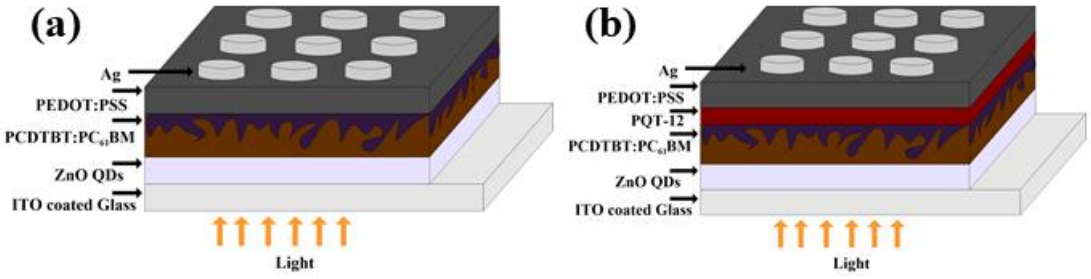

Figure 2.3: Device structure of fabricated OSCs (a) Device 1 and (b) Device 2.

2.3 Results and Discussion

In this section, thin-film and electrical as well as optical characterization of the PCDTBT:$PC_{61}BM$ based BHJ organic solar cell have been carried out.

2.3.1 Thin Film Characterization

The optical absorbance of the thin films was measured by UV/Vis/NIR spectroscopy (Model V-750 from Jesco, Japan). The photoluminescence (PL) from various thin-film

structures is measured by using a spectrometer (FLS 980 from Edinburgh Instruments, UK). The electrical characterization (current density vs. voltage, J-V) was carried out by using a semiconductor parameter analyzer (Model B1500A from Keysight, USA). The standard solar spectrum was obtained from a solar simulator (Model SS50AAA, A.M. 1.5G from Photo Emission Technology Inc., USA). The power density (light intensity) of the obtained solar spectrum is calibrated using a standard silicon reference cell (Model 60623 provided by Photo Emission Technology Inc., USA). The external quantum efficiency (EQE) was calculated with the help of a discrete spectrum obtained from a halogen lamp with the help of a monochromator (Model SP2150i from Princeton Instruments, USA).

The energy band diagram for both the OSCs structures fabricated using blend film of PCDTBT:$PC_{61}BM$ are shown in Figure 2.4. In Device 1, PEDOT:PSS as HTL blocks the electron and transports the hole, as shown in Figure 2.4 (a). In Device 2, the insertion of the PQT-12 IL between the active layer and PEDOT:PSS enhance hole transportation with a good energy band alignment, as shown in Figure 2.4 (b). Since the PEDOT:PSS is not in direct contact with the active layer, the insertion of PQT-12 IL also enhances the stability of the BHJ OSC under study. The absorption spectra of the ZnO/ PCDTBT:$PC_{61}BM$ and ZnO/PCDTBT:$PC_{61}BM$/PQT-12 films are shown in Figure 2.5. The solar spectrum of energy higher than 1.8 eV is absorbed by PCDTBT:$PC_{61}BM$ polymer blend. However, due to the thin film of the active layer (~80 nm), a significant part of the solar spectrum with energy higher than 1.8 eV is transmitted to PQT-12. The absorption spectra shown in Figure 2.5 illustrate that the use of FTM coated PQT-12 as the IL enhances the absorption in the active layer of the device. The charge extraction from the active layer

(PCDTBT:$PC_{61}BM$) at the interface is investigated using steady-state photoluminescence measurements [115]. The measurements for three film structures ZnO/PCDTBT:$PC_{61}BM$, ZnO/ PCDTBT:$PC_{61}BM$/PEDOT:PSS,and ZnO/PCDTBT:$PC_{61}BM$/PQT-12/PEDOT:PSS respectively are performed from glass side at an excitation wavelength of 540 nm as shown in the Figure. 2.6. It is found that the PEDOT:PSS only HTL quenched PL intensity slightly due to transfer of hole from the active layer to PEDOT:PSS. This PL intensity quenching further increases in the ZnO/ PCDTBT:$PC_{61}BM$/PQT-12/PEDOT:PSS film structures due to insertion of PQT-12 IL results in more efficient charge transfer at the interface (also seen from band diagram of Figure 2.4).

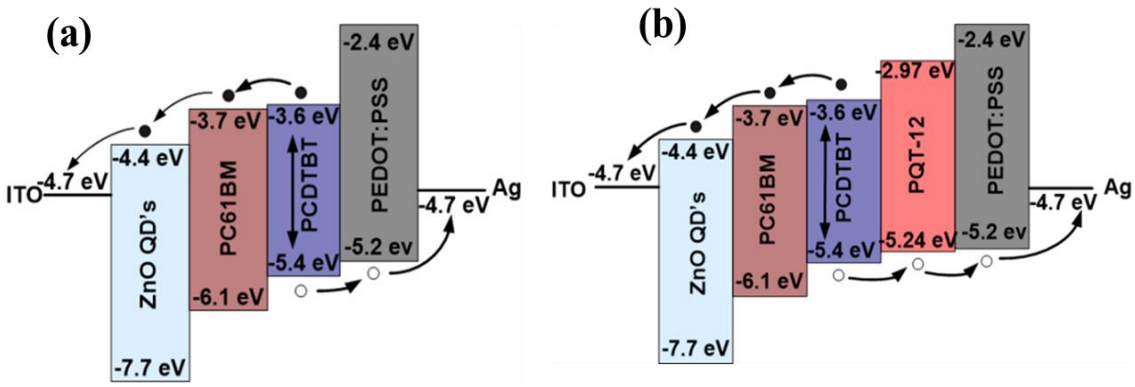

Figure 2.4: Energy band diagram of (a) Device 1 and (b) Device 2.

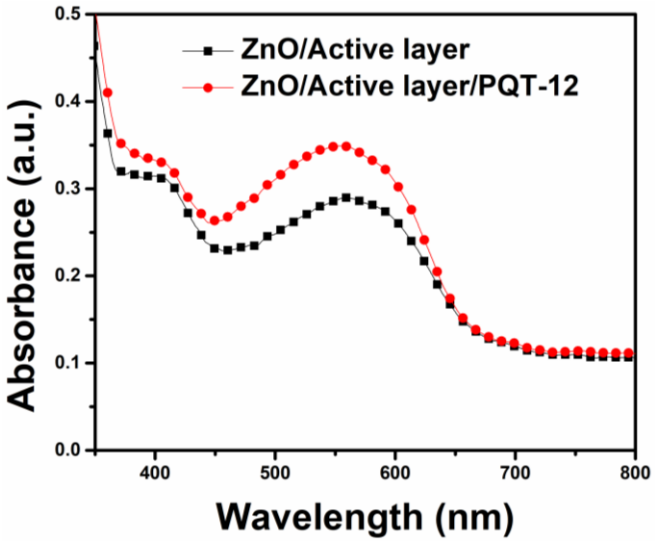

Figure 2.5: Absorption spectra of ZnO/Active layer and ZnO/Active layer/PQT-12 films.

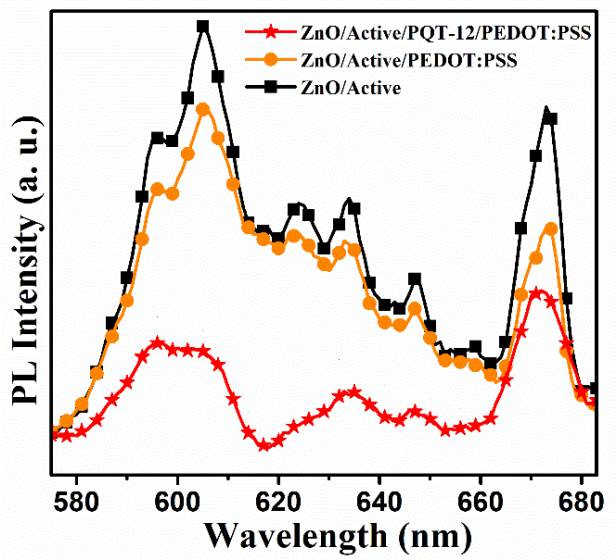

Figure 2.6: Photoluminescence (PL) spectra of ZnO/Active, ZnO/Active/PEDOT:PSS, and ZnO/Active/PQT-12/PEDOT:PSS films taken from glass side at an excitation of 540 nm.

2.3.2 Solar Cell Characterization

The *J-V* characteristics shown in Figure 2.7 are measured under illuminated conditions for both the BHJ OSCs under study. The non-ideal or S-shape J-V characteristics in the

figure are attributed to the rectifying contact between the hole collecting electrode and PEDOT:PSS layer resulted from the increased sheet resistance of the PEDOT:PSS based HTL [116]. It is believe that the PEDOT:PSS layer near the electrode contact gets dissolved in water and increases the sheet resistance of the PEDOT:PSS layer. Another possible reason behind the non-ideal or S-shape J-V curves is the reduced surface recombination velocity at the electrode/HTL interface [117]. The performance parameters of the BHJ OSCs are summarized in Table 2.1. The better power conversion, as well as other parameters in Device 2 over Device 1 listed in Table 2.1, are attributed to the FTM-based PQT-12 film as IL in the device. The maximum power conversion efficiency of 1.05% achieved in Device 2 attributed to the improved hole transfer and enhanced optical absorption, as observed in Figure 2.5. The best results for the open-circuit voltage (V_{OC}), short circuit current density (J_{SC}), and fill factor (FF) of 0.562 V, 5.62 mA/cm^2, and 0.33, respectively, are also obtained in Device 2. The V_{OC} closely depends on the difference of HOMO of electron donor polymer and LUMO of electron acceptor polymer [118]. According to Shockley's formula, the current density of the diode (heterostructure) is expressed as:

$$J = J_0[\exp(qV/nkT) - 1] \tag{2.1}$$

Where J_0 is reverse saturation current density, *k* is the Boltzmann constant, *T* is temperature, and *n* is the ideality factor of the diode. Including the effects of series resistance (R_S) and shunt resistance (R_{sh}), equation 2.1 can be modified as equation. 2.2 [40]:

$$J = \frac{Rsh+Rs}{Rsh}\left\{J_0\left[\left(\exp\frac{q(V-JRs)}{nKT}\right) - 1\right] + \frac{V}{Rsh}\right\} - J_{ph} \tag{2.2}$$

Using $V = V_{OC}$ and J=0 in the equation. 2.2 and assuming $R_{sh} >> R_s$, the open-circuit voltage

V_{OC} can be written as:

$$V_{OC} = \frac{nkT}{q} ln\left(\frac{J_{ph}}{J_0} + 1\right) \quad (2.3)$$

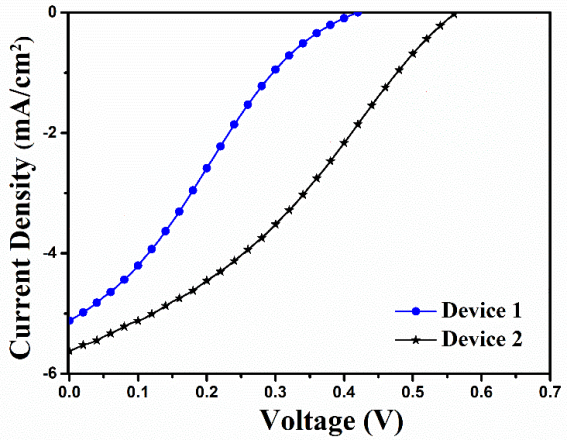

Figure 2.7: Current density versus voltage (J-V) characteristic of the fabricated OSCs.

Table 2.1: Performance parameters of the OSC devices

Device structure	V_{oc} (mV)	J_{sc} (mA/cm^2)	Fill factor (FF)	Efficiency η (%)
Device 1	419	5.12	0.24	0.53
Device 2	562	5.62	0.33	1.05

Table 2.2: Reverse saturation current of the OSC devices

Device structure	Voc (mV)	J_0 (A/cm^2)
Device 1	419	7.87×10^{-5}
Device 2	562	1.74×10^{-5}

The reverse saturation current density J_0 in equation 2.3 has been extracted from the measured J-V characteristics by following the method described in [119], [120]. The

obtained values of J_0 are in good agreement with equation 2.3 and V_{OC} calculated under the illumination of 1 sunlight. The values of J_0 are listed in Table 2.2 and compared with the corresponding V_{OC}. The barrier between HTL and the electrode, as shown in the band diagram of Figure 2.4, also supports the dark current characteristics.

The external quantum efficiency (EQE) of both devices has been shown in Figure 2.8. The enhancement in EQE in Device 2 over Device 1 is a result of improved absorption and better energy band alignment due to the insertion of the PQT-12 IL. The improved band alignment reduces the recombination and enhances the EQE by improving the transportation of selective charge carriers toward their respective electrodes (i.e., electrons toward ITO and holes toward Ag) in the BHJ OSCs.

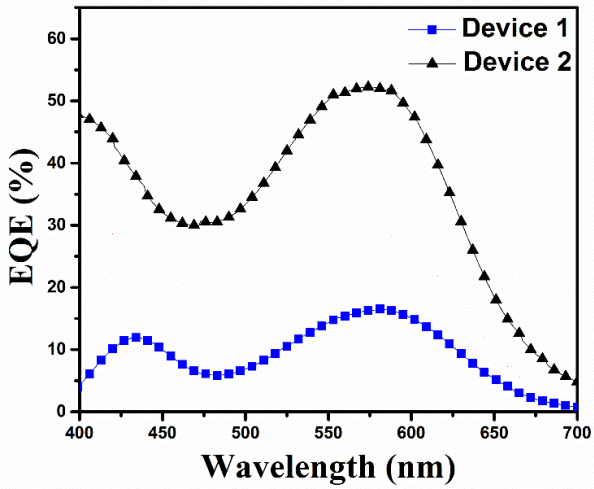

Figure 2.8: External quantum efficiency of the fabricated OSCs.

The impedance spectroscopy is performed for the measurement of resistance and capacitance associated with OSCs equivalent circuit. The impedance spectroscopy analysis of our OSCs is performed by using the Nyquist plot where x-axis represents the real (Z_1) and y-axis shows the imaginary (Z_2) part of the impedances. The frequency is varied in

such a way that it is decreased with the increase in the distance from the origin. The Nyquist plots (Cole-Cole plots) of the fabricated OSCs under dark condition are shown in Figure 2.9 (a) at an applied bias corresponding to their respective open circuit voltages, V_{OC}. Figure 2.9 (a) shows the semicircle which corresponds to the parrelel RC circuit shown in Figure 2.9 (b). The parallel resistance R_2 in the RC circuit represents the diameter of the semicircle which corresponds to the bulk resistance. On the other hand, C_2 in the RC circuit corresponds to the simple geometrical capacitance of the device [121]. Cole-Cole plots or Nyquist plots of the fabricated OSCs under dark condition are shown in Figure 2.9 (a) at an applied bias corresponding to their V_{OC}. The data obtained from Nyquist plots can be modeled for an equivalent circuit, as shown in Figure 2.9 (b). The resistance R_1 in series with the parallel combination of the resistance R_2 and capacitor C_2 is due to the resistive losses and interface mismatch [121]. The higher value of resistance R_1 is observed in Device 1, whereas lower R_1 is observed in Device 2. This reduction in the value of R_1 in Device 2 is due to better phase matching of the active layer with FTM-based PQT-12 as IL compared to that without IL between the active layer and PEDOT:PSS. The smallest semicircle for Device 2 in the Nyquist plot confirms the best charge transportation due to its lowest resistance value R_1. Further, Device 2 is illuminated with the light of 1 sun and the corresponding Nyquist plot is shown in Figure 2.9 (c). Under the illumination of light, two partial semicircles are formed as visible from Figure 2.9 (c). Therefore, a relatively more complex equivalent circuit model as shown in Figure 2.9 (d) is required to fit the solar cell impedance characteristic under illumination condition [121]. The second part ($R_3\|C_3$) of the equivalent circuit observed by the second semicircle is due to the generation/recombination of charge carriers and charge transfer at the interfaces.

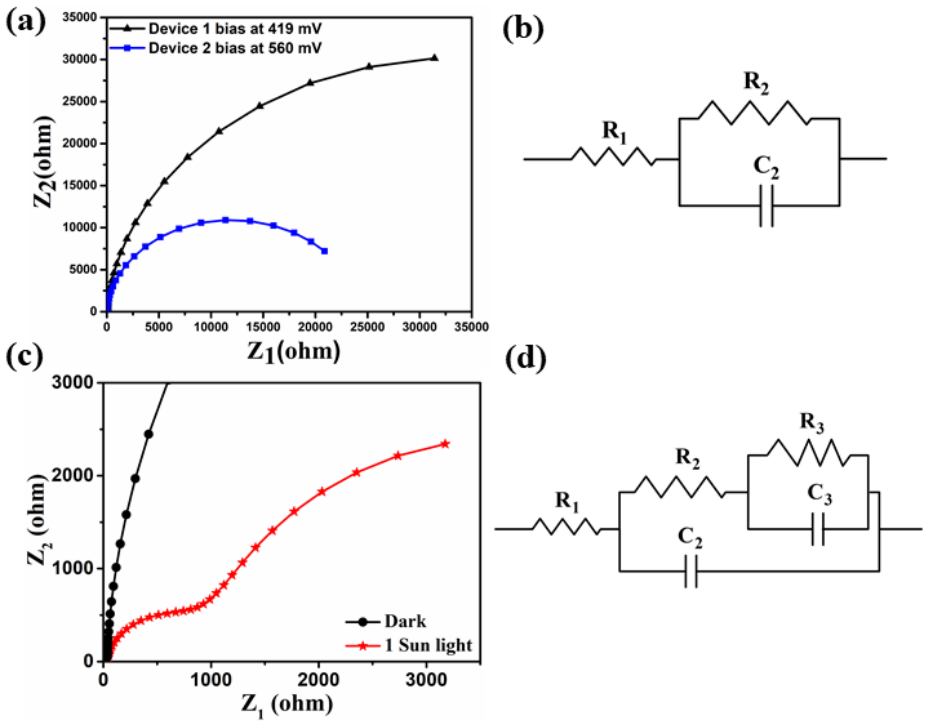

Figure 2.9: (a) Nyquist plot of the fabricated OSCs under dark condition, (b) Equivalent circuit of the OSCs under dark, (c) Nyquist plot of Device 2 under dark and light illumination, and (d) Equivalent circuit of the Device 2 under dark and light illumination.

2.4 Conclusion

In this chapter, the incorporation of FTM-based PQT-12 as an interface layer between the active layer and HTL shows better performance and stability. Well-matched HOMO level of PQT-12 (5.24 eV) and PEDOT:PSS (5.2 eV) with that of PCDTBT (5.4 eV) donor material have been used to facilitate better hole transportation to Ag electrode. The maximum values of J_{SC} (= 5.62 mA/cm^2), V_{OC} (= 562 mV), FF (= 0.33), and PCE (= 1.05%) have been measured in the OSC with PQT-12 as IL. The efficient hole transfer from the active layer to the electrode also enhanced the EQE to the maximum when PQT-

12 IL layer is inserted between the active layer and PEDOT:PSS. The impedance spectroscopy analysis is performed for the modelling of BHJ OSCs to obtain a simplified equivalent circuit of the OSCs under study. The FTM based PQT-12 as IL shows significant PL quenching and improves absorbance in the active layer, which, in turn, improves the PCE.

CHAPTER 3

Effects of HTL and ETL Thicknesses on the Performance of PQT-12/PCDTBT:$PC_{61}BM$/ZnO QDs Organic Solar Cells

Contents

*Part of this work has been published as:

Amit Kumar et al., "Effects of HTL and ETL Thicknesses on the Performance of PQT-12/PCDTBT:$PC_{61}BM$/ZnO QDs Solar Cells," *IEEE Photonics Technology Letters*,32 (12), 677-680, 2020.

CHAPTER 3

Effects of HTL and ETL Thicknesses on the Performance of PQT-12/PCDTBT:$PC_{61}BM$/ZnO QDs Organic Solar Cells

3.1 Introduction

In Chapter-2, we discussed the effect of FTM coated PQT-12 as an interface layer on the performance of ITO/ZnO QDs/PCDTBT:$PC_{61}BM$/PQT-12/PEDOT:PSS/Ag BHJ organic solar cells (OSCs). It was observed that the PQT-12 interface layer between the PCDTBT:$PC_{61}BM$ and PEDOT:PSS improved the performance over the device without the PQT-12 layer. It is reported that the use of PEDOT:PSS as the hole transport layer (HTL) degrades the performance of the OSCs [122], [123]. Thus, the FTM based PQT-12 may be used as a better replacement of PEDOT:PSS for the HTL due to its better stability [57] and energy band alignment with the PCDTBT than those of the PEDOT:PSS as discussed in Chapter-2.

The photovoltaic parameters such as open-circuit voltage (Voc), short circuit current density (Jsc), and fill factor (FF) are highly sensitive to the thicknesses of the electron transport layer (ETL) and HTL [124], [125]. In addition to the thicknesses, the deposition techniques used for the ETL and HTL also affect the performance of BHJ OSCs. The FTM has recently been successfully employed for fabricating low-cost, large-area, multi-layered devices [109], [110]. The FTM based PQT-12 films have been successfully used in the OSCs in Chapter-2. In this chapter, we have investigated the effects of the thicknesses of FTM derived PQT-12 based ETL and ZnO QDs based HTL on the performance of ITO/ZnO QDs/PCDTBT:$PC_{61}BM$/PQT-12/Ag BHJ OSCs. The ZnO QDs have been synthesized using the solution method and the floating-film

transfer method (FTM) has been used for fabricating the PQT-12 based HTL as considered in Chapter-2. The outline of the rest of this chapter is given as follows:

Section 3.2 deals with the experimental details regarding the fabrication of the proposed ITO-coated glass/ZnO QDs/PCDTBT:$PC_{61}BM$/PQT-12/Ag based BHJ OSC. Section 3.3 comprises various results and discussions regarding electrical (J-V characteristic, Nyquist plot) and optical (absorption, external quantum efficiency) characterization. Finally, Section-3.4 summarizes the objectives and concludes the major observations of this chapter.

3.2 Experimental Details

3.2.1 Materials and Synthesis

The useful polymers, PQT-12, PCDTBT, $PC_{61}BM$, and other chemicals required for cleaning purposes were purchased already mentioned in Chapter-2. The ZnO QDs (~2.53 nm) were synthesized using the chemical solution method described in [101]. In short, zinc acetate dihydrate (precursor) was dissolved in 2-methoxy ethanol under a nitrogen environment until the temperature reached up to 65ºC. Now equivalent molar of monoethanolamine (MEA) as stabilizing reagent was injected in the solution and kept the resulting solution (of ZnO QDs) for 24 hours at room temperature. The prepared ZnO QDs solution was then filtered by using a 0.22 μm PVDF filter to remove any unreacted part.

3.2.2 Solar Cell Fabrication

The BHJ OSCs were made on cleaned ITO coated glass substrate in an open-air environment (without using a glove box) unless any specific condition was mentioned. The ZnO QD was spin-coated at 3000 rpm for 30 s on cleaned ITO glass substrate and

then heated at 150ºC for preparing ETL. Finally, the ETL was annealed at 200ºC for 30 minutes in an ambient environment to act as the ETL. To prepare the organic active layer, 5 mg of PCDTBT in 1 ml dichlorobenzene and the solution was stirred at 60ºC for nearly 10 hours. After that 15 mg of $PC_{61}BM$ was mixed into PCDTBT solution and then stirred for uniform mixing for 2 hours prior to final deposition. The resultant PCDTBT:$PC_{61}BM$ solution was spin-coated on the previously deposited ZnO QDs based ETL layer at 1500 rpm for 50 seconds and then annealed at 120ºC for 30 minutes in an argon environment to fabricate the active layer (~110 nm).

The PQT-12 film was then deposited for HTL on the active layer by the FTM technique [114], [126], [127] as demonstrated in Figure 3.1 (a). In brief, PQT-12 hydrophobic solution (in chloroform) was dispersed on the hydrophilic solution of ethylene glycol and glycerol (prepared in 1:1 ratio) in a petri dish. The dispersed PQT-12 film was then stamped on the hydrophobic surface of the active layer. The good adhesive nature of the active layer to PQT-12 ensures a good active layer/HTL interface [114], [126]. The samples were finally dried up by heating at 120°C for 10 min in an argon environment. Now finally, the shadow masking technique was used to fabricate 100 nm silver (Ag) metal dots of 2 mm diameter on the HTL for the top electrode by a thermal evaporation method (Model no. FL400 SMART COAT 3.0 A from HHV, India).

The energy band diagram for the fabricated OSCs structure is shown in Figure 3.1 (b). It is observed from Figure 3.1 (b) that the band alignment of PQT-12 based HTL with the active layer is assisted with the separation of electron-hole pairs in the active layer that reduces recombination. Clearly, FTM-based PQT-12 film serves as an efficient HTL in the OSCs structure. The cross-sectional image of the fabricated

optimized structure without the Ag electrode is shown in Figure 3.2. The complete schematic of the proposed BHJ OSCs is shown in the inset of Figure 3.2. Four fabricated OSCs samples with fixed HTL thickness of 20 nm but with different ETL thicknesses of 20 nm, 25 nm, 30 nm, and 35 are denoted by ZnO (20), ZnO (25), ZnO (30), and ZnO (35), respectively. The performance of the solar cells is reported to be degraded with increased ZnO based ETL thickness due to increase in the contact resistance between ZnO layer and active layer [125]. That is why, we have restricted the ETL thickness up to 35 nm only. On the other hand, three OSCs with a fixed ETL thickness of 20 nm but with three different HTL thicknesses of 20 nm, 40 nm, and 60 nm are denoted by PQT-12 (20), PQT-12 (40), and PQT-12 (60), respectively.

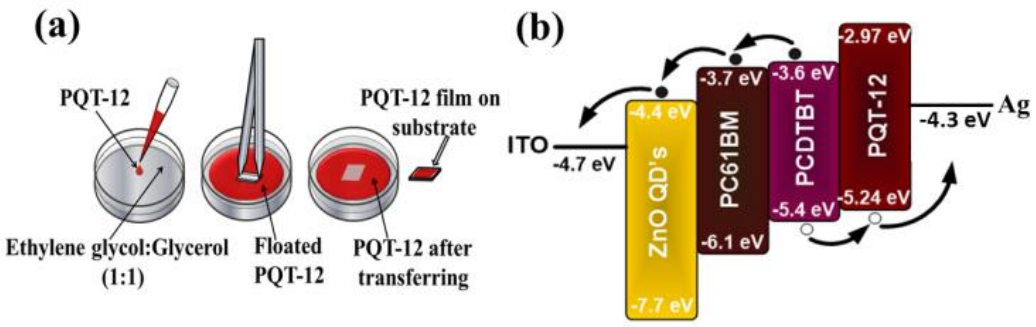

Figure 3.1: (a) FTM deposition steps for PQT-12 film and (b) Energy band diagram for the OSCs structure.

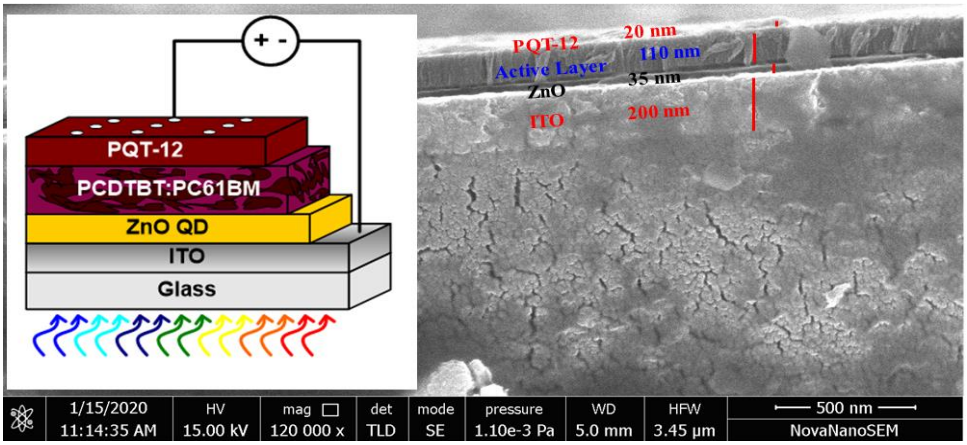

Figure 3.2: HRSEM cross-sectional image of the optimized OSC structure without Ag and complete OSC device structure in the inset.

3.3 Results and Discussion

In this section, optical as well as electrical characterizations of the fabricated BHJ OSCs have been discussed in detail.

3.3.1 Optical Characterization

The absorbance spectra of the PCDTBT:$PC_{61}BM$ based active layer and PQT-based HTL are shown in Figure 3.3. Figure 3.3 shows significant absorption of the visible spectrum in the active layer. The absorption of a part of the visible spectrum also takes place in the HTL. Thus, the active layer along with the HTL enhances the overall optical absorption in the visible spectrum. The transmittance spectra of the ZnO QDs based ETL are shown in Figure 3.4 for different thicknesses. The ETL appears to be nearly transparent (> 80%) in the visible range. This ensures that the significant part of the visible light enters into the active layer to contribute photocurrent in the device. However, light reduction in the transmittance with increased ETL thickness may be attributed to increased reflectance at higher wavelengths due to the plasma resonance of electron gas in the conduction band of the active layer [128].

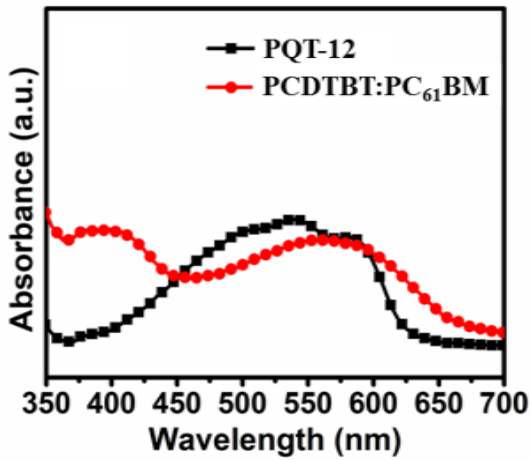

Figure 3.3: Absorbance of PQT-12 and PCDTBT:$PC_{61}BM$ film.

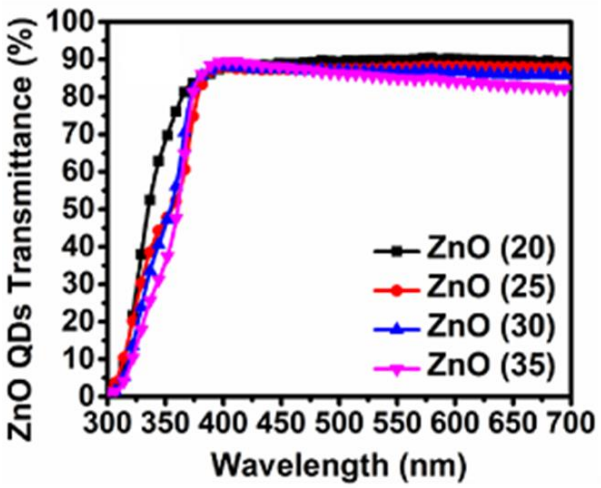

Figure 3.4: Transmittance of ZnO QDs thin film with different thicknesses.

The external quantum efficiency (EQE) calculated from the *J-λ* characteristics [129], which is measured using the monochromator unit (Model No. SP2150i from Princeton Instruments, USA) and attached halogen light source have been shown for different HTL thicknesses in Figure 3.5 and for different ETL thicknesses in and Figure 3.6. Since the absorptions in HTL and ETL regions also contribute to the photocurrent to some extent, the EQE peaks are observed to be red-shifted slightly with increased HTL and ETL thicknesses. The OSC with 20 nm HTL thicknesses and 35 nm ETL thicknesses shows the highest EQE among all the samples under study.

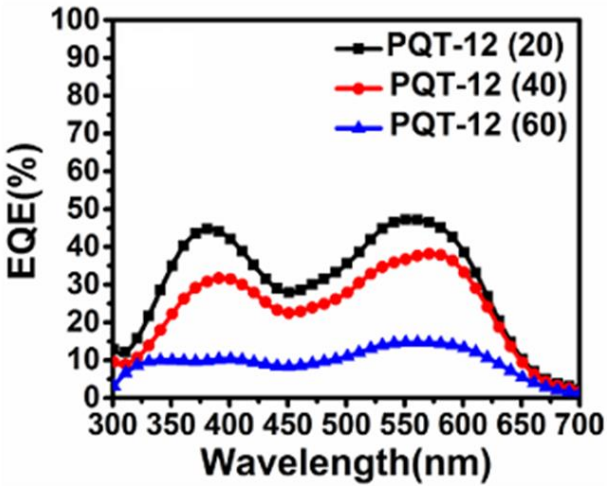

Figure 3.5: EQE characteristics for different HTL thicknesses with fixed ZnO of 20 nm.

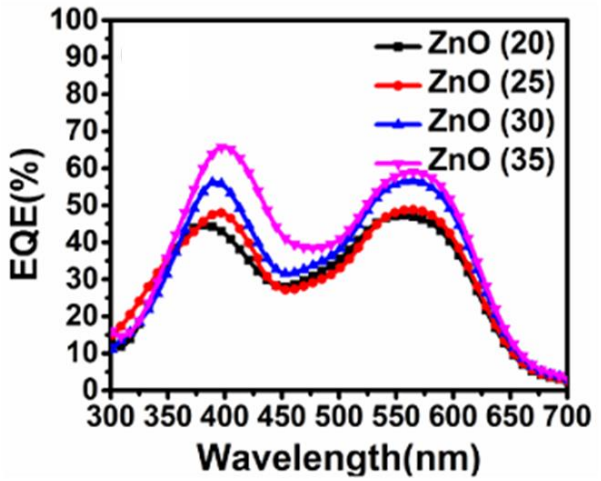

Figure 3.6: EQE characteristics for different ETL thicknesses with fixed PQT-12 of 20 nm.

3.3.2 Electrical Characterization

The current densities (J) vs. voltage (V) characteristics of OSCs under one sunlight are measured by a parameter analyzer (Model No. B1500A from Keysight, USA) in ambient open-air conditions. The standard solar light spectrum has been obtained using the solar simulator (Model SS50AAA from Photo Emission Technology, USA), which is calibrated for AM 1.5 G standard sunlight with a light intensity of 100 mW/cm^2 using a standard reference cell (Model No. 60623 from National Renewable Energy Laboratory, USA). The measured *J-V* characteristics of PQT-12 (20), PQT-12 (40), and PQT-12 (60) are shown in Figure 3.7. The PQT-12 (20 nm) based OSC shows the highest J_{SC} of 6.62 mA/cm^{2,} whereas the J_{SC} of PQT-12 (40 nm) and PQT-12 (60 nm) samples are 5.86 mA/cm^2 and 2.94 mA/cm^2, respectively. The values of other parameters with the variable thickness of PQT-12 are summarized in Table 3.1. The PCE and fill factor can be improved further by carrying out the fabrication and characterization of the OSCs in a controlled environment using a glove box. It is found that the PCE deteriorates with the increase in the PQT-12 based HTL thickness due to a reduction in hole transfer rate through the HTL.

Table 3.1: Photovoltaic Parameters with Varying PQT-12 Thickness

S.No.	PQT-12 (nm)	ZnO (nm)	J_{sc} (mA/cm^2)	V_{oc} (mV)	FF (%)	PCE (%)
1	20	20	6.62	566	28	1.05
2	40	20	5.86	495	29	0.84
3	60	20	2.94	612	27	0.49

Table 3.2: Photovoltaic Parameters with Varying ZnO QDs thickness

S.No.	PQT-12 QD (nm)	ZnO (nm)	J_{sc} (mA/cm^2)	V_{oc} (mV)	FF (%)	PCE (%)
1	20	20	6.62	566	28	1.05
2	20	25	6.85	602	32	1.31
3	20	30	9.44	656	35	2.16
4	20	35	10.42	672	38	2.66

The effect of ETL thickness for a fixed HTL thickness of 20 nm the *J-V* characteristics of OSCs are shown in Figure 3.8. The Figure shows that J_{SC} is increased with the ZnO QDs based ETL thickness. Almost more than 80 % transmittance is shown by the various thickness of ZnO shown in Figure 3.4; therefore, a similar amount of visible light will reach even with increasing thickness of ZnO. The variations in the other parameters of the OSCs are listed in Table 3.2. The maximum PCE of 2.66% is obtained for the OSC with 35 nm ETL thickness and 20 nm HTL thickness. The increased PCE with ETL thickness may be attributed to the enhanced charge transport as well as charge extraction in the OSCs [125]. Improved charge transportation and extraction with increased ZnO QDs based ETL thickness reduce the recombination,

which, in turn, enhances the dissociation of more photo-generated electron-hole pairs into electrons and holes. Enhanced numbers of dissociated photo-generated electrons and holes move toward their respective electrodes to improve the performance of the BHJ OSCs.

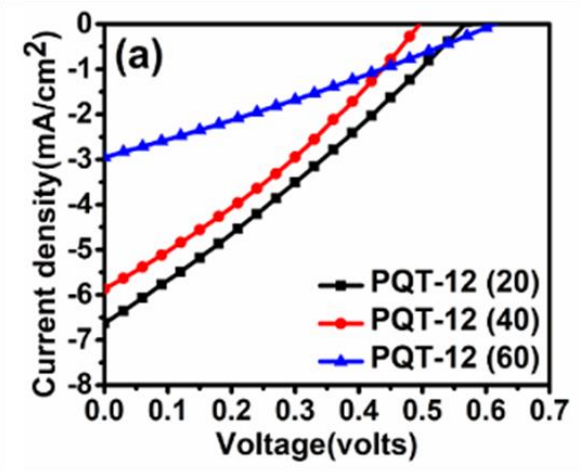

Figure 3.7: J-V characteristics of solar cells for fixed ETL thickness of 20 nm and different PQT-12 thicknesses of 20 nm, 40 nm, and 60 nm.

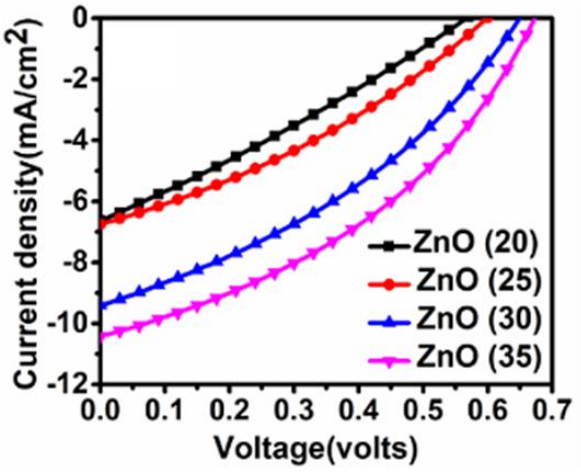

Figure 3.8: J-V characteristics of solar cells for a fixed PQT-12 based HTL thickness of 20 nm with four different ZnO QDs based ETL thicknesses of 20 nm, 25 nm, 30 nm, and 35 nm.

To analyze the stability of the proposed OSC in the ambient air conditions, the J-V characteristics of the OSC (with PQT-12 layer thickness of 20 nm and ZnO QDs layer thickness of 35 nm) are measured every day for a period over 7 days after the

fabrication of the device. The results are shown in Figure. 3.9. Day-wise performance parameters are shown in Table 3.3. About 11.36% degradation in the PCE is observed after 7 days in open environments. The performance degradation can be prevented by proper packaging of the device.

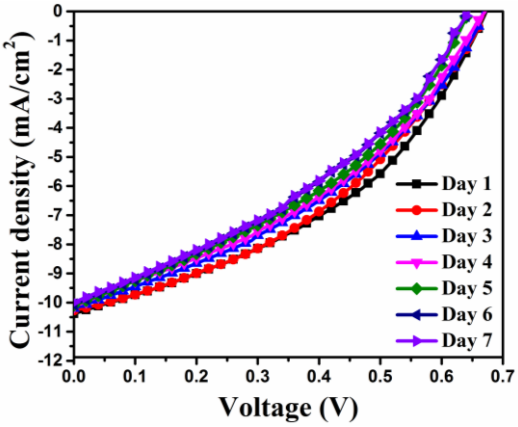

Figure. 3.9. J-V characteristics of device with 20 nm and 35 nm of PQT-12 and ZnO QDs, respectively to realize seven days stability.

Table. 3.3. Seven days analysis of the device with 20 nm and 35 nm of PQT-12 and ZnO QDs, respectively.

S.No	Days	Jsc (mA/cm^2)	Voc (mV)	FF (%)	PCE (%)
1	Day 1	10.38	670	38	2.64
2	Day 2	10.27	670	38	2.61
3	Day 3	10.20	668	37	2.52
4	Day 4	10.14	668	37	2.50
5	Day 5	10.10	644	36	2.34
6	Day 6	10.05	642	36	2.32
7	Day 7	10.00	642	36	2.31

We will now consider the impedance analysis in the 1 kHz -1 MHz frequency range at respective open-circuit voltages of OSCs under solar illumination. The Nyquist plots for different HTL and ETL thicknesses are shown in Figure 3.10 and Figure 3.11, respectively. The decreased diameter of semicircles with reduced (enhanced) HTL (ETL) thickness implies that the charge transportation (and hence the mobility) can be improved by reducing (increasing) the HTL (ETL) thickness [130]. In brief, an increase (decrease) in ETL (HTL) thickness thus reduces the recombination and enhances charge transportation in the active layer. Thus, the results of Figure 3.10 and Figure 3.11 confirm that the OSC with HTL thickness of 20 nm and ETL thickness of 35 nm possesses the highest performance among all the OSCs under study. The results of Figure 3.10 and Figure 3.11 also agree with the *J-V* and EQE analysis.

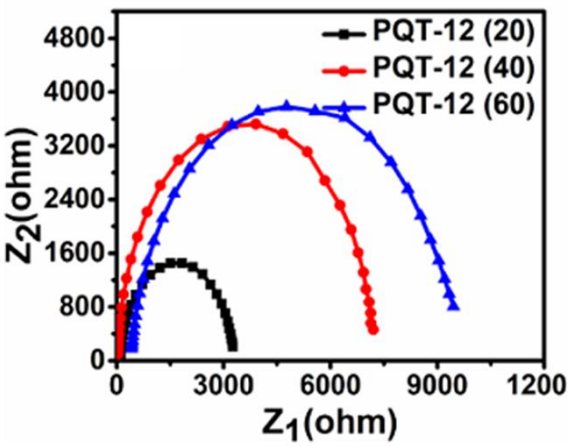

Figure 3.10: Nyquist plot with variation in PQT-12 thickness with fixed ZnO QDs of 20 nm.

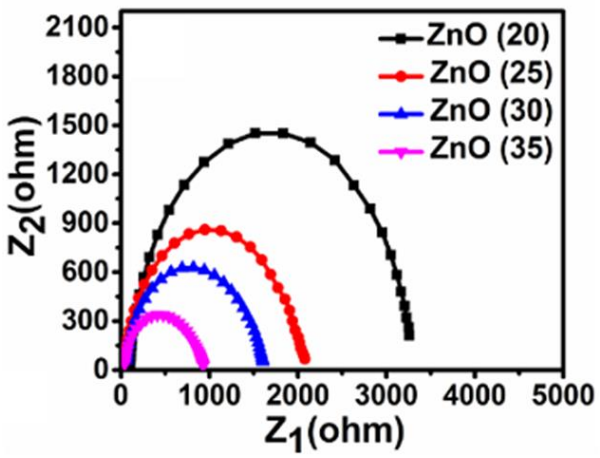

Figure 3.11: Nyquist plot with variation in ZnO QDs thickness with fixed PQT-12 of 20 nm.

3.4 Conclusion

The effects of ZnO QDs based ETL and FTM transferred PQT-12 film based HTL thicknesses on ITO/ZnO QDs/PCDTBT:PC_{61}BM/PQT-12/Ag structured BHJ solar cells have been investigated in this chapter for the first time. It is observed that a better PCE can be obtained for smaller HTL thickness and larger ETL thickness of the OSCs. Three OSCs with three different HTL thicknesses of 20 nm, 40 nm, and 60 nm but with a fixed ETL thickness of 20 nm fabricated to investigate the effects of the FTM transferred PQT-12 film based HTL thickness on the performance of the solar cells under study. On the other hand, four OSCs with a fixed HTL thickness of 20 nm but four different ETL thicknesses of 20 nm, 25 nm, 30 nm, and 35 nm are used for studying the effect of ETL layer thickness on the PCDTBT:PC_{61}BM based BHJ OSCs. The OSC with ~20 nm thin PQT-12 based HTL and ~35 nm thin ZnO QDs based ETL shows the highest performance parameters with J_{SC}, V_{OC}, and PCE of 10.42 mA/cm^2, 672 mV, and 2.66%, respectively. The present study can be used for the optimization of the other BHJ OSCs by optimizing the ETL and HTL layer thicknesses of the device.

CHAPTER 4

Synergistic Effect of CdSe Quantum Dots (QDs) and $PC_{61}BM$ in PCDTBT:$PC_{61}BM$:CdSe QDs Bulk Heterojunction Based Organic Solar Cells

Contents

*Part of this work has been published as:

Amit Kumar et al., "Synergistic Effect of CdSe Quantum Dots (QDs) and $PC_{61}BM$ on Ambient-Air Processed ZnO QDs/PCDTBT:$PC_{61}BM$:CdSe QDs/MoO_3 Based Ternary Organic Solar Cells," *Nanotechnology*, 31, 465404, 2020.

CHAPTER 4

Synergistic Effect of CdSe Quantum Dots (QDs) and $PC_{61}BM$ in PCDTBT:$PC_{61}BM$:CdSe QDs Bulk Heterojunction Based Organic Solar Cells

4.1 Introduction

Incorporation of metallic (Au and Ag) or semiconducting (CdSe, CdS, PbSe, PbS, and Cu_2S) nanoparticles in the photoactive layers is reported to enhance the photovoltaic parameters of BHJ OSCs [131]–[135]. The blend of semiconducting nanoparticles of CdSe, CdS, PbSe, PbS, and Cu_2S with organic materials in the form of organic-inorganic hybrid nanostructures as the active layer is reported to enhance the absorption and charge transport properties of the photoactive layer in various photo detection devices [108], [136]–[138]. After investigating the performance of the PCDTBT:$PC_{61}BM$ in Chapter-2 and Chapter-3, the synergistic effect of CdSe QDs and PCDTBT:$PC_{61}BM$ on the performance of ITO/ZnO QDs/PCDTBT:$PC_{61}BM$:CdSe QDs /MoO_3/Ag based organic-inorganic solar cells structure has been investigated in the present chapter. The ZnO QDs layer is used as the ETL as in the previous chapters while the MoO_3 layer is used for the HTL in the present study. In the present study, the PQT-12 HTL layer has been replaced by MoO_3 HTL layer due to its better energy band alignment with the active layer for achievoing better hole blocking capability as compared to that obtained from the previously used PQT-12 based HTL [139]. The layout of the rest of the chapter is given below:

Section 4.2 discusses the experimental details for fabricating the ITO/ZnO QDs/PCDTBT:$PC_{61}BM$:CdSe QDs /MoO_3/Ag structured BHJ OSC. Section 4.3

provides some important results related to the electrical and optical characteristics of fabricated ITO/ZnO QDs/PCDTBT:$PC_{61}BM$:CdSe QDs /MoO_3/Ag structure BHJ OSC which includes the current-voltage characteristics, Nyquist plots, external quantum efficiency, and absorbance. Finally, Section 4.4 concludes the major observations and findings of this chapter.

4.2 Experimental Details

In this section, PCDTBT:$PC_{61}BM$:CdSe QDs based ternary BHJ organic solar cell is fabricated and analyzed the effect of CdSe QDs on the performance parameters of the device.

4.2.1 Materials and Synthesis

ZnO QDs were synthesized using the chemical route described in ref. [101]. In brief, 100 mM of zinc acetate dihydrate was dissolved in 20 ml of 2-methoxy ethanol under nitrogen environment and kept the solution at 65ºC for stirring until the solution changed to smooth milky white. Further, 100 mM of monoethanolamine (MEA), used as stabilizing reagent, was injected into the resulting solution under controlled condition. The solution was later kept at room temperature for 24 hours at the continuous stirring condition. The synthesized colloidal ZnO QDs solution was then filtered by using a 0.22 µm PVDF filter to remove the unreacted part. The synthesized ZnO QDs solution had an average particle size of ~2.87 nm. On the other hand, the kinetic growth procedure was used for the synthesis of CdSe QDs. The precursor preparation steps were used as reported in ref. [140] for quantum dots synthesis with slight modification. In brief, the stock selenium solution was made by mixing 30 mg of selenium into the mix solution consists of 5 ml of octadecene and 0.4 ml of trioctylphosphine. Further, a cadmium precursor was prepared by sum-up three

chemicals, namely 13 mg of CdO, 0.6 ml of oleic acid, and 10 ml of octadecane, respectively, in a 25 ml round bottom flask and heated till the temperature reached 225°C. At a temperature of 225°C, 1 ml of stock selenium solution was quickly injected into the prepared cadmium solution as shown in Figure 4.1. The resulting orange colour solution was then centrifuged and washed three times with ethanol to extract the CdSe QDs. Finally, extracted CdSe QDs with average particle size of ~4.58 nm were dispersed in chloroform and used for the solar cell fabrication.

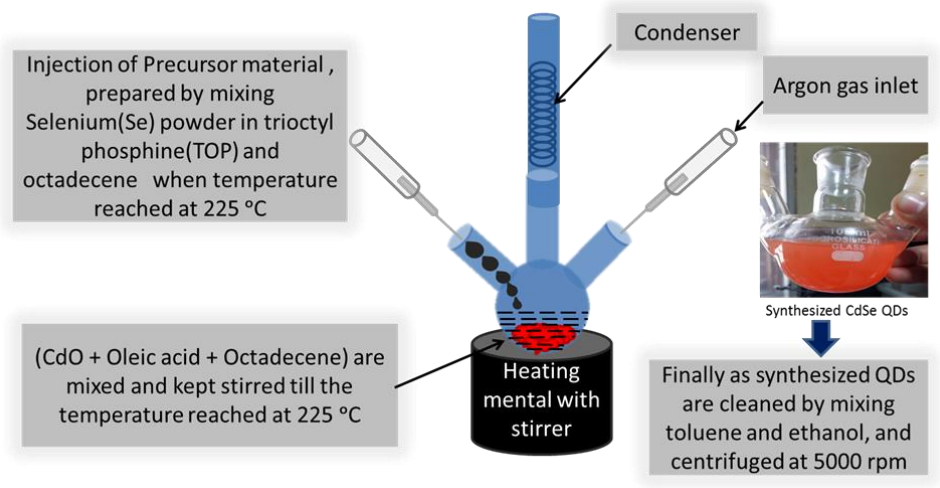

Figure 4.1: Synthesis process of CdSe QDs

4.2.2 Solar Cell Fabrication

Indium doped tin oxide (ITO) coated soda-lime glass substrates (15 × 15 mm^2) were used to fabricate the binary and ternary OSCs. The fabrication process was carried out in an ambient air atmosphere unless specific conditions are mentioned. The substrates were cleaned and dried in the oven under the flow of nitrogen gas. The ZnO QDs ETL was deposited using a spin coating technique at 2000 rpm for 40 s. The resultant film was dried at 110°C for 10 min, and this deposition was repeated multiple times to achieve a thickness of ~35 nm. Finally, the ZnO QDs film was annealed at 200°C for 30 min in an ambient air atmosphere to work efficiently as an ETL for the

OSCs. Two separate active layer solutions were prepared for the fabrication of two types of BHJ OSCs. The first active layer solution was prepared by blending p-type PCDTBT (5 mg ml^{-1}dissolved in dichlorobenzene) and n-type $PC_{61}BM$(15 mg ml^{-1}dissolved in chloroform). The solution for the second active layer was prepared by mixing 1 ml of each separate solution of PCDTBT (15 mg ml^{-1} in dichlorobenzene), $PC_{61}BM$ (30 mg ml^{-1} in chloroform), and CdSe QDs(15 mg ml^{-1} in chloroform). Initially, the solution of PCDTBT was stirred using a magnetic bead. Subsequently, the solutions of $PC_{61}BM$ and CdSe QDs were added to the solution of PCDTBT with continuous stirring for 24 h. The obtained ternary solution was well dispersed in 3 ml (20 mg ml^{-1}).

The mixing of an equivalent amount of CdSe QDs to the p-type polymer resulted in the best charge transportation [108]. Both prepared active layer solutions were continuously stirred overnight to get the evenly mixed solutions. Further, the prepared solutions were deposited upon ZnO QDs coated substrate for the identical thickness of the active layer and heated at 120°C in the oven under a nitrogen environment for 30 min. Over the active layer, an HTL layer of 10 nm thin MoO_3 was deposited using the thermal evaporation unit (FL400 SMART COAT 3.0 A from Hind High Vacuum, India) at a vacuum level of $\sim 3 \times 10^{-6}$ mbar and a constant rate of 0.1 Å s^{-1}. Finally, a circular electrode of Ag having a diameter of 2 mm and a thickness of 100 nm was deposited using a shadow masking technique inside the thermal evaporation unit. The two different types of device structures, namely binary and ternary, were fabricated as ITO/ ZnO QDs/PCDTBT:$PC_{61}BM$/MoO_3/Ag and ITO/ZnO QDs/PCDTBT:$PC_{61}BM$:CdSe QDs/MoO_3/Ag, respectively. Diagrams of the fabricated BHJ OSCs are shown in Figure 4.2.

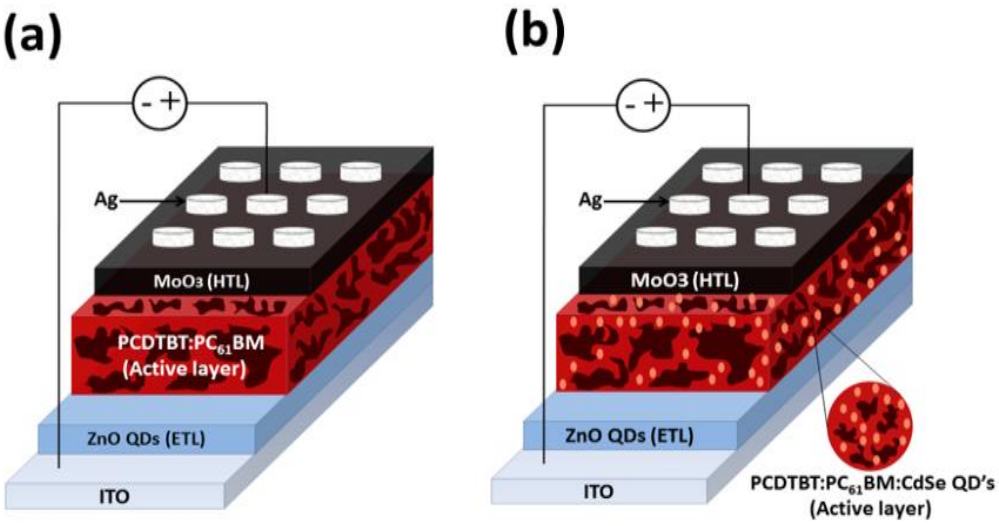

Figure 4.2: Device structure (a) Binary OSC without CdSe QDs (b) Ternary OSC with CdSe QDs.

4.2.3 Film and Device Characterization

The absorption spectra of the devices were carried out by using a UV/VIS spectrophotometer (Model V-730 from Jesco, Japan). The spectrometer (FLS 980 from Edinburgh Instruments, UK) was used to measure the photoluminescence (PL) of the devices. The semiconductor parameter analyzer (Model B1500A from Keysight, USA) was used to obtain the electrical characterization (current density vs. voltage, *J-V*). The standard 1 sunlight was obtained by using a solar simulator (Model SS50AAA, A.M. 1.5 G from Photo Emission Technology Inc., USA). Calibration of the 1 sunlight was assured by using a standard silicon reference cell (Model 60623) provided by Photo Emission Technology Inc., USA. The calculation of the external quantum efficiency (EQE) was done by using a monochromator (Model SP2150i from Princeton Instruments, USA) attached with a halogen lamp source.

4.3 Results and Discussion

In this section, the optical and electrical characteristics of fabricated

PCDTBT:$PC_{61}BM$:CdSe QDs based BHJ organic solar cell have been carried out to analyze the effect of CdSe QDs on PCDTBT:$PC_{61}BM$ based BHJ organic solar cell.

4.3.1 Optical Characterization

The effect of CdSe QDs loading in the absorption of the active layer is analyzed in the wavelength range of 350 nm to 800 nm. The absorption spectra of the ZnO QDs thin film, CdSe QDs thin film, ZnO QDs/PCDTBT:$PC_{61}BM$ stacked thin film, and ZnO QDs/PCDTBT:PC6$_1$BM:CdSe QDs stacked thin films are shown in Figure 4.3. Most of the visible spectrum passed through the ZnO QDs layer and absorbed by the active layer. The absorption in ZnO QDs/ PCDTBT:$PC_{61}BM$:CdSe QDs is slightly higher than that of ZnO QDs/ PCDTBT:$PC_{61}BM$ due to increased absorption in CdSe QDs around 515 nm shown in figure 4.3 [141]. In order to understand the charge transfer phenomena between PCDTBT and $PC_{61}BM$ by incorporating the CdSe QDs, photoluminescence (PL) characteristics have been determined in the wavelength range of 600 to 850 nm. Figure 4.4 exhibits the PL spectra of the active layer PCDTBT:$PC_{61}BM$ and PCDTBT:$PC_{61}BM$:CdSe QDs. The maximum excitation peak has been observed at 460 nm, shown in the inset of Figure 4.4. PCDTBT:$PC_{61}BM$ exhibits the maximum PL peak around 700 nm when excited at 460 nm. After mixing of CdSe QDs in the active layer, a considerable quenching of the peak around 700 nm has been observed. This quenching of the peak around 700 nm when CdSe QDs are added to PCDTBT:$PC_{61}BM$, suggests that the incorporation of CdSe QDs facilitates the improved charge transfer from PCDTBT to $PC_{61}BM$ through CdSe QDs [142].

This enhancement in the charge transfer rate could be attributed to the larger interfacial area formed when CdSe QDs have been added to the PCDTBT:$PC_{61}BM$. The energy band diagram of the binary and ternary OSCs is shown in Figure 4.5. Figure 4.5 (a) and (b) clearly show that the electrons and hole are separated efficiently towards

respective electrodes supported by ZnO QDs ETL and MoO_3 HTL. The charge transport in PCDTBT:$PC_{61}BM$ binary films occurs from PCDTBT to $PC_{61}BM$. Since the energy band levels of CdSe QDs lie in between those of PCDTBT and $PC_{61}BM$, the charge transport in PCDTBT:$PC_{61}BM$:CdSe QDs occurs through CdSe QDs as shown in Figure 4.6. The incorporation of CdSe QDs thus provides a better band alignment. As a result, the extra charge carriers generated in PCDTBT under solar light illumination are easily transported via a two-step process due to CdSe QDs as demonstrated in Figure 4.6.

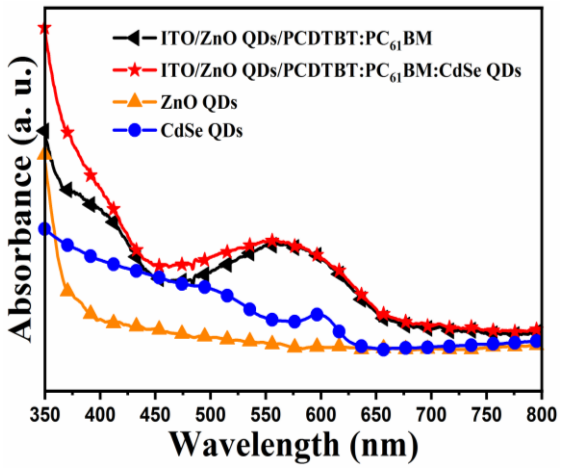

Figure 4.3: The absorbance in ZnO QDs thin film, CdSe QDs thin film, ZnO QDs/PCDTBT:$PC_{61}BM$ and, ZnO QDs/PCDTBT:$PC_{61}BM$:CdSe QDs.

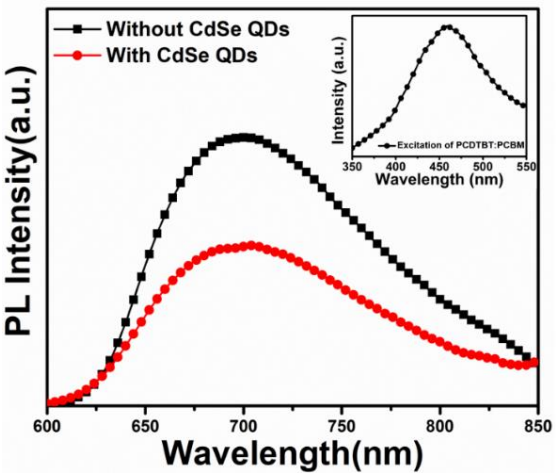

Figure 4.4: Photoluminescence (PL) spectra of PCDTBT:$PC_{61}BM$ and PCDTBT:$PC_{61}BM$:CdSe QDs.

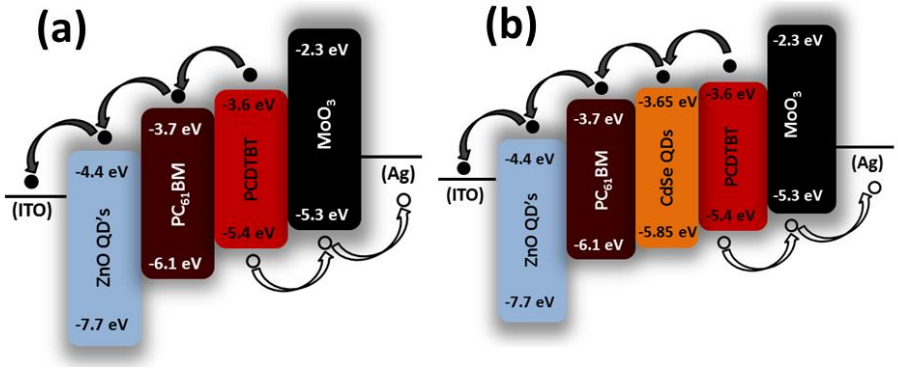

Figure 4.5: Energy band diagram (a) Binary OSC without CdSe QDs, and (b) Ternary OSC with CdSe QDs.

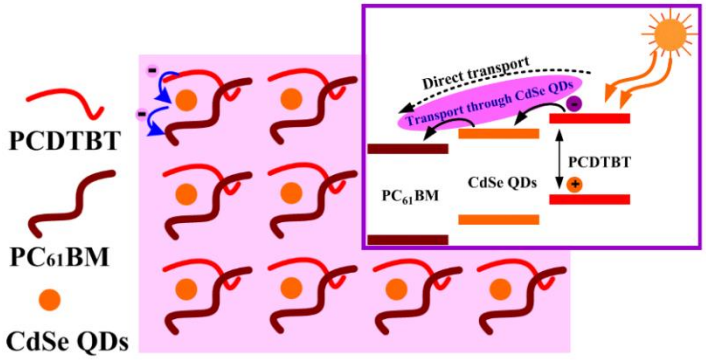

Figure 4.6: Ternary thin film made of PCDTBT, $PC_{61}BM$, and CdSe QDs. The charge carrier transport through CdSe QDs due to better band alignment.

To further understand the optical behaviour of both the OSC devices, the EQE has been plotted with respect to the wavelength ranging from 300 to 750 nm and shown in Figure 4.7. The calculation of the EQE has been completed using the relation described in [143].

$$\mathrm{EQE} = 1240 \times \left(\frac{R}{\lambda}\right) \times 100\ \% \qquad (4.1)$$

Where "R" and "λ" represent the responsivity and wavelength of the device, respectively.

Considerable enhancement has been found in the EQE of the ternary OSC (with CdSe QDs) as compared to the binary OSC (without CdSe QDs). The incorporation of CdSe

QDs in PCDTBT:$PC_{61}BM$ leads to a larger interfacial area which improves the charge transportation/extraction capability and thus improved external quantum efficiency (EQE), clearly shown in Figure 4.7.

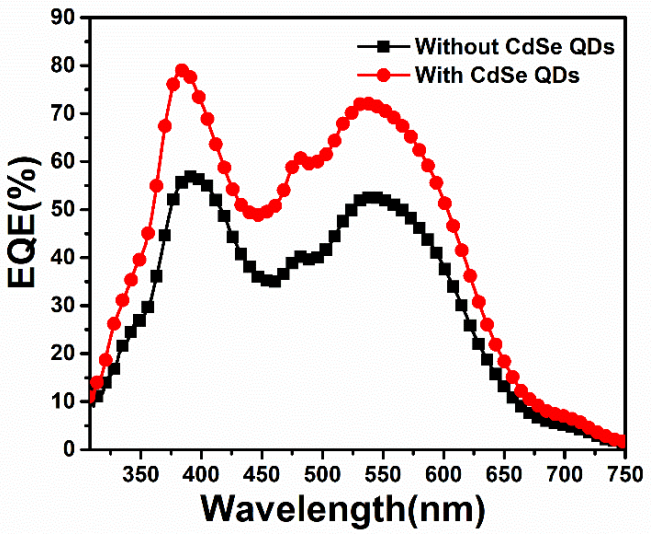

Figure 4.7: The external quantum efficiency of the fabricated binary and ternary OSC devices.

4.3.2 Electrical Characterization

To analyze the electrical behavior of the BHJ OSCs, the current density versus voltage (J-V) characteristics of both the binary and ternary OSC devices under 1 sun

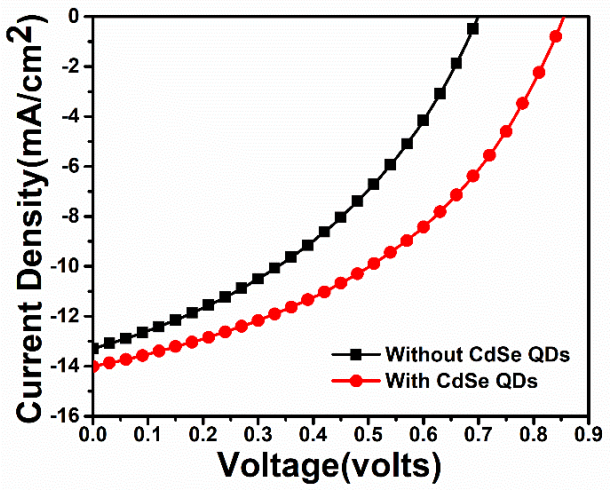

Figure 4.8: J-V characteristics of the fabricated binary and ternary OSCs.

illumination have been carried out and is shown in Figure 4.8. The calculated short

circuit current density (J_{SC}) and open-circuit voltage (V_{OC}) from the measured J-V characteristic of the binary OSC are 13.30 mA/cm^2 and 699 mV, respectively. Whereas the values of J_{SC} and V_{OC} are 14 mA/cm^2 and 854 mV for the ternary OSC. This significant enhancement in the photovoltaic parameter J_{SC} is attributed to the better charge transportation from PCDTBT to $PC_{61}BM$ via CdSe QDs in the ternary OSC [144]. We know that the V_{OC} of organic solar cells mainly depends on the energy difference (offset) between the lowest unoccupied molecular orbital (LUMO) level of the acceptor and the highest occupied molecular orbital (HOMO) level of the donor [40], [145]. Therefore, this improvement in the V_{OC} from 699 to 854 mV by the synergistic effect of CdSe QDs and $PC_{61}BM$ is due to the energy offset enhancement which could be seen clearly in the energy band diagram in Figure 4.5. All other photovoltaic parameters of the devices are detailed in table 4.1.

Table 4.1: Photovoltaic parameters of the binary and ternary OSCs.

Structure	J_{SC} (mA/cm^2)	V_{OC} (mV)	Fill Factor (FF)	PCE (%)
Binary	13.30	699	0.39	3.62
Ternary	14	854	0.42	5.02

The charge transport in the fabricated device structures has been investigated using impedance spectroscopy. Impedance spectroscopy in the frequency range of 1 kHz to 1 MHz is performed to understand the charge transportation and recombination mechanism. The Nyquist plots obtained under 1 sun illumination and operated at their open-circuit voltages for both the fabricated devices are shown in Figure 4.9. Both the devices show the semicircles, which correspond to the equivalent circuit shown in the inset of Figure 4.9. The ternary OSC shows the smaller semicircle, which implies better charge transportation from PCDTBT to the $PC_{61}BM$ via CdSe QDs is taking place.

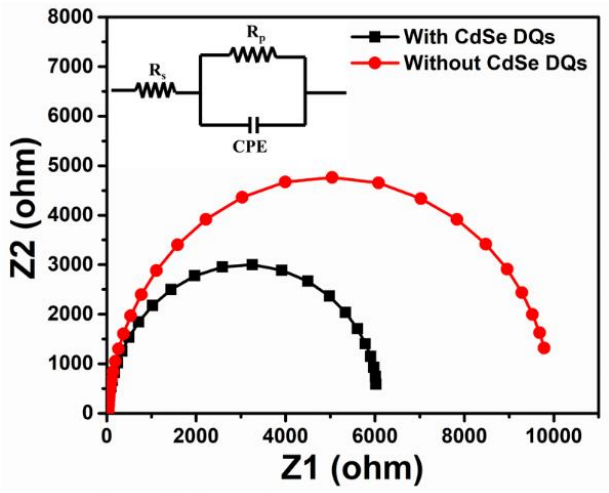

Figure 4.9: Nyquist plot of binary and ternary OSC devices under 1 sun illumination at zero applied voltage.

In order to extend some more depth of the charge transportation phenomena between donor and acceptor, the imaginary impedance Z_2 vs. frequency graph has been plotted. This plot gives an idea about the relaxation frequency of most resistive phenomena, and this relaxation frequency (fmax) is universally proportional to the relaxation time (τ) (fmax α1/ τ). Relaxation time (τ) gives an idea about the charge transfer rate between the donor and acceptor interface in the active material. The relaxation time must be as low as possible for better dissociation of excitons between donor and acceptor and thus better charge transportation [142], [146]. Figure 4.10 clearly shows that the ternary BHJ OSC exhibits a peak (relaxation frequency- fmax) shift towards the higher frequency region, which confirms that it has a lower relaxation time and thus better charge transportation as compared to the binary BHJ OSC. Now, Figure 4.11 shows the frequency-dependent real part of the impedance, which corresponds to the Rp shown in the inset of Figure 4.9. In Figure 4.11, the ternary OSC shows the lower value of impedance in the frequency ranging from 1000 to 15000 kHz compared to the binary BHJ OSC, which implies that the ternary BHJ OSC provides the better interface between donor and acceptor [146] and so better charge transportation.

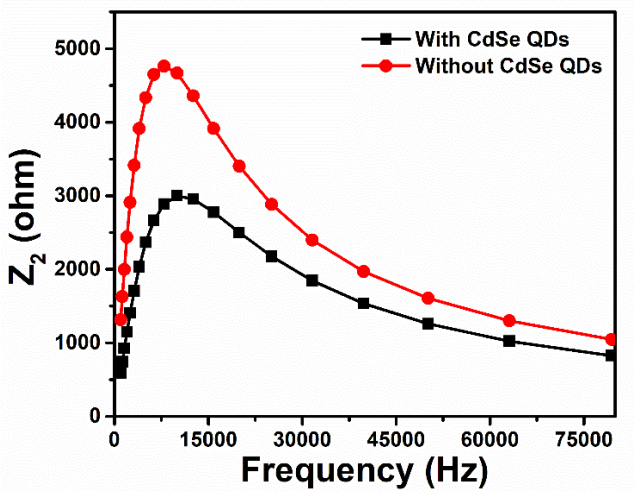

Figure 4.10: Frequency vs. imaginary part of impedance (Z_2) of the binary and ternary OSC devices.

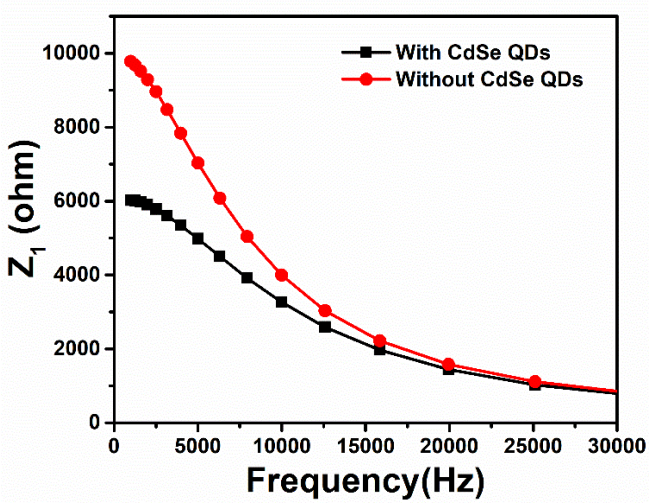

Figure 4.11: Frequency vs. real part of impedance (Z_1) of the binary and ternary OSC devices.

4.4 Conclusion

The photovoltaic performance of PCDTBT:$PC_{61}BM$ and PCDTBT:$PC_{61}BM$:CdSe QDs based binary and ternary OSCs have been investigated in this chapter. The charge transportation and photoabsorption in the photoactive thin layer of PCDTBT:$PC_{61}BM$ are tailored using the mixing of colloidal QDs of CdSe. The synergistic effect of CdSe QDs and $PC_{61}BM$ results in enhanced photoabsorption and charge transportation of the active layer of the device. The binary BHJ OSC fabricated in ITO/ZnO QDs/PCDTBT:$PC_{61}BM$/MoO3/Ag and the ternary BHJ OSC fabricated in ITO/ZnO

QDs/PCDTBT:$PC_{61}BM$:CdSe QDs/MoO3/Ag structures are characterized under the light of 1 sun. It has been found that the ternary BHJ OSC has better photovoltaic parameters compared to the binary BHJ OSC. The blending of CdSe QDs with PCDTBT:$PC_{61}BM$ improves J_{SC} from 13.30 to 14 mA/cm^2, V_{OC} from 699 to 854 mV, and the PCE from 3.62 to 5.02% due to enhanced charge transportation. The impedance measurements are used to validate the effective charge transportation in the binary and ternary BHJ OSCs.

CHAPTER 5

Conclusion and Future Scope

Contents

CHAPTER 5

Conclusion and Future Scope

5.1 Introduction

The thesis is mainly focused on investigating and improving the photovoltaic performance parameters of the PCDTBT:PC_{61}MB-based bulk heterojunction organic solar cell (BHJ OSC) fabricated by low-cost solution process. This chapter includes the chapter-wise objectives and major findings of the thesis as described in the following section.

5.2 Chapter-Wise Major Observations

Chapter-1 introduces the inorganic/organic semiconductors and the charge transport phenomena involved with them. Different types of organic solar cell structures have been discussed. The bulk heterojunction (BHJ)-based organic solar cells (OSCs) have been discussed in detail. The working principle and photovoltaic parameters of the OSCs have also been introduced. A detailed literature survey on PCDTBT:PC_{61}BM and other related active layers based BHJ OSCs have been discussed. OSCs with an electron transport layers (ETL) of ZnO and a hole transport layer (HTL) of PEDOT:PSS, PQT-12, and MoO_3 have also been reviewed. Based on the research gaps observed from the literature survey, the scope of the thesis is outlined at the end of this chapter.

Chapter-2 reports the fabrication and characterization of PCDTBT:PC_{61}BM based BHJ OSCs. Two distinct BHJ OSCs with device structures of ITO/ZnO QDs (ETL)/PCDTBT:PC_{61}BM (Active layer)/PEDOT:PSS (HTL)/Ag and ITO/ZnO QDs (ETL)/PCDTBT:PC_{61}BM (Active layer)/PQT-12 (Interface layer)/PEDOT:PSS

(HTL)/Ag have been studied. The floating film transfer method (FTM) derived PQT-12 film is used as an interface layer in between the PCDTBT:$PC_{61}BM$ active layer and PEDOT:PSS HTL layer. The major observations and findings from the chapter are summarized below:

- The effect of the FTM-derived PQT-12 as an interface layer between PCDTBT:$PC_{61}BM$ and PEDOT:PSS has been investigated by analyzing the electrical as well as optical behaviour of the fabricated BHJ OSC.
- The electrical characterization has been performed by current-voltage and Nyquist plots, whereas the optical characterization has been performed by absorption, photoluminescence (PL), and external quantum efficiency plots.
- Insertion of FTM-derived PQT-12 as an interface layer results in improved photovoltaic parameters compare to the device without interface layer of PQT-12.
- Improvement in the photovoltaic parameters such as short circuit density (Jsc) from 5.12 to 5.62 mA/cm^2, open-circuit voltage (Voc) from 419 to 562 mV, and fill factor from 0.24 to 0.33 are observed and attributed to the enhancement in charge transportation as well as absorption due to insertion of PQT-12 as an interface layer.
- Although the photovoltaic parameters (power conversion efficiency from 0.53 to 1.05 %) have been improved, the OSC's performance is still low, and hence further enhancement is needed.

Chapter-3 investigates the effects of the thicknesses of the ZnO QDs ETL and PQT-12 HTL on the performance of the ITO/ZnO QDs/PCDTBT:$PC_{61}BM$/ PQT-12/Ag based BHJ OSC. The PQT-12 film is grown by the floating-film transfer method (FTM)

while the colloidal ZnO QDs have been used for the ETL as discussed in Chapter-2. The major findings of this chapter are summarized as follows:

- PQT-12 used as HTL layer in the ITO/ZnO QDs/PCDTBT:$PC_{61}BM$/PQT-12/Ag shows better performance over the ITO/ZnO QDs/PCDTBT:$PC_{61}BM$/ PEDOT:PSS /Ag device considered in Chapter-2. This shows that FTM based PQT-12 can act as a better HTL material than the PEDOT:PSS in the BHJ OSCs.
- The performance parameters for different thicknesses of solution-processed spin-coated ZnO ETL and FTM-derived PQT-12 HTL have been investigated. Based on the results, the best suitable values of the ZnO QDs ETL and PQT-12 thicknesses have been obtained for the ITO/ZnO QDs/PCDTBT:$PC_{61}BM$/PQT-12/Ag BHJ OSC under study.
- The ZnO QDs ETL of 35 nm and PQT-12 HTL of 20 nm thicknesses show the best photovoltaic parameters. It offers a short circuit current density (Jsc) of 10.42 mA/cm^2, open-circuit voltage (Voc) of 672 mV, fill factor of 0.38, and power conversion efficiency of 2.66 %. The above results are much higher than those obtained for other values of the thicknesses the ETL and HTL of the OSC under study.
- The maximum obtained power conversion efficiency with the 35 nm of ZnO QDs ETL and 20 nm of PQT-12 HTL is 2.66 %. It is relatively low which opens up the opportunities for further improvement.

Chapter-4 investigates the performance of the CdSe QDs:PCDTBT:$PC_{61}BM$ based inorganic-organic hybrid Nano composites based BHJ OSC. The performance parameters of ITO/ZnO QDs/PCDTBT:$PC_{61}BM$/MoO_3/Ag and ITO/ZnO

QDs/PCDTBT:$PC_{61}BM$:CdSe QDs/MoO_3/Ag based BHJ OSCs have been compared. The ZnO QDs and MoO_3 are used as the ETL and HTL, respectively in these structures. The major observations and findings from the chapter are summarized below:

- The proposed PCDTBT:$PC_{61}BM$:CdSe QDs active layer based BHJ OSC of ITO/ZnO QDs/PCDTBT:$PC_{61}BM$: CdSe QDs/MoO_3/Ag structure shows better photovoltaic parameters over the ITO/ZnO QDs/PCDTBT:$PC_{61}BM$/ PQT-12/Ag structure studied in Chapter-3.
- The electrical and optical characterizations have been carried out to investigate the synergistic effect of CdSe QDs and PCDTBT:$PC_{61}BM$ in the photoactive layer to improve the performance of the BHJ OSCs.
- Significant improvement in the photovoltaic parameters such as short circuit density (Jsc) from 13.30 mA/cm^2 to 14 mA/cm^2, open-circuit voltage (Voc) from 699 mV to 854 mV, and fill factor from 0.38 to 0.42 have been observed when PCDTBT:$PC_{61}BM$ is replaced by PCDTBT:$PC_{61}BM$:CdSe QDs as the active layer in the BHJ OSC structure under study.
- The proposed ITO/ZnO QDs/PCDTBT:$PC_{61}BM$:CdSe QDs/MoO_3/Ag BHJ OSC shows the maximum power conversion efficiency of 5.02 % which is much higher than that of the PCDTBT:$PC_{61}BM$ based BHJ OSCs considered in Chapter-2 and Chapter-3.

5.3 Future Scope of Work

Based on the research expertise gained through the works carried out in the present thesis, some scopes of future research in the related area can be outlined as follows:

- PCDTBT:$PC_{61}BM$ bulk heterojunction organic solar cell may be fabricated on a flexible substrate such as polyamide, PET, PEN, etc.

- Various metal nanoparticles such as Au, Ag and Al, etc., may be used upon/under the PCDTBT:$PC_{61}BM$ film to produce a plasmonic effect to further enhance OSC performance.
- Different nanostructures, such as nanowires, nanorods, and nanotubes of metal oxides such as ZnO, TiO_2, MoO3, etc., may be used for transport layers, which may improve the optical property of the PCDTBT:$PC_{61}BM$ based BHJ OSC.
- Another donor polymer may be mixed with the PCDTBT:$PC_{61}BM$ active layer for better collect solar spectrum range using ternary structure.
- Doped ZnO and MoO_3 may be used as ETL and HTL, respectively, in the PCDTBT:$PC_{61}BM$ based BHJ OSC to improve the charge transportation and hence performance of the OSC.

REFERENCES

[1] N. Girouard, E. Konialis, C. Tam, and P. Taylor, "OECD Green Growth Studies," 2012.

[2] "Electricity and the environment," *eia.gov*, 2018. [Online]. Available: https://www.eia.gov/energyexplained/electricity/electricity-and-the-environment.php.

[3] "Renewable Energy: Various Resources," *studymumbai.com*, 2018. [Online]. Available: https://www.studymumbai.com/renewable-energy-resources/.

[4] "Photosynthesis converts solar energy into chemical energy," *asknature.org*, 2018. [Online]. Available: https://asknature.org/strategy/photosynthesis-converts-solar-energy-into-chemical-energy/.

[5] W. W. Anderson and Y. G. Chai, "Becquerel effect solar cell," *Energy Convers.*, vol. 15, pp. 85–94, 1976.

[6] W. G. Adam and R.E.Day, "On the action of light on Selenium," *Nature*, vol. 13, no. 334, p. 407, 1876.

[7] W. Schottky, "Vereinfachte und erweiterte Theorie der Randschicht-gleichrichter," *Zeitschrift für Phys.*, vol. 118, pp. 539–592, 1941.

[8] M. A. Green, "Photovoltaics: Technology overview," *Energy Policy*, vol. 28, no. 14, pp. 989–998, 2000.

[9] D. M. Chapin, C. S. Fuller, and G. L. Pearson, "A new silicon p-n junction photocell for converting solar radiation into electrical power," *J. Appl. Phys.*, vol. 25, no. 5, pp. 676–677, 1954.

[10] M. Tao, "Inorganic photovoltaic solar cells: Silicon and beyond," *Electrochem.*

Soc. Interface, vol. 17, no. 4, pp. 30–35, 2008.

[11] K. P. Bhandari, J. M. Collier, R. J. Ellingson, and D. S. Apul, "Energy payback time (EPBT) and energy return on energy invested (EROI) of solar photovoltaic systems: A systematic review and meta-analysis," *Renew. Sustain. Energy Rev.*, vol. 47, pp. 133–141, 2015.

[12] H. Spanggaard and F. C. Krebs, "A brief history of the development of organic and polymeric photovoltaics," *Sol. Energy Mater. Sol. Cells*, vol. 83, no. 2–3, pp. 125–146, 2004.

[13] C. W. Tang, "Two-layer organic photovoltaic cell," *Appl. Phys. Lett.*, vol. 48, no. 2, pp. 183–185, 1986.

[14] H. Letheby, "On the Production of a Blue Substance by the Electrolysis of Sulphate of Aniline," *J. Chem. Soc.*, vol. 15, pp. 161–163, 1862.

[15] A. Köhler and B. Heinz, *Electronic Processes in Organic Semiconductors*. 2015.

[16] I. G. Hill, A. Kahn, Z. G. Soos, and R. A. Pascal, "Charge-separation energy in films of π -conjugated organic molecules," *Chem. Phys. Lett.*, vol. 327, pp. 181–188, 2000.

[17] X. Y. Zhao and H. J. Liu, "Review of polymer materials with low dielectric constant," *Polym. Int.*, vol. 59, no. 5, pp. 597–606, 2010.

[18] T. Xu and L. Yu, "How to design low bandgap polymers for highly efficient organic solar cells," *Mater. Today*, vol. 17, no. 1, pp. 11–15, 2014.

[19] M. Benghanem and A. Almohammedi, "Organic Solar Cells: A Review," *Adv. Struct. Mater.*, vol. 128, pp. 81–106, 2020.

[20] A. K. Ghosh, D. L. Morel, T. Feng, R. F. Shaw, and C. A. Rowe, "Photovoltaic and rectification properties of Al/Mg phthalocyanine/Ag schottky-barrier cells," *J. Appl. Phys.*, vol. 45, no. 1, pp. 230–236, 1974.

[21] D. Chirvase, Z. Chiguvare, M. Knipper, J. Parisi, V. Dyakonov, and J. C.

Hummelen, “Electrical and optical design and characterisation of regioregular poly(3-hexylthiophene-2,5diyl)/fullerene-based heterojunction polymer solar cells,” *Synth. Met.*, vol. 138, pp. 299–304, 2003.

[22] A. Ltaief, J. Davenas, A. Bouazizi, R. Ben Chaa, P. Alcouffe, and H. Ben Ouada, “Film morphology effects on the electrical and optical properties of bulk heterojunction organic solar cells based on MEH-PPV / C 60 composite,” *Mater. Sci. Eng.*, vol. 25, pp. 67–75, 2005.

[23] T. Martens, T. Munters, Z. Beelen, L. Goris, J. Manca, D. Vanderzande, L. De Schepper, and R. Andriessen, “Disclosure of the nanostructure of MDMO-PPV : PCBM bulk hetero-junction organic solar cells by a combination of SPM and TEM,” *Synth. Met.*, vol. 138, pp. 243–247, 2003.

[24] P. Vemulamada, G. Hao, T. Kietzke, and A. Sellinger, “Efficient bulk heterojunction solar cells from regio-regular- poly(3,3‴-didodecyl quaterthiophene)/PC70BM blends,” *Org. Electron.*, vol. 9, no. 5, pp. 661–666, 2008.

[25] N. Yeh and P. Yeh, “Organic solar cells: Their developments and potentials,” *Renew. Sustain. Energy Rev.*, vol. 21, pp. 421–431, 2013.

[26] Y. Zhang, E. Bovill, J. Kingsley, A. R. Buckley, H. Yi, A. Iraqi, T. Wang, and D. G. Lidzey, “PCDTBT based solar cells: one year of operation under real-world conditions.,” *Sci. Rep.*, vol. 6, p. 21632, 2016.

[27] S. M. Ryno, M. K. Ravva, X. Chen, H. Li, and J. L. Brédas, “Molecular Understanding of Fullerene – Electron Donor Interactions in Organic Solar Cells,” *Adv. Energy Mater.*, vol. 7, no. 10, pp. 1–22, 2017.

[28] U. Vongsaysy, D. M. Bassani, L. Servant, B. Pavageau, G. Wantz, and H. Aziz, “Formulation strategies for optimizing the morphology of polymeric bulk heterojunction organic solar cells: a brief review,” *J. Photonics Energy*, vol. 4, no. 1, p. 040998, 2014.

[29] L. Zhu, M. Zhang, G. Zhou, T. Hao, J. Xu, J. Wang, C. Qiu, N. Prine, J. Ali, W. Feng, X. Gu, Z. Ma, Z. Tang, H. Zhu, L. Ying, Y. Zhang, and F. Liu, "Efficient Organic Solar Cell with 16.88% Efficiency Enabled by Refined Acceptor Crystallization and Morphology with Improved Charge Transfer and Transport Properties," *Adv. Energy Mater.*, vol. 10, no. 18, pp. 1–9, 2020.

[30] A. Opitz, R. Banerjee, S. Grob, M. Gruber, A. Hinderhofer, U. Hörmann, J. Kraus, T. Linderl, C. Lorch, A. Steindamm, A. K. Topczak, A. Wilke, N. Koch, J. Pflaum, F. Schreiber, and W. Brütting, "Charge separation at nanostructured molecular donor–Acceptor interfaces," *Adv. Polym. Sci.*, vol. 272, pp. 77–108, 2017.

[31] S. Tiwari, T. Tiwari, S. A. Carter, J. C. Scott, and J. V. Yakhmi, "Advances in polymer-based photovoltaic cells: Review of pioneering materials, design, and device physics," in *Handbook of Ecomaterials*, vol. 2, 2019, pp. 1055–1101.

[32] M. A. A. Suzon, "Pathways towards efficiency improvement of Kesterite based solar cell," 2019.

[33] D. R. Kozub, K. Vakhshouri, S. V. Kesava, C. Wang, A. Hexemer, and E. D. Gomez, "Direct measurements of exciton diffusion length limitations on organic solar cell performance," *Chem. Commun.*, vol. 48, no. 47, pp. 5859–5861, 2012.

[34] J. L. Brédas, J. E. Norton, J. Cornil, and V. Coropceanu, "Molecular understanding of organic solar cells: The challenges," *Acc. Chem. Res.*, vol. 42, no. 11, pp. 1691–1699, 2009.

[35] K. Ellmer, "Past achievements and future challenges in the development of optically transparent electrodes," *Nat. Photonics*, vol. 6, no. 12, pp. 809–817, 2012.

[36] A. Andersson, N. Johansson, P. Bröms, N. Yu, D. Lupo, and W. R. Salaneck, "Fluorine tin oxide as an alternate to indium tin oxide in polymer LEDs," *Adv. Mater.*, vol. 10, no. 11, pp. 859–863, 1998.

[37] H. Ishii, K. Sugiyama, E. Ito, and K. Seki, "Energy level alignment and interfacial electronic structures at organic/metal and organic/organic interfaces," *Adv. Mater.*, vol. 11, no. 8, pp. 605–625, 1999.

[38] R. Po, C. Carbonera, A. Bernardi, and N. Camaioni, "The role of buffer layers in polymer solar cells," *Energy Environ. Sci.*, vol. 4, no. 2, pp. 285–310, 2011.

[39] M. Diantoro, T. Suprayogi, A. Hidayat, A. Taufiq, A. Fuad, and R. Suryana, "Shockley's equation fit analyses for solar cell parameters from I-V curves," *Int. J. Photoenergy*, vol. 2018, p. 9214820, 2018.

[40] N. K. Elumalai and A. Uddin, "Open circuit voltage of organic solar cells: An in-depth review," *Energy Environ. Sci.*, vol. 9, no. 2, pp. 391–410, 2016.

[41] B. Qi and J. Wang, "Fill factor in organic solar cells," *Phys. Chem. Chem. Phys.*, vol. 15, no. 23, pp. 8972–8982, 2013.

[42] O. Dupré, B. Niesen, S. De Wolf, and C. Ballif, "Field Performance versus Standard Test Condition Efficiency of Tandem Solar Cells and the Singular Case of Perovskites/Silicon Devices," *J. Phys. Chem. Lett.*, vol. 9, no. 2, pp. 446–458, 2018.

[43] M. Hiramoto and Y. Shinmura, "Organic Solar Cells," in *Springer Handbook of Electronic and Photonic Materials*, 2017, pp. 1329–1338.

[44] W. H. Simpson, "Electrical Characteristics of Chlorophyll a films," *Discuss. Faraday Soc.*, vol. 51, pp. 288–292, 1971.

[45] V. Y. Merritt and H. J. Hovel, "Organic solar cells of hydroxy squarylium," *Appl. Phys. Lett.*, vol. 29, no. 7, pp. 414–415, 1976.

[46] A. K. Ghosh and T. Feng, "Merocynanine organic solar cells," *J. Appl. Phys.*, vol. 49, no. 12, pp. 5982–5989, 1978.

[47] M. Hiramoto, H. Fujiwara, and M. Yokoyama, "Three-layered organic solar cell with a photoactive interlayer of codeposited pigments," *Appl. Phys. Lett.*, vol. 58,

no. 10, pp. 1062–1064, 1991.

[48] M. Hiramoto, H. Fujiwara, and M. Yokoyama, "P-I-N Like Behavior in Three-Layered Organic Solar Cells Having a Co-Deposited Interlayer of Pigments," *J. Appl. Phys.*, vol. 72, no. 8, pp. 3781–3787, 1992.

[49] N. S. Sariciftci, D. Braun, C. Zhang, V. I. Srdanov, A. J. Heeger, G. Stucky, and F. Wudl, "Semiconducting polymer-buckminsterfullerene heterojunctions: Diodes, photodiodes, and photovoltaic cells," *Appl. Phys. Lett.*, vol. 62, no. 6, pp. 585–587, 1993.

[50] J. B. Whitlock, "Investigations of materials and device structures for organic semiconductor solar cells," *Opt. Eng.*, vol. 32, no. 8, p. 1921, 1993.

[51] G. Yu, J. Gao, J. C. Hummelen, F. Wudl, and A. J. Heeger, "Polymer photovoltaic cells: Enhanced efficiencies via a network of internal donor-acceptor heterojunctions," *Am. Assoc. Adv. Sci.*, vol. 270, no. 5243, p. 1789, 1995.

[52] C. Y. Yang and A. J. Heeger, "Morphology of composites of semiconducting polymers mixed with C60," *Synth. Met.*, vol. 83, no. 2, pp. 85–88, 1996.

[53] L. Chen, D. Godovsky, O. Inganäs, J. C. Hummelen, R. A. J. Janssens, M. Svensson, and M. R. Andersson, "Polymer photovoltaic devices from stratified multilayers of donor-acceptor blends," *Adv. Mater.*, vol. 12, no. 18, pp. 1367–1370, 2000.

[54] F. Padinger, D. Gebeyehu, C. J. Brabec, T. Fromherz, N. S. Sariciftci, and J. C. Hummelen, "The interconnection between efficiency and morphology of two component systems in plastic solar cells," *Mater. Res. Soc. Symp. - Proc.*, vol. 598, pp. 1–6, 2000.

[55] T. Fromherz, F. Padinger, D. Gebeyehu, C. Brabec, J. C. Hummelen, and N. S. Sariciftci, "Comparison of photovoltaic devices containing various blends of polymer and fullerence derivatives," *Sol. Energy Mater. Sol. Cells*, vol. 63, no. 1,

pp. 61–68, 2000.

[56] I. Riedel and V. Dyakonov, “Influence of electronic transport properties of polymer-fullerene blends on the performance of bulk heterojunction photovoltaic devices,” *Phys. Status Solidi Appl. Res.*, vol. 201, no. 6, pp. 1332–1341, 2004.

[57] A. P. Yuen, A. M. Hor, S. M. Jovanovic, J. S. Preston, R. A. Klenkler, N. M. Bamsey, and R. O. Loutfy, “Improved stability of solution processed photovoltaic devices using PQT-12,” *Sol. Energy Mater. Sol. Cells*, vol. 94, no. 12, pp. 2455–2458, 2010.

[58] N. Blouin, A. Michaud, and M. Leclerc, “A low-bandgap poly(2,7-carbazole) derivative for use in high-performance solar cells,” *Adv. Mater.*, vol. 19, no. 17, pp. 2295–2300, 2007.

[59] X. Yang and A. Uddin, “Effect of thermal annealing on P3HT:PCBM bulk-heterojunction organic solar cells: A critical review,” *Renew. Sustain. Energy Rev.*, vol. 30, pp. 324–336, 2014.

[60] O. A. Abdulrazzaq, V. Saini, S. Bourdo, E. Dervishi, and A. S. Biris, “Organic solar cells: A review of materials, limitations, and possibilities for improvement,” *Part. Sci. Technol.*, vol. 31, no. 5, pp. 427–442, 2013.

[61] S. Beaupré and M. Leclerc, “PCDTBT: En route for low cost plastic solar cells,” *J. Mater. Chem. A*, vol. 1, no. 37, pp. 11097–11105, 2013.

[62] K. Borse, R. Sharma, D. Gupta, and A. Yella, “Interface engineering through electron transport layer modification for high efficiency organic solar cells,” *RSC Adv.*, vol. 8, no. 11, pp. 5984–5991, 2018.

[63] M. T. Lloyd, C. H. Peters, A. Garcia, I. V. Kauvar, J. J. Berry, M. O. Reese, M. D. McGehee, D. S. Ginley, and D. C. Olson, “Influence of the hole-transport layer on the initial behavior and lifetime of inverted organic photovoltaics,” *Sol. Energy Mater. Sol. Cells*, vol. 95, no. 5, pp. 1382–1388, 2011.

[64] R. Steim, F. R. Kogler, and C. J. Brabec, “Interface materials for organic solar

cells," *J. Mater. Chem.*, vol. 20, no. 13, pp. 2499–2512, 2010.

[65] J. You, C. C. Chen, L. Dou, S. Murase, H. S. Duan, S. A. Hawks, T. Xu, H. J. Son, L. Yu, G. Li, and Y. Yang, "Metal oxide nanoparticles as an electron-transport layer in high-performance and stable inverted polymer solar cells," *Adv. Mater.*, vol. 24, no. 38, pp. 5267–5272, 2012.

[66] V. Shrotriya, G. Li, Y. Yao, C. W. Chu, and Y. Yang, "Transition metal oxides as the buffer layer for polymer photovoltaic cells," *Appl. Phys. Lett.*, vol. 88, no. 7, p. 073508, 2006.

[67] S. Chen, J. R. Manders, S. W. Tsang, and F. So, "Metal oxides for interface engineering in polymer solar cells," *J. Mater. Chem.*, vol. 22, no. 46, pp. 24202–24212, 2012.

[68] H. O. Seo, S. Y. Park, W. H. Shim, K. D. Kim, K. H. Lee, M. Y. Jo, J. H. Kim, E. Lee, D. W. Kim, Y. D. Kim, and D. C. Lim, "Ultrathin TiO2 films on ZnO electron-collecting layers of inverted organic solar cell," *J. Phys. Chem. C*, vol. 115, no. 43, pp. 21517–21520, 2011.

[69] H. Sun, J. Weickert, H. C. Hesse, and L. Schmidt-Mende, "UV light protection through TiO2 blocking layers for inverted organic solar cells," *Sol. Energy Mater. Sol. Cells*, vol. 95, no. 12, pp. 3450–3454, 2011.

[70] F. J. Lim, K. Ananthanarayanan, J. Luther, and G. W. Ho, "Influence of a novel fluorosurfactant modified PEDOT:PSS hole transport layer on the performance of inverted organic solar cells," *J. Mater. Chem.*, vol. 22, no. 48, pp. 25057–25064, 2012.

[71] M. S. White, D. C. Olson, S. E. Shaheen, N. Kopidakis, and D. S. Ginley, "Inverted bulk-heterojunction organic photovoltaic device using a solution-derived ZnO underlayer," *Appl. Phys. Lett.*, vol. 89, no. 14, p. 143517, 2006.

[72] T. Hori, H. Moritou, N. Fukuoka, J. Sakamoto, A. Fujii, and M. Ozaki, "Photovoltaic properties in interpenetrating heterojunction organic solar cells

utilizing MoO3 and ZnO charge transport buffer layers," *Materials (Basel).*, vol. 3, no. 11, pp. 4915–4921, 2010.

[73] S. Kundu, S. R. Gollu, R. Sharma, G. Srinivas, A. Ashok, A. R. Kulkarni, and D. Gupta, "Device stability of inverted and conventional bulk heterojunction solar cells with MoO3 and ZnO nanoparticles as charge transport layers," *Org. Electron.*, vol. 14, no. 11, pp. 3083–3088, 2013.

[74] B. H. Hoppe, M. Niggemann, C. Winder, J. Kraut, R. Hiesgen, A. Hinsch, D. Meissner, and N. S. Sariciftci, "Nanoscale Morphology of Conjugated Polymer / Fullerene-Based Bulk-Heterojunction Solar Cells," *Adv. Funct. Mater.*, vol. 14, no. 10, pp. 1005–1011, 2004.

[75] M. Wright, R. Lin, M. J. Y. Tayebjee, and G. Conibeer, "Effect of Blend Composition on Bulk Heterojunction Organic Solar Cells: A Review," *Sol. RRL*, vol. 1, pp. 1–31, 2017.

[76] S. Alem, T.-Y. Chu, S. C. Tse, S. Wakim, J. Lu, R. Movileanu, Y. Tao, F. Bélanger, D. Désilets, S. Beaupré, M. Leclerc, S. Rodman, D. Waller, and R. Gaudiana, "Effect of mixed solvents on PCDTBT:PC70BM based solar cells," *Org. Electron.*, vol. 12, no. 11, pp. 1788–1793, 2011.

[77] T. M. Clarke, J. Peet, A. Nattestad, N. Drolet, G. Dennler, C. Lungenschmied, M. Leclerc, and A. J. Mozer, "Charge carrier mobility, bimolecular recombination and trapping in polycarbazole copolymer: Fullerene (PCDTBT:PCBM) bulk heterojunction solar cells," *Org. Electron.*, vol. 13, no. 11, pp. 2639–2646, 2012.

[78] J. S. Moon, J. Jo, and A. J. Heeger, "Nanomorphology of PCDTBT:PC70BM bulk heterojunction solar cells," *Adv. Energy Mater.*, vol. 2, no. 3, pp. 304–308, 2012.

[79] F. Etzold, I. A. Howard, R. Mauer, M. Meister, T. D. Kim, K. S. Lee, N. S. Baek, and F. Laquai, "Ultrafast exciton dissociation followed by nongeminate charge recombination in PCDTBT:PCBM photovoltaic blends," *J. Am. Chem. Soc.*, vol. 133, no. 24, pp. 9469–9479, 2011.

[80] T. Y. Chu, S. Alem, P. G. Verly, S. Wakim, J. Lu, Y. Tao, S. Beaupŕ, M. Leclerc, F. Ɓlanger, D. Ɗsilets, S. Rodman, D. Waller, and R. Gaudiana, "Highly efficient polycarbazole-based organic photovoltaic devices," *Appl. Phys. Lett.*, vol. 95, no. 6, p. 063304, 2009.

[81] E. L. Ratcliff, J. Meyer, K. X. Steirer, N. R. Armstrong, D. Olson, and A. Kahn, "Energy level alignment in PCDTBT:PC70BM solar cells: Solution processed NiOx for improved hole collection and efficiency," *Org. Electron. physics, Mater. Appl.*, vol. 13, no. 5, pp. 744–749, 2012.

[82] E. A. Parlak, T. AslTumay, N. Tore, Ş. Saroğlan, P. Kavak, and F. Türksoy, "Efficiency improvement of PCDTBT solar cells with silver nanoparticles," *Sol. Energy Mater. Sol. Cells*, vol. 110, pp. 58–62, 2013.

[83] M. Piralaee, Z. Ebrahimpour, and A. Asgari, "The improved performance of BHJ organic solar cells by random dispersed metal nanoparticles through the active layer," *Curr. Appl. Phys.*, vol. 20, no. 4, pp. 531–537, 2020.

[84] Y. Zhu, L. Yang, S. Zhao, Y. Huang, Z. Xu, Q. Yang, P. Wang, Y. Li, and X. Xu, "Improved performances of PCDTBT:PC $_{71}$ BM BHJ solar cells through incorporating small molecule donor," *Phys. Chem. Chem. Phys.*, vol. 17, no. 40, pp. 26777–26782, 2015.

[85] C. H. Peters, I. T. Sachs-Quintana, W. R. Mateker, T. Heumueller, J. Rivnay, R. Noriega, Z. M. Beiley, E. T. Hoke, A. Salleo, and M. D. McGehee, "The mechanism of burn-in loss in a high efficiency polymer solar cell," *Adv. Mater.*, vol. 24, no. 5, pp. 663–668, 2012.

[86] M. A. Faist, S. Shoaee, S. Tuladhar, G. F. A. Dibb, S. Foster, W. Gong, T. Kirchartz, D. D. C. Bradley, J. R. Durrant, and J. Nelson, "Understanding the reduced efficiencies of organic solar cells employing fullerene multiadducts as acceptors," *Adv. Energy Mater.*, vol. 3, no. 6, pp. 744–752, 2013.

[87] Y. H. Huh and B. Park, "Interface-engineering additives of poly(oxyethylene tridecyl ether) for low-band gap polymer solar cells consisting of

PCDTBT:PC70BM bulk-heterojunction layers," *Opt. Express*, vol. 21, p. 178491, 2013.

[88] B. C. Schroeder, Z. Li, M. A. Brady, G. C. Faria, R. S. Ashraf, C. J. Takacs, J. S. Cowart, D. T. Duong, K. H. Chiu, C.-H. Tan, J. T. Cabral, A. Salleo, M. L. Chabinyc, J. R. Durrant, and I. McCulloch, "Enhancing Fullerene-Based Solar Cell Lifetimes by Addition of a Fullerene Dumbbell," *Angew. Chemie*, vol. 126, no. 47, pp. 13084–13089, 2014.

[89] L. D'Olieslaeger, M. Pfannmöller, E. Fron, I. Cardinaletti, M. Van Der Auweraer, G. Van Tendeloo, S. Bals, W. Maes, D. Vanderzande, J. Manca, and A. Ethirajan, "Tuning of PCDTBT:PC71BM blend nanoparticles for eco-friendly processing of polymer solar cells," *Sol. Energy Mater. Sol. Cells*, vol. 159, pp. 179–188, 2017.

[90] T. Pratyusha, G. Sivakumar, A. Yella, and D. Gupta, "Novel Ternary Blend of PCDTBT, PCPDTBT and PC70BM for the Fabrication of Bulk Heterojunction Organic Solar Cells," *Mater. Today Proc.*, vol. 4, no. 4, pp. 5067–5073, 2017.

[91] M. T. Khan, V. Agrawal, A. Almohammedi, and V. Gupta, "Effect of traps on the charge transport in semiconducting polymer PCDTBT," *Solid. State. Electron.*, vol. 145, pp. 49–53, 2018.

[92] A. Aghassi and C. D. Fay, "Effects of IPA treatment on the photovoltaic performance of bulk heterojunction organic solar cells," *J. Phys. Chem. Solids*, vol. 130, pp. 136–143, 2019.

[93] S. Rafique, S. M. Abdullah, K. Sulaiman, and M. Iwamoto, "Fundamentals of bulk heterojunction organic solar cells : An overview of stability/degradation issues and strategies for improvement," *Renew. Sustain. Energy Rev.*, vol. 84, pp. 43–53, 2018.

[94] H. Yüksel Güney, Z. Avdan, and H. Yetkin, "Optimization of annealing temperature and the annealing effect on life time and stability of P3HT:PCBM-based organic solar cells," *Mater. Res. Express*, vol. 6, no. 4, p. 045103, 2019.

[95] S. K. Shah, K. Hayat, and K. Ali, “Effect of TiO2 interlayer on the performance of inverted polymeric solar cells,” *Mater. Res. Express*, vol. 6, no. 6, p. 065102, 2019.

[96] S. Lattante, “Electron and Hole Transport Layers: Their Use in Inverted Bulk Heterojunction Polymer Solar Cells,” *Electronics*, vol. 3, no. 1, pp. 132–164, 2014.

[97] A. Babusenan, S. Mondal, S. Ramaswamy, S. Dutta, M. Gopalakrishnan, and J. Bhattacharyya, “Investigation of non-linear dependence of exciton recombination efficiency on PCBM concentration in P3HT:PCBM blends,” *Mater. Res. Express*, vol. 6, no. 8, p. 085309, 2019.

[98] S. Savagatrup, A. D. Printz, T. F. O’Connor, A. V. Zaretski, D. Rodriquez, E. J. Sawyer, K. M. Rajan, R. I. Acosta, S. E. Root, and D. J. Lipomi, “Mechanical degradation and stability of organic solar cells: molecular and microstructural determinants,” *Energy Environ. Sci.*, vol. 8, pp. 55–80, 2015.

[99] P. Vanlaeke, a. Swinnen, I. Haeldermans, G. Vanhoyland, T. Aernouts, D. Cheyns, C. Deibel, J. D’Haen, P. Heremans, J. Poortmans, and J. V. Manca, “P3HT/PCBM bulk heterojunction solar cells: Relation between morphology and electro-optical characteristics,” *Sol. Energy Mater. Sol. Cells*, vol. 90, no. 14, pp. 2150–2158, 2006.

[100] S. Rafique, S. M. Abdullah, M. M. Shahid, M. O. Ansari, and K. Sulaiman, “Significantly improved photovoltaic performance in polymer bulk heterojunction solar cells with graphene oxide /PEDOT:PSS double decked hole transport layer,” *Sci. Rep.*, vol. 7, p. 39555, 2017.

[101] Y. Kumar, H. Kumar, G. Rawat, C. Kumar, and A. Sharma, “Colloidal ZnO Quantum Dots Based Spectrum Selective Ultraviolet Photodetectors,” *IEEE Photonics Technol. Lett.*, vol. 29, no. 4, pp. 361–364, 2017.

[102] Z. Hu, J. Zhang, Z. Hao, and Y. Zhao, “Influence of doped PEDOT:PSS on the performance of polymer solar cells,” *Sol. Energy Mater. Sol. Cells*, vol. 95, no.

10, pp. 2763–2767, 2011.

[103] Z. He, C. Zhong, S. Su, M. Xu, H. Wu, and Y. Cao, "Enhanced power-conversion efficiency in polymer solar cells using an inverted device structure," *Nat. Photonics*, vol. 6, no. 9, pp. 591–595, 2012.

[104] E. Vitoratos, S. Sakkopoulos, E. Dalas, N. Paliatsas, D. Karageorgopoulos, F. Petraki, S. Kennou, and S. A. Choulis, "Thermal degradation mechanisms of PEDOT : PSS," *Org. Electron.*, vol. 10, pp. 61–66, 2009.

[105] B. S. Ong, W. U. Yiliang, and P. Liu, "Design of high-performance regioregular polythiophenes for organic thin-film transistors," *Proc. IEEE*, vol. 93, no. 8, pp. 1412–1419, 2005.

[106] C. Kumar, G. Rawat, H. Kumar, Y. Kumar, S. Ratan, R. Prakash, and S. Jit, "Poly (3, 3'"-dialkylquaterthiophene) Based Flexible Nitrogen Dioxide Gas Sensor," *IEEE Sensors Lett.*, vol. 2, no. 1, p. 4500104, 2018.

[107] C. Kumar, G. Rawat, H. Kumar, Y. Kumar, R. Prakash, and S. Jit, "Flexible poly (3, 3'"- dialkylquaterthiophene) based interdigitated metal-semiconductor-metal ammonia gas sensor," *Sensors Actuators B Chem.*, vol. 255, pp. 203–209, 2018.

[108] C. Kumar, G. Rawat, H. Kumar, Y. Kumar, A. Kumar, R. Prakash, and S. Jit, "Electrical and Ammonia Gas Sensing Properties of PQT-12/CdSe Quantum Dots Composite Based Organic Thin Film Transistors," *IEEE Sens. J.*, vol. 18, no. 15, pp. 6085–6091, 2018.

[109] T. Morita, V. Singh, S. Nagamatsu, S. Oku, W. Takashima, and K. Kaneto, "Enhancement of Transport Characteristics in Poly(3-hexylthiophene) Films Deposited with Floating Film Transfer Method," *Appl. Phys. Express*, vol. 2, p. 111502, 2009.

[110] C. Kumar, G. Rawat, H. Kumar, Y. Kumar, R. Prakash, and S. Jit, "Electrical and Optical Characteristics of PQT-12 Based Organic TFTs Fabricated by Floating-Film Transfer Method," *IEEE Trans. Nanotechnol.*, vol. 17, no. 6, pp. 1111–

1117, 2018.

[111] M. Pandey, S. Nagamatsu, S. S. Pandey, S. Hayase, and W. Takashima, "Enhancement of carrier mobility along with anisotropic transport in non-regiocontrolled poly (3-hexylthiophene) films processed by floating film transfer method," *Org. Electron. physics, Mater. Appl.*, vol. 38, pp. 115–120, 2016.

[112] A. Dauendorffer, S. Nagamatsu, W. Takashima, and K. Kaneto, "Optical and transport anisotropy in poly(9,9'-dioctyl-fluorene-alt- bithiophene) films prepared by floating film transfer method," *Jpn. J. Appl. Phys.*, vol. 51, no. 5, p. 055802, 2012.

[113] C. Kumar, G. Rawat, H. Kumar, Y. Kumar, R. Prakash, and S. Jit, "Electrical and ammonia gas sensing properties of poly (3, 3‴-dialkylquaterthiophene) based organic thin film transistors fabricated by floating-film transfer method," *Org. Electron.*, vol. 48, pp. 53–60, 2017.

[114] R. K. Pandey, W. Takashima, S. Nagamatsu, A. Dauendorffer, K. Kaneto, and R. Prakash, "Macroscopic self ordering of solution processible poly(3,3‴-dialkylquaterthiophene) by floating film transfer method," *J. Appl. Phys.*, vol. 114, no. 5, p. 054309, 2013.

[115] T. Jiang and W. Fu, "Improved performance and stability of perovskite solar cells with bilayer electron-transporting layers," *RSC Adv.*, vol. 8, no. 11, pp. 5897–5901, 2018.

[116] A. Zekry and G. Eldallal, "Effect of MS contact on the electrical behaviour of solar cells," *Solid- State Electron.*, vol. 31, no. 1, pp. 91–97, 1988.

[117] A. Wagenpfahl, D. Rauh, M. Binder, C. Deibel, and V. Dyakonov, "S-shaped current-voltage characteristics of organic solar devices," *Phys. Rev. B - Condens. Matter Mater. Phys.*, vol. 82, no. 11, pp. 1–9, 2010.

[118] Z. S. Ma, Q. K. Wang, C. Li, Y. Q. Li, D. D. Zhang, W. Liu, P. Wang, and J. X. Tang, "Efficient inverted polymer solar cells integrated with a compound

electron extraction layer," *Optics Communications*, vol. 356, no. 2. pp. 541–545, 2015.

[119] G. Rawat, H. Kumar, Y. Kumar, C. Kumar, D. Somvanshi, and S. Jit, "Effective Richardson Constant of Sol-Gel Derived TiO_2 Films in n-TiO2/p-Si Heterojunctions," *IEEE Electron Device Lett.*, vol. 38, no. 5, pp. 633–636, 2017.

[120] D. Somvanshi and S. Jit, "Mean barrier height and richardson constant for Pd/ZnO Thin film-based Schottky Diodes grown on n-Si substrates by thermal evaporation method," *IEEE Electron Device Lett.*, vol. 34, no. 10, pp. 1238–1240, 2013.

[121] B. J. Leever, C. A. Bailey, T. J. Marks, M. C. Hersam, and M. F. Durstock, "In situ characterization of lifetime and morphology in operating bulk heterojunction organic photovoltaic devices by impedance spectroscopy," *Adv. Energy Mater.*, vol. 2, no. 1, pp. 120–128, 2012.

[122] K. Kawano, R. Pacios, D. Poplavskyy, J. Nelson, D. D. C. Bradley, and J. R. Durrant, "Degradation of organic solar cells due to air exposure," *Sol. Energy Mater. Sol. Cells*, vol. 90, no. 20, pp. 3520–3530, 2006.

[123] H. J. Son, H. K. Park, J. Y. Moon, B. K. Ju, and S. H. Kim, "Thermal degradation related to the PEDOT:PSS hole transport layer and back electrode of the flexible inverted organic photovoltaic module," *Sustain. Energy Fuels*, vol. 4, no. 4, pp. 1974–1983, 2020.

[124] Y. Long, "Effects of metal electrode reflection and layer thicknesses on the performance of inverted organic solar cells," *Sol. Energy Mater. Sol. Cells*, vol. 94, no. 5, pp. 744–749, 2010.

[125] S. K. Gupta, A. Sharma, S. Banerjee, R. Gahlot, N. Aggarwal, Deepak, and A. Garg, "Understanding the role of thickness and morphology of the constituent layers on the performance of inverted organic solar cells," *Sol. Energy Mater. Sol. Cells*, vol. 116, pp. 135–143, 2013.

[126] C. Kumar, G. Rawat, H. Kumar, Y. Kumar, R. Prakash, and S. Jit, "Electrical and ammonia gas sensing properties of poly (3, 3‴- dialkylquaterthiophene) based organic thin film transistors fabricated by floating-film transfer method," *Org. Electron.*, vol. 48, pp. 53–60, 2017.

[127] A. Kumar, S. Ratan, D. K. Jarwal, A. K. Mishra, C. Kumar, A. P. Singh, B. Mukherjee, and S. Jit, "Effect of PQT-12 interface layer on the performance of PCDTBT: PCBM bulk heterojunction solar cells," *Mater. Res. Express*, vol. 6, no. 11, p. 115514, 2019.

[128] B. Z. Dong, G. J. Fang, J. F. Wang, W. J. Guan, and X. Z. Zhao, "Effect of thickness on structural, electrical, and optical properties of ZnO: Al films deposited by pulsed laser deposition," *J. Appl. Phys.*, vol. 101, no. 3, p. 033713, 2007.

[129] D. K. Jarwal, A. Kumar, S. Member, A. K. Mishra, S. Ratan, C. Kumar, D. Upadhyay, and B. Mukherjee, "Efficiency Improvement of TiO 2 Nanorods Electron Transport Layer Based Perovskite Solar Cells by Solvothermal Etching," *IEEE J. Photovoltaics*, vol. 9, no. 6, pp. 1699–1707, 2019.

[130] M. Bag, L. A. Renna, S. P. Jeong, X. Han, C. L. Cutting, D. Maroudas, and D. Venkataraman, "Evidence for reduced charge recombination in carbon nanotube/perovskite-based active layers," *Chem. Phys. Lett.*, vol. 662, pp. 35–41, 2016.

[131] P. K. Shin, P. Kumar, A. Kumar, S. Kannappan, and S. Ochiai, "Effects of organic solvents for composite active layer of PCDTBT/PC71BM on characteristics of organic solar cell devices," *Int. J. Photoenergy*, vol. 2014, p. 786468, 2014.

[132] Y. Q. Wong, H. Y. Wong, C. S. Tan, and H. F. Meng, "Performance optimization of organic solar cells," *IEEE Photonics J.*, vol. 6, no. 4, pp. 1–26, 2014.

[133] J. W. Lee, Y. S. Choi, H. Ahn, and W. H. Jo, "Ternary Blend Composed of Two Organic Donors and One Acceptor for Active Layer of High-Performance

Organic Solar Cells," *ACS Appl. Mater. Interfaces*, vol. 8, no. 17, pp. 10961–10967, 2016.

[134] T. L. Benanti and D. Venkataraman, "Organic solar cells: An overview focusing on active layer morphology," *Photosynth. Res.*, vol. 87, no. 1, pp. 73–81, 2006.

[135] S. J. Lou, J. M. Szarko, T. Xu, L. Yu, T. J. Marks, and L. X. Chen, "Effects of additives on the morphology of solution phase aggregates formed by active layer components of high-efficiency organic solar cells," *J. Am. Chem. Soc.*, vol. 133, no. 51, pp. 20661–20663, 2011.

[136] L. Ren, S. Wang, M. Holtz, and J. Qiu, "The synergistic effect of nanocrystal integration and process optimization on solar cell efficiency," *Nanotechnology*, vol. 23, no. 7, p. 075401, 2012.

[137] J. Y. Lek, Y. M. Lam, J. Niziol, and M. Marzec, "Understanding polycarbazole-based polymer:CdSe hybrid solar cells," *Nanotechnology*, vol. 23, no. 31, p. 315401, 2012.

[138] R. Sharma, S. Bhalerao, and D. Gupta, "Effect of incorporation of CdS NPs on performance of PTB7 : PCBM organic solar cells," *Org. Electron.*, vol. 33, pp. 274–280, 2016.

[139] A. Kumar, D. K. Jarwal, A. K. Mishra, S. Ratan, C. Kumar, R. K. Upadhyay, B. Mukherjee, and S. Jit, "Effects of HTL and ETL Thicknesses on the Performance of PQT-12/PCDTBT:PC61BM/ZnO QDs Solar Cells," *IEEE Photonics Technol. Lett.*, vol. 32, no. 12, pp. 677–680, 2020.

[140] E. M. Boatman, G. C. Lisensky, and K. J. Nordell, "A Safer , Easier , Faster Synthesis for CdSe Quantum Dot Nanocrystals," *J. Chem. Educ.*, vol. 82, no. 11, pp. 1697–1699, 2005.

[141] H. Kumar, Y. Kumar, B. Mukherjee, G. Rawat, C. Kumar, B. N. Pal, and S. Jit, "Electrical and Optical Characteristics of Self-Powered Colloidal CdSe Quantum Dot-Based Photodiode," *IEEE J. Quantum Electron.*, vol. 53, no. 3, pp. 1–8,

2017.

[142] S. K. Dwivedi, D. C. Tiwari, S. K. Tripathi, P. K. Dwivedi, P. Dipak, T. Chandel, and N. E. Prasad, “Fabrication and properties of P3HT: PCBM/Cu2SnSe3 (CTSe)nanocrystals based inverted hybrid solar cells,” *Sol. Energy*, vol. 187, pp. 167–174, 2019.

[143] D. K. Jarwal, A. Kumar, A. K. Mishra, S. Ratan, C. Kumar, D. Upadhyay, B. Mukherjee, and S. Jit, “Efficiency Improvement of TiO2 Nanorods Electron Transport Layer Based Perovskite Solar Cells by Solvothermal Etching,” *IEEE J. Photovoltaics*, vol. 9, no. 6, pp. 1699–1707, 2019.

[144] Y. J. Park, K. S. Lee, G. H. Lim, H. W. Seo, S. W. Kim, M. Kim, Y. Yi, H. S. Lee, and D. I. Son, “Role of CdSe and CdSe@ZnS quantum dots interlayers conjugated in inverted polymer solar cells,” *Org. Electron.*, vol. 82, p. 105707, 2020.

[145] Y. Shen, L. Scudiero, and M. C. Gupta, “Temperature dependence of HOMO-LUMO levels and open circuit voltage for P3HT:PCBM organic solar cells Yang,” *Mater. Res. Soc. Symp. Proc.*, vol. 1360, p. 80601, 2012.

[146] Y. Zhang, L. Li, S. Yuan, G. Li, and W. Zhang, “Electrical properties of the interfaces in bulk heterojunction organicsolar cells investigated by electrochemical impedance spectroscopy,” *Electrochim. Acta*, vol. 109, pp. 221–225, 2013.

AUTHOR'S RELEVANT PUBLICATIONS

Journals:

1. **Amit Kumar**, Smrity Ratan, Deepak Kumar Jarwal, Ashwini Kumar Mishra, Chandan Kumar, Abhinav Pratap Singh Bratindranath Mukherjee, and Satyabrata Jit, "Effect of PQT-12 interface layer on the performance of PCDTBT:PCBM bulk heterojunction solar cells," ***Material Research Express***, vol. 6, no. 11, 115514, 2019.
2. **Amit Kumar**, Deepak Kumar Jarwal, Ashwini Kumar Mishra, Smrity Ratan, Chandan Kumar, Rishibrind Kumar Upadhyay, Bratindranath Mukherjee, and Satyabrata Jit, "Effects of HTL and ETL Thicknesses on the Performance of PQT-12/PCDTBT:$PC_{61}BM$/ZnO QDs Solar Cells," ***IEEE Photonics Technology Letters***, vol. 32, no. 12, pp. 677-680, 2020.
3. **Amit Kumar**, Deepak Kumar Jarwal, Ashwini Kumar Mishra, Smrity Ratan, Chandan Kumar, Deep Chandra Upadhyay, Bratindranath Mukherjee and Satyabrata Jit, "Synergistic Effect of CdSe Quantum Dots (QDs) and $PC_{61}BM$ on Ambient-Air Processed ZnO QDs/PCDTBT:$PC_{61}BM$:CdSe QDs/MoO_3 Based Ternary Organic Solar Cells," ***Nanotechnology***, vol. 31, no. 46, 465404, 2020.

Conferences:

1. **Amit Kumar**, Deepak Kumar Jarwal, Ashwini Kumar Mishra, Smrity Ratan, Chandan Kumar, Rishibrind Kumar Upadhyay, Abhinav Pratap Singh, Bratindranath Mukherjee, and Satyabrata Jit, "Effect of Electron transport Layer (ZnO QDs) thickness on the performance of PCDTBT: PCBM based bulk heterojunction organic solar cells" **(MSSND 2019)**, Jadavpur University,

Kolkata, India, 2019